U.PORTO
FEUP FACULDADE DE ENGENHARIA
UNIVERSIDADE DO PORTO

Delivery of biomolecules by functionalized inorganic/organic nanoparticles

by

Sílvia Maria de Castro Coelho

Thesis submitted to the University of Porto for a Doctor of Philosophy in Chemical and Biological Engineering

Supervisor: Manuel Álvaro Neto Coelho
Co-supervisors: Maria do Carmo da Silva Pereira
Sandra Cristina Pinto da Rocha

Porto, 2013

GOVERNO DE PORTUGAL
Lepae Laboratory for Process, Environmental and Energy Engineering
UNIÃO EUROPEIA Fundo Social Europeu
FCT Fundação para a Ciência e a Tecnologia MINISTÉRIO DA EDUCAÇÃO E CIÊNCIA
COMPETE PROGRAMA OPERACIONAL FACTORES DE COMPETITIVIDADE
POPH PROGRAMA OPERACIONAL POTENCIAL HUMANO
QREN QUADRO DE REFERÊNCIA ESTRATÉGICO NACIONAL PORTUGAL 2007.2013

To my Family ...

"Valeu a pena? Tudo vale a pena
Se a alma não é pequena.
Quem quer passar além do Bojador
Tem que passar além da dor."

in Mar Português de F. Pessoa

Abstract

In this study the enhancement of the proteasome inhibitor activity by colloidal gold nanoparticle delivery was evaluated in pancreatic and prostate cell lines. Chitosan-gum Arabic-gold nanoparticle structures are also proposed as another approach for specific drug delivery to cancer cells.

Proteasome inhibition is a current therapeutic strategy used in the treatment of multiple myeloma. Drugs controlling proteasome activity are ideally suited for unidirectional manipulation of cellular pathways such as apoptosis. The first proteasome inhibitor approved in clinics was bortezomib. This drug is currently used in combination with other anticancer agents.

The cellular uptake of the two nanosystems - gold nanoparticles coated with poly(ethylene glycol) and chitosan-gum Arabic matrix- gold nanoparticle - was studied in pancreatic (S2-013 and hTERT-HPNE) and prostate (Du145) cell lines by laser scanning confocal microscopy. Adenocarcinoma and normal cells internalized pegylated gold nanoparticles, which show no toxicity up to concentrations of 1.0 nM. The formation of endocytic vesicles with high electron density particles was observed and might explained the activity of the proteasome inhibitor at very low concentrations in the presence of the gold nanoparticles. The internalization of bortezomib promoted by the particles leads to its rapid accumulation and diffusion in the cytoplasm yielding to an increased toxicity to the cancer cells when compared to the drug alone. Concerning Du145 cells, it was observed a significant cell viability reduction with bortezomib concentrations as low as 4 nM in the presence of gold nanoparticles. The proteasome inhibitor alone had to be present at concentrations of at least 120 nM to induce identical cytotoxicity response.

Cytotoxic assays established that the positively charged nanosystem - chitosan-gum Arabic-gold nanoparticles - reduces the cell growth and cell proliferation of S2-013s but this effect was not observed in hTERT-HPNE cells.

The capacity of chitosan-gum Arabic nanocarriers to deliver gold nanoparticles/anticancer drug is showed and a decrease of the drug concentration needed to cause toxicity in HPNE cells was demonstrated.

These findings demonstrate that gold nanoparticles can be used as effective delivery system, enhancing the permeation and retention of the drug in pancreatic and prostate cells and open the possibility to decrease multi-drug resistance. *In vitro* results of functionalized gold nanoparticles, internalized by cancer cells, pave the way for a more efficient proteasome inhibitor delivery and release in adenocarcinoma cells.

Resumo

O presente estudo visa estudar a atividade de um inibidor de proteassomas transportados em nanopartículas de ouro em linhas celulares neoplásicas do adenocarcinoma pancreático e prostático. Outra abordagem neste estudo consiste no desenvolvimento de nanopartículas de quitosano-goma-arábica como sistemas de libertação de fármacos anticancerígenos.

A inibição de proteassomas é uma estratégia terapêutica usada no tratamento de mieloma múltiplo. Na verdade, os fármacos controladores da atividade do proteassoma são fundamentais na manipulação e degradação de proteínas responsáveis pelo ciclo celular e iniciadores da apoptose. O bortezomib é o primeiro inibidor de proteassomas aprovado em tratamentos clínicos. Este medicamento é, atualmente, utilizado em combinação com outros agentes anticancerígenos.

Os estudos de internalização celular dos dois nano-sistemas – as nanopartículas de ouro funcionalizadas com polietilenoglicol e as nanopartículas de ouro encapsuladas numa matriz de quitosano-goma-arábica foram estudados em linhas celulares pancreáticas (S2-013 e hTERT-HPNE) e prostáticas (Du145) por microscopia confocal. As nanopartículas de ouro internalizadas pelas células neoplásicas e não neoplásicas não mostram citotoxicidade para concentrações até 1.0 nM. A formação de vesículas endocíticas de nanopartículas com uma elevada densidade eletrónica são observados e poderá explicar a atividade inibidora do proteassoma, com concentrações bastante baixas de fármaco, na presença de nanopartículas de ouro. A internalização do bortezomib promovida pelas nanopartículas conduz à rápida acumulação e difusão no citoplasma, levando ao aumento de toxicidade nas células neoplásicas quando comparado com o fármaco. Nas células Du145 foi observada uma significativa redução na viabilidade celular com a concentração de bortezomib de 4

nM na presença de nanopartículas de ouro. Quando o inibidor é utilizado sozinho, a sua concentração será de 120 nM para induzir uma resposta idêntica à anteriormente nomeada.

Os ensaios de citotoxicidade com os nano-sistemas permitiram verificar que há uma redução do crescimento e proliferação celulares das S2-013, mas a mesma resposta não foi observada nas hTERT-HPNE.

A capacidade dos nano-transportadores de quitosano-goma-arábica para a entrega de nanopartículas de ouro/agentes anti-tumorais é apresentada e é demonstrada a minimização de toxicidade das drogas em células HPNE.

Estes resultados demonstram que as nanopartículas de ouro podem ser utilizadas como sistemas de transporte de fármacos, que permitem aumentar o efeito de permeabilidade e retenção tanto nas células pancreáticas como nas células prostáticas. Este sistema poderá conduzir à diminuição de resistência a múltiplas drogas. Os resultados *in vitro* da internalização de nanopartículas de ouro funcionalizadas por células neoplásicas possibilitam a eficiência no transporte e libertação dos inibidores de proteassomas.

Acknowledgments

The present work was carried out in the group of Professor Manuel Coelho at the LEPABE, Faculty of Engineering of the University of Porto (FEUP, Porto, Portugal).

I would like to express my deepest gratitude to Professor Manuel Coelho for accepting me as a PhD student and the opportunity to work in his group, supervising the work and always available for scientific discussions. I want to thank his encouragement, expertise and valuable ideas, which were indispensable to accomplish my research. I also would like to thank Professor Maria do Carmo Pereira for the guidance and help in many points, which contributed to my knowledge.

A special thanks to Doctor Sandra Rocha who received me in the laboratory during my first experiments and supported me with her teaching, helpful suggestions and comments.

Dr. Petras Juzenas welcomed me in his group at the Department of Radiation Biology, Institute for Cancer Research at the Norwegian Radium Hospital (Oslo, Norway). Both he and all the members of his group were always open to many work discussions of the project, introducing me to the *in vitro* cell studies.

Furthermore, I want to thank Doctor Filipe Santos and Doctor Gabriela Almeida for providing the opportunity to develop my work in collaboration with IPATIMUP as well as for their contribution in our scientific discussions. To Doctor Paula Sampaio (Advanced Light Microscopy), Doctor Rui Fernandes (Histology and Electron Microscopy), Professor Susana Moreno Flores and Professor José Luis Toca-Herrera (Surface Probe Microscopy) for the assistance and effort providing me help in this research work. I thank to CEMUP for the technical support (scanning electron microscopy); to my colleague and friend Leonor Ricardo for helping me and giving me

knowledge about gold nanoparticles; to my colleagues Andreia Sousa and Cristina Teixeira for sharing their laboratorial expertise.

My acknowledgment to the Lepae members and Department of Chemical Engineering of FEUP, especially, to my work group who were friendly and helpful in scientific facilities. My recognition to D. Fátima Ribeiro through her help with bureaucratic questions.

I am thankful to my friends, in particular, to Joana Ângelo, Ana Catarina Duarte, Paula Dias, António Meireles, Filipa Duarte for their friendship and recommendations. A special thanks to Vera Gonçalves, who supports me all the time with her incentive and friendly dedication.

I would like to thank my mother and father for their love and continuous support, encouraging me with my choices and challenges. Moreover, a special word to my brother for his patience and understanding my temperament. Last but not least, I am grateful to my boyfriend for all the love, inspiration, comprehension and always being with me.

The research work was supported by FCT research project PTDC/QUI/BIQ/115449/2009 and by the Research Council of Norway with the Yggdrasil - young guest and doctoral researchers' annual scholarships.

Table of Contents

List of Figures

List of Tables

Abbreviations and Symbols

Abbreviations

A	Absorbance
AFM	Atomic force microscopy
AFU	Arbitrary fluorescence uits
ATR	Attenuated total reflectance
AuNPs	Gold nanoparticles
BTZ	Bortezomib
C	Concentration
Ch	Chitosan
D	Diameter
DI	Deionized water
DLS	Dynamic light scattering
DMEM	Dulbecco's modified Eagle's medium
DMSO	Dimethyl sulfoxide
DNA	Deoxyribonucleic acid
DNA	Deoxyribonucleic acid
Du145	Human prostate carcinoma
EGFR	Epidermal growth factor receptor
FBS	Fetal bovine serum
FTIR	Fourier transform infrared spectroscopy
GA	Gum Arabic
GI_{50}	Concentration for 50% growth inhibition
h	hour
hTERT-HPNE	Immortalized human pancreatic duct epithelial cells
KBr	Potassium bromide
LDV Laser	Doppler Velocimetry
LSCM	Laser Scanning Confocal Microscopy

MB	Methylene blue
MDR	Multi-drug resistance
min	minutes
mV	milivolts
nm	nanometers
PB	PrestoBlue®Cell Viability Reagent
PBS	Phosphate buffered saline
PdI	Polydispersity index
PEG	Polyethylene glycol
PEGAuNPs	Pegylated gold nanoparticles
$R_{GA/Ch}$	GA/Ch weight ratios
RPMI-1640	Roswell Park Memorial Institute-1640
S2-013	Human pancreatic cell
SEM	Scanning electron microscopy
SRB	Sulforhodamine B
T	absolute temperature value
TCA	Tricloroacetic acid
TEM	Transmission electron microscopy
ZP	Zeta potential

Symbols

D_S	Translational diffusion coefficient
ε	Extinction coefficient
ε	Dielectric constant
F	Force of interaction between the tip and the surface of the sample
$f(ka)$	Henrys function
I_0	Incident light intensity
I	Light intensity that passes through a volume of solution
k	Spring contact of the cantilever
k	Boltzmann's constant

L	Distance through the sample
R_H	Hydrodynamic radius of the scattering particle
S_0	ground state
S_1	excited state
T	Transmittance
T	Turbidity
μ_E	Electrophoretic mobility
η	Viscosity
ζ	Zeta potential
x_c	Deflection of the cantilever

Legal Regulations

According to the Law n° 216/92 of 13th October and to the Regulations of PhD by the University of Porto, we clarify that all the experiments, results and discussion presented on this thesis are our own, except if stated otherwise. The results from the work presented in this dissertation resulted from the following publications:

Coelho S, Moreno-Flores S, Toca-Herrera JL, Coelho MAN, Carmo Pereira M, Rocha S (2011) Nanostructure of polysaccharide complexes. Journal of Colloid and Interface Science 363 (2):450-455.
doi:http://dx.doi.org/10.1016/j.jcis.2011.07.098.

Coelho SC, Rocha S, Juzenas P, Sampaio P, Almeida GM, Silva FS, et al. (2013) Gold nanoparticle delivery-enhanced proteasome inhibitor effect in adenocarcinoma cells. Expert Opin Drug Deliv 10 (10): 1345-52.
doi:10.1517/17425247.2013.827659.

Coelho SC, Rocha S, Carmo Pereira M, Juzenas P, Coelho MAN (2013) Enhancing proteasome inhibitor effect by functionalized gold nanoparticles. J. Biomed. Nanotech. 9 (*in press)*.

Coelho SC, Rocha S, Sampaio P, Carmo Pereira M, Coelho MAN Encapsulation of a proteasome inhibitor with gold-polysaccharide nanocarriers. *Submitted to Journal of Nanoparticle Research*.

Chapter 1

1 Preface

Nanoparticle formulation, functionalization and characterization are important advances in biomedicine that contribute to the development of new approaches for the treatment and diagnosis of diseases such as cancer. Recent studies show that nanoparticle size, degree of hydrophobicity, stability and reduced toxicity are important factors that determine the ability of the systems to cross cell barriers in order to reach specific areas of the body and to deliver biomolecules to tissues [1].

Nanoparticles have shown to be promising delivery systems for cancer therapy applications and diagnostics. Different approaches are currently being investigated for the targeted delivery of anticancer drugs with minimal side effects [2, 3]. Some nanosystems have been developed due to their specific properties, biocompatibility and biodegradability [4, 5]. Some vehicles have been successfully applied in the clinic [4]. Nonetheless it is fundamental a continuous investigation for developing safe nanomaterials as nanocarriers for therapeutic and diagnostics applications.

This thesis focuses on the delivery of an anticancer drug, bortezomib, by inorganic based nanocarriers for cancer treatment. Bortezomib (BTZ) is a dipeptide boronic acid, FDA-approved inhibitor of 26S proteasome function, crucial to induce toxicity and apoptosis in tumour cells [6]. Functionalized gold and gold-polysaccharide (chitosan-gum Arabic) nanoparticles were developed in order to (a) enhance the drug therapeutic efficacy in cells leading to effective combination therapies against cancer and low toxicity; (b) ability to deliver the anticancer drugs to specific sites and (c) understand the internalization mechanism of the particles by cancer cells.

The present thesis is organized into six chapters. This chapter, Introduction, presents the purposes and scope of this research. Chapter 2, Background, introduces the state-of-art of drug delivery systems in biomedical applications, particularly in cancer therapies. In Chapter 3, Material and Methods, the preparation and

characterization of the nanosystems are described. In Chapter 4, the BTZ loaded pegylated gold nanoparticle system is presented and its toxicity in prostate and pancreatic cells is evaluated. Chapter 5 presents the system of BTZ+pegylated gold nanoparticles loaded in chitosan-gum Arabic nanoparticles and the results concerning their toxicity in pancreatic cells. Chapter 6, Concluding Remarks, sums up the main outcomes of this thesis.

.

Chapter 2

2 Background

Contents

2.1 Introduction

Drug delivery systems (DDS) have been of a considerable focus of attention as promising tools to attain better retention and release of therapeutic and diagnostic agents and thus to overcome the limitations of conventional therapies. The increase of the treatment efficacy by targeting the anticancer drugs selectively to cancer cells is a challenge of nanotechnology-based DDS [7]. Nanosystems are currently being developed to transport and distribute the drugs, in a direct and controlled way, as well as to activate them *in situ* [8]. This leads to a decrease of the relative anticancer drug concentration and side effects in normal host tissues [2, 3, 5, 7, 9-12].

Nanosystems like dendrimers, liposomes, metal based nanoparticles, micelles, vesicles, nanoemulsions, quantum dots and polymer nanoparticles have been developed to solve limitations of the myriad existing drugs, such as poor solubility at physiological pH, biodistribution and cell uptake [2, 7, 10, 13-19]. Biocompatibility, biodegradability and stability are also crucial factors that should be taken into consideration [4, 5, 10, 15, 16]. Physical-chemical properties such as chemical composition, shape, roughness, hydrophobicity or hydrophilicity, hydrodynamic diameter and

surface charge influence the biocompatibility and stability of the nanosystems [1, 4]. Table 2.1 highlights some types of materials used in nanocarrier preparation for application as drug delivery systems [3, 5, 20, 21].

Table 2.1 Nanosystems in drug delivery applications.

Dendrimers	Poly(amidoamine).
Fullerenes	Carbon based nanocarriers.
Inorganic nanoparticles	Gold nanoparticles (AuNPs); carbon nanotubes; mesoporous silica nanoparticles.
Polymer-based nanoparticles	Polylactic acid; Poly(cyano)acrylates. Polyethyleinemine; Polysaccharides including alginate, chitosan, gum Arabic; Phospholipids;
Liposomes	Phospholipids.

An overview of polymeric and metal-based nanoparticles, in particular, polysaccharides nanoparticles and AuNPs, for cancer therapy is presented.

2.2 Design of nanoparticles for anticancer drug delivery

Nanoparticles (NPs) have potential in therapeutics and diagnostics applications. They can improve several limitations of the chemotherapy agents [14]. Chemotherapy agents used in cancer treatment are capable of blocking critical cell cycle phases leading to apoptosis of tumour cells [10]. However chemotherapy success rate has limitations and depends on each patient. The anticancer activity is not selective in tumour tissues, often causing damage to healthy tissues [8, 10, 21, 22]. The unfavorable pharmacokinetics, and administration at high doses of the agents with poor solubility leads to a low circulation time in the body associated to the limitations of conventional chemotherapy [2, 4, 8, 14, 23]. The effectiveness of the anticancer drug

targeting to a specific site by nanoparticles will have an enormous impact in cancer treatments [15].

NPs offer advantages such as the improvement of bioavailability, controlled time release, modifications on pharmacologic and pharmacodynamics properties of the active drugs and a significant reduction of unwanted systemic side effects [21, 22, 24]. The advantages and disadvantages of nanoparticles are summarized in Table 2.2.

Table 2.2 Nanoparticles advantages and disadvantages.

Nanoparticles advantages
Easy modification to achieve transport drug targeting
Biocompatibility
Low toxicity
Drug protection and controlled release
Good stability
Increase solubility of the anticancer drug preserving its activity
Targeting delivery at site
Reduction of side effects
Nanoparticles disadvantages
Possibility of toxicity of the materials
Need for surgical intervention either for the systems' applications or removal
Particle aggregation, making physical handling of nanoparticles difficult in liquid and dry forms
High cost of drug production

NPs can increase the anticancer drug concentration in tumour cells by passively or actively targeting the tumour tissue [20, 25].

Through active targeting, specific marker agents for cancer cells are used, modifying the drug nanosystem. A targeted moiety having selective affinity for interacting with a specific tissue or cell is conjugated to the nanocarrier. The molecules that acts as penetration enhancers are capable to recognize and bind to

other biomolecules [7, 10]. The targets could be receptors, enzymes, peptides and antibodies [25].

Nanosystems can be accumulate, gradually, at the target site, in solid tumours via the enhancing the permeation and retention (EPR) effect (Figure 2.1), decreasing the toxicity while therapeutic effects are maintained [5, 7, 8, 20, 21, 25, 26].

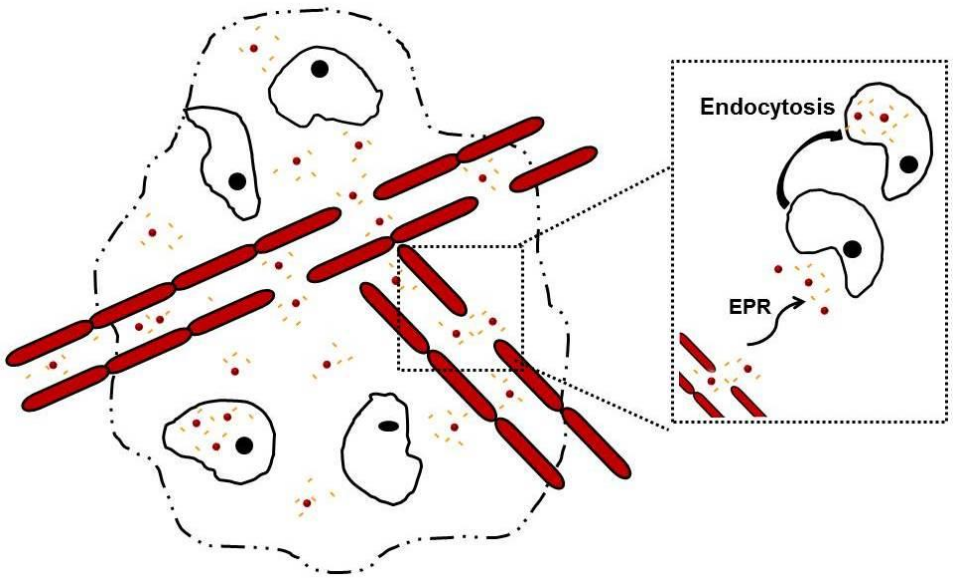

Figure 2.1 Passive targeting delivery – the EPR effect.

Solid tumours have particular pathophysiological characteristics such as abnormal angiogenesis [27]. Angiogenesis is the process that involves the growth of new blood and lymphatic vessels which is stimulated when tumour tissues require nutrients and oxygen [28, 29]. Consequently, angiogenesis is the crucial process that generates the development and growth of disease, particularly the growth of tumours [29]. Figure 2.2 shows the tumour angiogenesis process. This occurs due to disorders in the balance between stimulating and inhibiting elements [29]. Therefore, solid tumours reveal hyper vascular permeability, defective vascular architecture and poor lymphatic drainage compared with normal tissues [3, 21, 22, 27, 30, 31]. These features of

solid tumours are described as EPR effect. Leaky blood vessels are present with irregular shape and the endothelial cells are disorganized [22, 32]. Nanocarriers have the capacity to deliver high anticancer drug doses, increasing their half-life time and reducing their side effects by selective targeting tumour tissues and vasculature [8, 10, 21, 30, 31, 33]. Several studies reported nanocarriers that contribute to the EPR effect [22, 27].

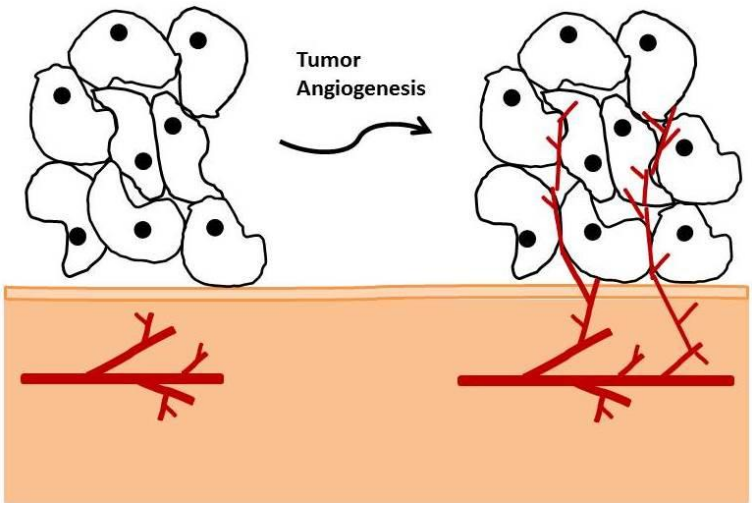

Figure 2.2 Angiogenesis process.

It is reported by several studies that nanoparticles are internalized into cancer cells through endocytosis (Figure 2.1) [34, 35]. The nanosystem is confined in endocytic vesicles. Usually, incubation with nanoparticles in cell media leads to adsorption of serum proteins on nanoparticles' surface that facilitates their uptake mechanism by cells [36]. Kim *et al.* studied the influence of nanoparticle internalization on the cell cycle phase [37]. The uptake of nanoparticles by cells was studied and characterized by transmission electron microscopy (TEM) methods in order to understand the mechanisms of potential nanoparticle toxicity [34, 38-40].

Continuous research has been focused on nanosystems' behaviour within biological systems. When the nanocarriers are administered to the body, there is an immune response in order to protect it against the foreign NPs. It has been studied

that small NPs (10 to 100 nm) can avoid being detected and cleared by a component of the immune system, the reticuloendothelial system (RES), by the opsonisation process [41]. The intravenous administration of NPs leads to the recognition of the nanosystems by the immune system that are then cleared by phagocytes. Hence, it is important to decrease the adsorbed blood components - the opsonins – from the nanoparticle' surface, making them less visible to phagocytic cells [25]. This can be achieved by the development of NPs functionalized with hydrophilic polymers/surfactants such as poly(ethylene glycol) layer, poloaximine and polysorbate 80 [4, 8, 20]. The addition of modifiers to nanocarriers is possible through their surface functionalization leading to increased stability. Also, due to effective repulsive forces between nanocarriers, aggregation and precipitation are avoided, prolonging their *in vivo* circulation time [4, 5, 8]. Efficient loading of chemotherapeutic agents, such as doxorubicin, paclitaxel, carboplatin, into NPs has been reported [42-46]. Table 2.3 presents some colloidal carriers that are under development or on the market. These systems showed either equal or higher anticancer drug efficacy compared to regular chemotherapy. The anticancer drug agents can be loaded into the NPs by encapsulation, entrapment or surface attachment [14]. Also, NPs are able to overcome the resistance to several anticancer drugs developed by most of tumour cells and, consequently, target the drug to cells [8, 14]. Nanoparticles may be administered by different routes, which include intravenous, intramuscular, and subcutaneous injection, as well as peroral, ophthalmic and transdermal administration [47].

Table 2.3 Colloidal systems under development, clinical trials, or on the market.

Formulation	Drug	Product	Application	Status
Pegylated liposome		Doxil	Ovarian and metastatic breast cancer, multiple myeloma, kaposi's sarcoma [48-52]	On the market
NPs		Livatag	Hepatocellular carcinoma, liver cancer [53]	On the market
liposomes	Doxorubicin	Thermodox	Breast, liver cancer [54, 55]	Clinical trial Phase II and III On market
Polymeric micelles (PEG-poly(aspartic acid) block copolymer)		NK911	Solid tumours [56, 57]	Clinical trial Phase I
Polyisohexyl--cyanoacrylate NPs			Hepatocellular carcinoma [42]	Under development
Albumin NPs		Abraxane	Lung, advanced ovarian, breast, metastatic pancreatic cancer [58-61]	On the market
Polymeric micelles	Paclitaxel	Genexol-PM	Lung and breast cancer [62-64]	On the market Clinical trial Phase II
Cetyl alcohol/polysorbate NPs			Brain tumours: U-118, HCT-15 cells [65]	Under development
PEGAuNPs	Human tumour necrosis factor alpha, TNF	Aurimmune (CYT-6091)	Pancreatic, ovarian and breast cancer, melanoma, soft tissue sarcoma [66-68]	Clinical trial Phase II
Liposome	Uridine		Metastatic solid tumour [69]	Clinical trial Phase I

Formulation	Drug	Product	Application	Status
Polymeric micelles	Cisplatin	NC-6004	Advanced solid tumour [70, 71]	Clinical trial Phase I/II/III
Polymeric NPs	Docetaxel	Docetaxel-PNP	Advanced solid malignancies [72]	Clinical trial Phase I
Liposome	Daunorubicin	Daunoxome	Kaposi sarcoma [73]	On the market

The multidrug resistance (MDR) of the tumour cells conferred by the over expression of the plasma membrane p-glycoprotein might be reduced by NPs [15, 74]. P-glycoprotein recognizes the anticancer agent decreasing the influx agent and increasing the drug efflux out of the solid tumours, changing the apoptotic mechanism [8]. Generally, MDR is a decrease of the drug accumulation in the specific site of tumour because of the overexpression of ATP-dependent pumps for xenobiotic compounds [8, 74]. Several nanosystems have been evaluated to augment the drug control release and increase the tumour targeting, avoiding this problem of chemotherapy [74]. The nanoparticles loaded with anticancer drug will cross the cell membrane without triggering the p-glycoprotein pump augmenting the capacity of anticancer drug distribution into tissue and cells [8, 15]. Koziara *et al.* proposed a system able to overcome drug resistance in a human colon adenocarcinoma cell line (HCT-15) by paclitaxel entrapped in emulsifying wax NPs [75]. A cytotoxicity study of doxorubicin (DOX) loaded pegylated gold NPs (PEGAuNPs) in hepatocellular cell line HepG2R showed ability to overcome MDR compared to free anticancer drug [76]. The cytotoxicity study demonstrated that the Au-PEG-SS-DOX nanoconjugate system efficiently released the anticancer drug DOX and enhanced its cytotoxicity against MDR cancer cells. This study highlights the potential of using AuNPs for overcoming of MDR in cancer chemotherapy. Brown *et al.* revealed a significant growth inhibition of lung epithelial cancer cell line, A549, treated with oxaliplatin adsorbed onto PEGAuNPs [77].

The NPs may increase the activation of the anticancer drug in the site of action and drug targeting in combination with other cancer therapies like radiotherapy

treatment. Radiation induced deoxyribonucleic acid (DNA) damage to cancer cells leading to a reduction in size or destruction of the tumour [10, 78, 79]. Therefore, NPs act as radiopharmaceuticals or radiosensitizers in cancer treatment [10, 80]. Metallic NPs can enhance, effectively, the radiation therapy by scattering and/or absorbing high-energy electromagnetic waves (X-rays and gamma rays) [19]. This fact contributes to the damage of DNA and cancer cells organelles. NPs can have influence in total radiation dose, minimizing it, and thus decreasing the radiation side effects [81]. Several studies have been showing an increase in absorption of X-rays radiation when AuNPs are internalized in cancer cells [80, 82, 83]. Hainfield *et al.* reported AuNPs as radiosensitizers [84]. They increase the local dose concentration of drugs and enhance the effects of X-rays radiation. Results showed that the tumours were reduced by about 90% in size when treated with AuNPs and X-rays radiation, compared to radiation alone. The area of combination therapies in drug nanotechnology research is a highly emerging one.

2.3 Metal based Nanoparticles

Metal NPs have been studied for drug delivery applications. Inert metals such as gold and titanium are the most used for control release of anticancer drugs [85].

AuNPs have been the focus of increasing number of studies due to their inherent and unique optical and chemical properties [86]. AuNPs can be synthesized with different shape (spheres, rods, tubes, wires, ribbons, cubic, hexagonal, triangular) and size [86-89]. They present a characteristic surface plasmon resonance band, absorb light in the near infrared region rendering them active for biological purposes [14, 90 91]. The expectable and easy surface modification chemistry through thiol linkages due to their reactive surface area, provides them the ability to carry high drug doses [20, 91-93].

AuNPs can be synthesized via different methods. The biphasic Brust-Schiffrin method uses tetraoctylammonium bromide as the phase transfer reagent and sodium borohydride as reducing agent and allows the preparation of AuNPs with an

hydrodynamic diameter between 1 and 5 nm [94]. Turkevitch *et al.* synthesized AuNPs with diameter range from 10 to 100 nm by the reduction of $HAuCl_4$ with sodium citrate [95, 96].

Characteristics such as charge, functionalized surface and size of AuNPs are important since they affect their cellular uptake [97-99]. The mechanism of AuNP cellular uptake is controversial. Even though there are several studies reporting the fast uptake of positively-charged NPs by tumour cells, the presence of positive charges at the particle surface also leads to immune reactions [21]. Neutral and negative NPs are considered better systems for clinical applications [21, 100]. The most efficient cell internalization of NPs was observed for particles with size ranging between 20 and 50 nm. Chan *et al.* showed that AuNPs with a diameter between 14 and 74 nm are able to be internalized by a HeLa cell model [101].

AuNPs are used for many biomedical applications including as a drug delivery vectors based on covalent reaction, drug encapsulation, electrostatic adsorption and non-covalent conjugation [12, 20, 24, 41, 102-104]. They can increase the anticancer effect of drugs by delivering them to cancer cells [105]. This fact is facilitated by passive or active targeting mechanisms [106]. Several studies showed that AuNPs interact with serum protein. Chithrani *et al.* studied the behavior of AuNPs when incubated with cell culture media. It was suggested that serum proteins are adsorbed at the particle surface, which mediate the AuNPs internalization via endocytosis process [101].

Also, AuNPs might be a potential vector to avoid the RES clearance and enhance endothelial [3, 12]. Mirkin *et al.* suggested that paclitaxel loaded oligonucleotide-AuNPs might overcome the drug-efflux in MDR cancers [107]. Another example is the doxorubicin conjugated AuNPs for the treatment of breast cancer [108]. The results showed an increase of cancer cell death compared to the free doxorubicin and an outgrown drug efflux from breast cancer cells. Patra *et al.* reported gemcitabine (anticancer drug) and cetuximab (anti-epidermal growth factor receptor) conjugated to AuNPs as an efficient nanosystem inhibitor of pancreatic tumour proliferation *in vitro* and *in vivo* [90].

Drug delivery by AuNPs delivery can be combined with non-invasive therapeutic effects such as radiofrequency ablation (RFA), photothermal therapy (PTT), photodynamic therapy (PDT) and radiotherapy [78, 105, 109, 110]. Different studies reported better anticancer effects when NPs were combined with anticancer drugs and nonionizing radiofrequency (RF) radiation. Glazer *et al.* showed *in vivo* an increase on the pancreatic cancer cell apoptosis with combined therapies – cetuximab - and PAM4-conjugated AuNPs and RF radiation [111]. El-Sayed et al. reported that the use of epidermal growth factor receptor (EGFR) coated AuNPs increased the photothermal therapy effect by 20 times of human oral squamous cell carcinoma, HSC3 [112].

PEGAuNPs are studied in several tumours and are systems that combined with chemotherapeutic agents offer a therapeutic strategy for advanced stage cancer patients [24, 113]. The first clinical trial with PEGAuNPs was performed with aurimune (CYT-6091) in advanced cancer patients could result in a significant decrease of cytotoxicity of anticancer drugs [113].

2.4 Polymeric Nanoparticles

Polymeric NPs using biocompatible, stable and biodegradable polymers have been formulated to encapsulate hydrophilic and hydrophobic anticancer drugs and proteins [10, 21, 26, 114, 115]. Polymeric NPs confer advantages for the deliver of drugs [21, 26, 116]. These advantages are:

- An increase of the drugs solubility and a better biodistribution;
- Increase in stability of biomolecules and increase of their half-life time [14, 117, 118];
- Accumulation of the anticancer drug polymeric NPs at the tumour tissue due to the EPR effect [119, 120];
- Targeting the drug to specific locations [121].

Polysaccharides are polymers derived from algae, plants, microbial population and animals [122]. Chitosan, alginate, heparin, hyaluronic acid and dextran are examples

of polysaccharides [123]. They are high molecular weight compounds, classified according to their surface charges in cationic polysaccharides – chitosan - anionic polysaccharides – gum Arabic, alginate, heparin, hyaluronic acid and nonionic polysaccharides – dextran [7, 26, 124]. Polysaccharide-based NPs can be prepared by different mechanisms: covalent crosslinking, ionic crosslinking, polyelectrolyte complexation and self-assembly of hydrophobically modified polysaccharides [123] (Table 2.4) [123, 125, 126].

Table 2.4 Methods used for the preparation of polysaccharide-based nanoparticles.

Method	Characteristics
Covalent crosslinking	Chemical interaction.
Ionic crosslinking	Polyanions/polycations with low molecular weight can act as ionic crosslinkers for charged polysaccharides. The most common crosslinker used is tripolyphosphate (TPP).
Polyelectrolyte complexation	Polymers with opposite charge surface can form polysaccharide NPs by electrostatic interaction.
Self-assembly of Hydrophobically modified polysaccharides	Spontaneous formation of micelles by polymeric amphiphiles through intermolecular connection between hydrophobic moieties.

Chitosan (Ch) is a natural heteropolymer of N-acetyl-D-glucosamine and D-glucosamine liked by beta-(1-4)glycosidic bonds and it is obtained by deacetylation of chitin [26, 127]. It presents low toxicity and it is hydrophilic, biodegradable and soluble in acidic solutions due to protonation of the amine groups [7]. Ch play an important role in cancer therapy and can be explored for tumour angiogenesis inhibition [128]. Ch has many advantages, including:

- the ability to control the release of active agents;
- avoiding the use of hazardous organic solvents while preparing particles;

- allowing for ionic crosslinking (cationic nature) with multivalent anions: it has mucoadhesive character, which increases the residual time at the site of absorption [129].

Gum arabic (GA) (Acacia) is a negatively charged branched polysaccharide. Its biocompatibility and biodegradability confer to this polyelectrolyte numerous advantages [130]. The composition analysis of GA reveals the presence of a main galactan chain carrying heavily branched galactose/arabinose side chains. The carbohydrate moiety is composed of D-galactose (40% of the residues), L-arabinose (24%), L-rhamnose (13%), and two types of uronic acids, responsible for the polyanionic character of the gum, D-glucuronic acid (21%) and 4-*O*-methyl-D-glucuronic acid (2%) [131]. Liu *et al*. suggested that AuNPs form a novel nanocomposite in the presence of GA [132]. The system can be promising as photothermal agents for cancer treatment [132]. Effiong *et al.* revealed that GA-modified magnetic NPs inhibit the proliferation of *E. coli* in media [133]. Avadi *et al.* developed a nanoparticulate system based on ionic gelation between Ch and GA for oral delivery of insulin [134].

NPs can entrap the anticancer drugs into their matrix or absorb them onto their surface [123] [127]. The loading efficacy depends on the NPs preparation and physicochemical properties of the anticancer drug/biomolecule. Anticancer drugs such as doxorubicin, paclitaxel, 5-fluoroaucil have been encapsulated using polymeric NPs. Fonseca *et al.* reported an increase of the inhibitory growth effect with paclitaxel loaded to poly(lactic-co-glycolic) acid (PLGA) NPs in human small cell lung cancer cell line, NCl-H69 when compared to free anticancer drug [135]. Another study showed similar results, supporting the use of these NPs as a promising drug delivery nanosystem. In fact, in HeLa cells, a higher inhibitory growth effect is revealed with paclitaxel-loaded PLGA NPs when compared to the drug alone [136].

Nah *et al.* prepared the paclitaxel loaded in water-soluble Ch NPs. The NPs were produced by conjugation of hydrophilic group, methoxy poly-(ethylene) glycol *p*-nitrophenyl carbonate and an hydrophobic group, cholesteryl chloroformate to the free amine groups of chitosan [137]. The results suggested a high nanoparticle

accumulation in a tumour induced murine model and, therefore, a considerable anticancer effect. Sahu *et al.* showed a good cytotoxicity of paclitaxel loaded folic acid (FA) modified chitosan NPs in tumour cells [138].

Chapter 3

3 Materials and Methods

Contents

3.1 Materials

Bortezomib (Velcade) was purchased from Selleck Chemicals LLC (USA). Chitosan 250 kDa (degree of deacetylation > 93%) was purchased from Altakitin (Portugal). High molecular weight chitosan (Ch, 310–375 kDa based on the viscosity range of 800–2000 mPa.s, degree of deacetylation > 75%), gum Arabic (GA, Mw ~ 250,000, viscosity 60 mPa s), glacial acetic acid, sodium hydroxide and sodium chloride, trisodium citrate dehydrate and tetrachloroauric (III) acid ($HAuCl_4$; 99.99% trace metals basis, 30 wt% in dilute HCl), acetic acid, Potassium bromide (KBr), dimethyl sulfoxide (DMSO), sulforhodamine B (SRB) and trypan blue were purchased from Sigma-Aldrich (Germany). Phosphate buffered saline (PBS: 0.01 M, 0.0027 M KCl, 0.137 M NaCl, pH 7.4) were purchased from Fluka (Germany). α-thiol-ω-carboxyl (polyethylene glycol) (molecular weight 394.57 Da) was purchased from Prochimia (Poland). Tricloroacetic acid (TCA) and Tris buffer were acquired from Merck (Darmstadt, Germany). Roswell Park Memorial Institute-1640 medium-(RPMI-1640 medium), fetal bovine serum (FBS), L-glutamine, penicillin and streptomycin were purchased from Invitrogen (Spain). Trypsin, Dulbecco's modified Eagle's medium (DMEM) and PrestoBlue®Cell Viability Reagent (PB) were obtained from Invitrogen Co. (Scotland, UK). 20S proteasome enzyme (human erythrocyte), substrate Suc-LLVY-AMC (molecular weight 763.9 Da), proteasome assay buffer were purchased from Enzo Life Sciences (Switzerland).

3.2 Systems

3.2.1 Synthesis of pegylated gold nanoparticles

Gold nanoparticles (AuNPs) (pH of 5.1) were synthesized by reduction of $HAuCl_4$ using sodium citrate (Turkevich-Frens method) [96, 139]. Briefly, $HAuCl_4$ aqueous solution was heated to slight boiling and stirred. Trisodium citrate was added and boiled for 15 min. Then, pegylated-modified gold nanoparticles (PEGAuNPs) were prepared by mixing AuNPs with α-thiol-ω-carboxyl (polyethylene glycol) (PEG) capped with a carboxylate group at a molar ratio of 1:1000. The mixture was stirred at room temperature for about 1 h. The resultant solution was centrifuged by three washing steps with water, at 13400 rpm (12000 g) during 10 min to remove the unbound PEG molecules. The pH of PEGAuNPs was 5.3. The concentration of the PEGAuNPs was determined by the Lambert-Beer Law assuming the molar absorptivity of the AuNPs plasmon resonance band at 526 nm being 2.33×10^8 M^{-1} cm^{-1} [140].

3.2.2 Mixture of bortezomib with functionalized gold nanoparticles

A fresh BTZ solution was prepared in DMSO at room temperature (0.01 mg· mL^{-1}). The mixture of BTZ and the PEGAuNPs (BTZ+PEGAuNPs) was prepared by adding BTZ to PEGAuNPs solution to obtain the final BTZ concentrations presented in Table 3.1. The samples were prepared in DMEM and RPMI-1640 medium (pH of 7.0-7.4) for pancreatic and prostate cell lines, respectively.

Table 3.1 BTZ concentrations used in prostate and pancreatic cancer cell assays.

Cell line type / C_{BTZ} (nM)	Prostate	Pancreatic
0.001		✓
0.01		✓
0.1		✓
1.0		✓
4.0	✓	
7.76	✓	
10.0		✓
15.5	✓	
46.4	✓	
50.0		✓
77.6	✓	
100.0		✓
124.2	✓	

The main objective was to use the solutions in the range of the BTZ concentrations as previously defined above, with PEGAuNPs concentrations range of 0.1, 0.5 and 1.0 nM.

3.2.3 Preparation of chitosan-gum Arabic complexes

Solutions of the complexes were prepared with two different initial concentrations of Ch, 0.04% 0.06% and 0.3% (w/v), and different GA concentrations according to the weight ratios.

Ch solutions were prepared by dissolving the suitable mass in 1% aqueous acetic acid solution, followed by the pH adjustment to 4.8, with 10% aqueous sodium hydroxide solution. GA was dissolved in ultrapure water. The pH of the GA solutions ranged from 5.0 to 5.6. The complex preparation involved the mixture of aqueous

phases of the two macromolecules, adding 5 mL of the correspondent GA solution to 5 mL of a Ch solution dropwise and under gentle magnetic stirring for 30 min at room temperature. The final pH was 4.8 and the ionic strength was 0.04 M. The charge ratios were calculated assuming 23% of charge residues for GA (glucoronic acids).

3.2.4 Preparation of PEGAuNPs loaded Ch-GA NPs

PEGAuNPs loaded complexes of chitosan-gum Arabic were prepared in the same conditions of Ch-GA NPs. PEGAuNPs were added to the GA under magnetic stirring for 15 min at room temperature, followed by the addition of Ch solution dropwise for more 15 min. The initial concentration of Ch was 0.04% (w/v) and Ch/GA weight ratio of 1:1.2. The final PEGAuNPs concentration in Ch-GA-PEGAuNPs was 2 nM. The pH of Ch-GA-PEGAuNP suspension was 4.7.

3.2.5 Preparation of BTZ loaded Ch-GA NPs

A fresh BTZ solution was prepared in DMSO at room temperature and was added to GA solution, under homogenization for 15 min at room temperature. After, Ch solution was added dropwise and homogenized for more 15 min. The initial concentration of Ch was 0.04% (w/v) and Ch/GA weight ratio was of 1:1.2. The final BTZ concentration was 200 nM. The BTZ loaded Ch-GA (Ch-GA-BTZ) NPs pH was 4.8.

3.2.6 Preparation of Ch-GA NPs loaded with BTZ+PEGAuNPs

The mixture of BTZ and the PEGAuNPs was prepared by adding BTZ to PEGAuNPs solution to obtain the final PEGAuNPs and BTZ concentrations of 2.0 and 200.0 nM, respectively. Briefly, followed the preparation of the fresh BTZ+PEGAuNPs, GA solution was added, drop by drop at room temperature. After 15 min of

continuous magnetic stirring, Ch solution (0.4% w/v) was added. Stirring was continued for 15 min. The Ch-GA NPs loaded with BTZ+PEGAuNPs (Ch-GA-BTZ+PEGAuNPs) pH was 4.6.

3.3 Methods

3.3.1 Dynamic Light Scattering

Dynamic light scattering (DLS) is the most popular experimental method for the characterization of complex liquids like colloidal suspensions, polymer solutions and others [141]. For this technique, it is necessary to know some parameters as the temperature and viscosity of the sample. The temperature value must be constant; if not, convection in the sample will implicate non-arbitrary movements and, consequently, incorrect interpretation of the particles size. One change on the surface of the particles will affect the diffusion speed and, thus, the size of the particles.

DLS determines the size of particles and their size distribution in dispersion. The incident light source from the laser illuminates the sample contained in a cell. This intensity of the scattered light depends on the Brownian motion of the particles, an *arbitrary* movement of the particles as a consequence of the contact with the solvent molecules and their thermal energy causing a Doppler Shift. The intensity of the scattered light that fluctuates with time is detected using a suitable optical arrangement and is correlated with the particle size.

The hydrodynamic diameter of the particles measured is that of a sphere having the equal translational diffusion coefficient as the particle being measured. In this case, it is assumed that the particles are spherical and the hydrodynamic radius value is calculated based on translational diffusion coefficient by using the Stokes-Einstein relation [142]:

$$D_S = \frac{kT}{6\pi\eta R_H} \tag{3.1}$$

where R_H is Laser hydrodynamic radius of the scattering particle; D_S is the translational diffusion coefficient, which depends on the size of the particle, on the surface structure and on the concentration and type of ions in solution; k is the Boltzmann's constant; T is the absolute temperature value and η is the viscosity.

The hydrodynamic diameter of the nanoparticle' suspension was analysed by dynamic light scattering (DLS) using a Zetasizer Nano ZS (Malvern Instruments Ltd., Malvern, UK), keeping the samples at 25ºC. Size measurements were performed at a scattering angle of 173º in a 12 mm square polystyrene cuvette (Sarstedt, Germany).

3.3.2 Zeta Potential

Zeta potential (ζ, ZP) corresponds to a physical property and gives an indication of the stability of the system. The zeta potential of particles is determined by applying an Electrophoresis and measuring the velocity of the particles by Doppler Velocimetry (LDV).

Electrophoresis is an electrokinetic effect and is based on the movement of the particles under an applied electric field to an electrode with opposite charge. Viscous forces on the particles tend to oppose this movement. When equilibrium is reached between these two opposing forces, the particles move with a constant velocity. The velocity depends on the viscosity (η), the zeta potential, the dielectric constant (ε) and it is denominated electrophoretic mobility (μ_E).

Henry's equation[143] relates electrophoretic mobility to zeta potential:

$$\mu_E = \frac{2\varepsilon \cdot \zeta \cdot f(ka)}{3\eta} \tag{3.2}$$

where $f(ka)$ is Henrys function and can be 1.5 or 1.0. It is 1.5 when it is a Smoluchowski approximation for an aqueous solution. For small particles with low dielectric constant and in non-aqueous solutions, the Henrys function is 1.0 and it is the called Huckel approximation.

A particle is considered stable if it has an absolute value of zeta potential of 30 mV or more. The particles will repel each other and there isn't tendency for flocculation [141].

The zeta potential of nanoparticle suspensions and complexes was determined by laser Doppler velocimetry, respectively, using a Zetasizer Nano ZS (Malvern Instrument s Ltd., Malvern, UK), at 25ºC. The zeta potential was obtained by using a disposable capillary cell (DTS 1060, Malvern).

3.3.3 Transmission Electron Microscopy

Transmission electron microscopy (TEM) is useful to interpreting the particle size, structure and geometry of samples [144]. In TEM a beam of electrons is transmitted through the sample, interacting with the specimen as it passes through [145]. The final image is two-dimensional. Negative staining is used to provide sufficient contrast to allow visualization of biological samples such as polymers and DNA. Uranyl acetate crystals is one of the most used negative staining dye. The presence of salt residues of buffers can decrease the contrast of the sample.

TEM images were acquired using a Jeol JEM-1400, JEOL operated at 60 kV. 5 µL of each sample was placed on carbon formvar-coated grid and let to adsorb for 2 min. The staining was performed with 1% (w/v) of filtered aqueous solution of uranyl acetate for 45 seconds. After, the grid was washed twice with deionized (DI) water to remove the excess.

3.3.4 Scanning Electron Microscopy

Scanning electron microscopy (SEM) uses electrons that interact with atoms of the surface sample producing radiation signals and allows to obtain images of high resolution. It is possible to have information about the topography and the composition of the sample.

An electron beam is generated by an electron gun and is focussed by a series of electromagnetic lenses. The scan coils are adjusted to focus the incident electron beam onto the sample; these adjustments cause fluctuations in the voltage, increasing/decreasing the speed in which the electrons come into contact with the surface of the sample. The electrons are released from the surface of the sample, creating a magnetic field that deflects the beam and radiation signals are produced. The signal is collected by detectors, converted into a voltage and amplified. The image corresponds to several points of intensity.

Scanning electron microscopy measurements were performed using a SEM (JEOL JSM-6301F, JEOL Ltd., Tokyo, Japan), to study the morphological properties and to confirm the size of PEGAuNPs.

3.3.5 Laser Scanning Confocal Microscopy

Laser scanning confocal microscopy (LSCM) detects structures obtaining by light from a single focal plane of the sample without light out of focus. The light out of focus, which is not originated from the microscope focal plane, is eliminated via a pinhole that is placed in front of the detector. The light that hits the sample, it excites fluorescence and this radiation is collected by the objective, it passes to the detector. The image corresponds to the intensity of the pixel that is directly proportional to the intensity of the fluorescence light detected.

Imaging experiments were performed with the prostate (Du145) and pancreatic (S2-013 and hTERT-HPNE) cell lines. The cells were grown for 24 h, in a 12-well µ-Chamber (ibidi, Germany) (800cells/well) under normal conditions (5% CO_2 humidified atmosphere at 37ºC). Then the cells were incubated with 0.5 nM of PEGAuNPs, 1 nM of BTZ alone and 1 nM BTZ + 5 nM PEGAuNPs for a period of incubation of 30 min and 48 h. In case of polysaccharides nanosystems the cellular uptake of Ch-GA-BTZ+PEGAuNPs with BTZ concentration of 100 nM was studied using pancreatic cells (S2-013) and immortalized human pancreatic duct epithelial cells (hTERT-HPNE) for

the same period of incubation. Following the incubation, the cells were rinsed with 1% of phosphate buffered saline (PBS) and fixated using 4% paraformaldehyde for 15 min. The cells were washed with PBS and mounted in a glycerol-based non-drying and non-hardening medium. Imaging was performed using a laser scanning confocal microscope TCS SP5 II (Leica Microsystems, Germany). To evaluate the nanoparticle internalization by cells, the control untreated cells were also imaged. Different areas were analysed and at least three images were acquired for each type of cell. Cell imaging showed reproducible results.

3.3.6 Atomic Force Microscopy

Atomic force microscopy (AFM) is a scanning probe microscopy technique used to study the topology of surfaces using force measurement and manipulate properties of chemical and biological surfaces, with little sample preparation, in three dimensions at the nanoscale [146]. AFM has better resolution than optical microscopes and it guarantees the best topographic contrast, not only by direct measurements of the surface but also by quantitative height information [147].

The basic physical principle of this scanning probe method is the interaction between a scanning probe and the sample. This interaction ranges between different kinds of forces and reflects the tip geometry and material [148]. Then, it contributes, by different way, to the measured force between the tip and sample on the basis of the cantilever deflection. The deflection of the cantilever is measured by a laser, which reflected off the back of the cantilever onto a photodetector. The piezoelectric tube moves the sample in the *z* direction for maintaining a constant force, and in *x* and *y* directions for scanning the sample. Hooke's law gives the tip-sample force by:

$$F = -k \cdot x_c \tag{3.3}$$

where F is the force of interaction between the tip and the surface of the sample, x_c is the deflection of the cantilever and k is the spring contact of the cantilever [149].

AFM can operate by two modes. In contact mode, the equipment operates by scanning a static tip across the sample. In this case, the AFM tip is brought close to the sample surface and the scanner makes the final adjustment on the tip. The piezo movements ΔZ are recorded as a function of x and y position. The height image is the final image and shows the sample surface topography.

In tapping mode AFM, also known as intermittent contact, the cantilever oscillates up and down, at a constant drive frequency and drive amplitude; while the tip scans the sample surface by intermittent contact, the amplitude drops. Thus, the tip lightly taps the surface of the sample, while rastering and only touches the sample at the bottom of each oscillation.

AFM imaging was performed in tapping mode (at about 14 kHz, near the resonant frequency of the cantilever) and in liquid (water), using a Veeco Multimode Nanoscope 4A. The cantilevers had a nominal radius of curvature of 20 nm. The samples were diluted (1:60) and a drop (50 µL) was deposited onto freshly mica surface and let to adsorb for at least 30 min, at room temperature. AFM imaging was acquired with unmodified silicon nitride tips (DNP, Veeco Instruments, USA). At least three regions of the surface of the complexes were examined to verify if morphology, shape and structure were similar in the sample. The images were analysed using the JPK Image Processing software.

3.3.7 Absorption Spectroscopy

The concentration of gold nanoparticles was estimated from UV absorbance (A) at around 526 nm according to the Beer-Lambert law:

$$A = \log_{10}(I_0 / I) = \varepsilon.C.L \qquad (3.4)$$

where I_0 is the intensity of the incident light at a given wavelength, I is the transmitted intensity, L is the distance through the sample and C is the concentration of the absorbing specie; ε is a constant known as the molar

absorptivity or extinction coefficient, which is a molecular property in a given solvent at a specific temperature and pressure.

UV-Vis absorption spectra of the samples PEGAuNPs and BTZ+PEGAuNPs were carried out using a 1 cm quartz cuvette, at room temperature by Shimadzu UV-1700 PharmaSpec spectrophotometer.

3.3.8 Fluorescence

The fluorescence intensity corresponds to a process of the emission of light by a molecule which is in an excited state (higher energy state) because it absorbed light energy before [150]. The intensity of fluorescence is dependent on the absorbance, according to Beer-Lambert law eq. 3.4.

When the molecule absorbs the energy light $h\nu_{ex}$, it changes to a higher quantum state of energy – excited state (S_1), and it can fluoresce. After that, the molecule stays instable and returns to the lowest energy state, the ground state (S_0), by emitting a photon with a characteristic energy [150, 151]. The time of excited state of the molecule is denominated excited lifetime. The difference of energy between both is denominated Stokes shift [150].

The fluorescence spectrometer is composed by a light source, which emits a range of different wavelengths of light. For one wavelength value, the light passes through an excitation monochromator and then through the sample cell. Afterward, in absorption and re-emission of the energy, many wavelengths may appear due to electron transitions and Stokes shift. To separate and analyze them, the fluorescent radiation passes through an emission monochromator and it is registered by a detector [152].

BTZ activity was studied with the 20S proteasome assay kit – BML-AK740 (Enzo Life Sciences). A fluorescence standard curve of BTZ was measured for concentrations between 10 nM and 300 nM.

Incubation assays with BTZ and BTZ plus PEGAuNPs were performed at 37ºC, during 50 min. BTZ activity alone and in the presence of PEGAuNPs was monitored as the reaction substrate's fluorescence emission (excitation at 360 nm, emission at 485 nm) using a microplate reader (PowerWave HT Microplate Spectrophotometer, BioTek).

3.3.9 ATR-FTIR

Fourier transform infrared spectroscopy (FTIR) is a technique used to identify chemical compounds and substituent groups by comparison with known spectra of compounds [153]. A compound exposed to infrared light absorbs infrared energy at its characteristic frequencies. During the analysis, the sample's transmittance and reflectance on the infrared region at various frequencies is converted and the result is a FTIR spectrum [154].

The Infrared region of the electromagnetic spectrum is usually divided into three regions: far-IR (400-20 cm^{-1} wavenumber), which has adjacent rotational energy level changes; mid-IR (400-1400 cm^{-1}), which has correlated to fundamental vibrational level changes, and near-IR (14000 – 4000 cm^{-1}), which causes vibrational and rotational level changes [155].

The transmittance (T) is:

$$T = \frac{I}{I_o} = \exp\left[-\alpha \times b\right] \tag{3.5}$$

where I is the intensity of the transmitted radiation by the sample, I_0 is intensity of the incident radiation [156].

The equipment used has a beam source that contains different frequencies of light at once and it measures how much of that beam is absorbed by the sample. The light shines according to configuration of mirrors denominated Michelson interferometer, which allows some wavelengths to pass through and blocks others. The light from the polychromatic infrared source is accumulated and directed to a

beam splitter. The best way is the light reflected from the two mirrors back to the beam splitter and 50% of the original light passes into the sample. After that, the light is refocused to the detector. Then, the measured signal (information about the characteristics frequencies and intensities of the spectrum) is digitized and sent to the computer where the Fourier transformation takes place. The raw data is a set of intensities measured for discrete values of retardation, being interpreted and manipulated according to algorithm Fourier Transform [157].

The BTZ+PEGAuNPs, PEGAuNPs and BTZ solutions were analysed by Attenuated total reflectance-Fourier transform infrared spectroscopy (ATR-FTIR). The samples were dried in a drying oven (Scientific, model BTC-9090) for 24 h. The dried samples were added to KBr and ATR-FTIR spectra were recorded with an ALPHA FTIR Spectrometer (Bruker) in the spectral range 4000-400 cm^{-1}, resolution of 4 cm^{-1} and 64 scans, at room temperature.

3.3.10 Turbidity measurements

Coacervation process between arabic gum and chitosan results in the formation of a complex that can be analysed by turbidimetric measurements [158].

The turbidity of the samples was measured with a Shimadzu UV-1700 spectrophotometer at a wavelength of 500 nm as a function of time at 25 ºC using 1 cm path length cuvette. The turbidity (T) was defined as:

$$T = -\ln\left(I / I_0 \right) \tag{3.6}$$

with I the light intensity that passes through a volume of solution in 1 cm^3 and I_0 the incident light intensity.

3.3.11 *In vitro* release studies

Drug release studies of the BTZ from the systems BTZ+PEGAuNPs, Ch-GA-BTZ NPs and Ch-GA-BTZ+PEGAuNPs were carried out at 37ºC by dialysis using a regenerated cellulose membrane (molecular weight cut off, MWCO: 8–10 KD, purchased from Spectrum Labs Europe BV, Netherlands). The initial PEGAuNPs and BTZ concentration were 5 nM and 210 μM, respectively. In case of the Ch-GA-BTZ NPs, Ch-GA-BTZ+PEGAuNPs, the BTZ concentration used was 200 μM. The solutions were incubated in 6 ml of DI water and in PBS 0.01 M, with constant magnetic stirring.

The BTZ concentration of the dialysate buffer was analysed with time using spectrophotometric analysis at 270 nm (Shimadzu UV-1700 PharmaSpec spectrophotometer). The concentration of BTZ that was released was calculated from the standard calibration curves of BTZ solution in DI water and in PBS 0.01 M.

3.3.12 *In vitro* cell assays

Du145 cell line, derived from solid tumour tissue (human prostate carcinoma) was grown using a standard RPMI, supplemented with 10% (v/v) fetal bovine serum, 1% L-glutamine, and 1% penicillin and streptomycin. The cell cultures were maintained at 37ºC in 95% humidified atmosphere and 5% CO_2.

Human pancreatic cancer cell line (S2-013) and immortalized human pancreatic duct epithelial cells (hTERT-HPNEs) were provided by Professor M. A. Hollingsworth (UNNC - Omaha, USA). The cells were maintained in DMEM medium, supplemented with 10% FBS under 5% CO_2 humidified atmosphere at 37 ºC.

All the procedures must be made under sterile conditions to avoid contaminations. Viable cells were counted using an automated Coulter counter (Vi-Cell XR, Beckman-Coulter Inc., Miami, FL, USA).

Radiotherapy principle of cancer

The use of X-rays is an innovation in cancer therapy that allows destruction/killing of cancer cells. This treatment can be used alone or associated with other anticancer treatment protocols as chemotherapy, surgery [159]. Radiation therapy works in a certain part of the body – local treatment. This can stop or control cancer cells from growing and spreading [160]. The SI unit of absorbed dose is the gray (Gy) and it is the amount of radiation required to deposit one joule of energy in one kilogram of any kind of matter [161].

When a high radiation kills cells by damaging DNA, their ability to grow is blocked. This is the basic principle of radiation therapy.

In vitro cytotoxicity study

The evaluation of the cytotoxicity of BTZ, PEGAuNPs, BTZ+PEGAuNPs was performed in prostate cancer cell line, Du145 by a colorimetric cell proliferation assay based on measuring the retention of methylene blue (MB) in ethanol-fixed cells; and in pancreatic cell lines, S2-013 and hTERT-HPNE by PrestoBlue (PB) and Sulforhodamine B (SRB) assays. Ch-GA-BTZ NPs and Ch-GA-BTZ+PEGAuNPs cytotoxicity study was evaluated against pancreatic cell lines by PB and SRB assays.

MB assay

The cell viability of Du145 cells incubated with the particles was determined by the colorimetric cell proliferation assay.

Cells were seeded in 96 well plates at a density of 6000 cell/well for 24 h. Samples – BTZ alone, PEGAuNPs and BTZ+PEGAuNPs, at different concentrations were added to the cells and incubated, at 37 ºC during 24 h at the BTZ concentrations ranging between 4.0 and 124.2 nM. After this period, the solution of each well was removed and fresh medium was added and the incubation proceeded for 24 h more.

For experiments using ionizing radiation the cells were irradiated with 160 kV X-rays. The 96-well plates with the cultured cells were placed inside a CP160 X-ray

cabinet (Faxitron Bioptics, Tucson, AZ). Low energy radiation in 50–250 kV range has been shown to yield significant radiosensitization with AuNPs in brachytherapy [162-166]. The dose rate was 1 Gy/min for 5 min and followed the incubation for 24 h more.

Cell viability was determined by the cellular protein assay (MB assay) [167]. The MB assay was found by Dent *et al.* to be a sensitive method for determining the response of cultured cells to growth factors with low variability [168]. The cells were washed twice with phosphate saline buffer and fixed with 90% ethanol for 5 min. After that, 30 μL of filtered MB working solution (Sigma-Aldrich Co.) was added to each well and incubated for 15 min at room temperature. The plates were washed with cool tap water; then, 200 μL of 0.1% HCl was added and left for 30 min. Absorbance was measured at 675 nm using a microplate reader (PowerWave HT Microplate Spectrophotometer, BioTek).

PB and SRB assays

The effects of the nanoparticles and drug on the cell growth in the tested pancreatic cell lines were evaluated by two different assays based on PB (fluorescence) and SRB (colorimetric). Both assays allow an indirect estimation of cell number: the PB assay by the metabolization of resazurin to resofurin, and the SRB assay by staining cellular proteins with the dye SRB [169, 170].

The S2-013 and hTERT-HPNE cells were seeded in 96-well plates (1000 cells per well) under normal conditions (5% CO_2 humidified atmosphere at 37ºC) and allowed to adhere for 24 h. The cells were then treated for 48 h with:

- BTZ, PEGAuNPs and BTZ+PEGAuNPs at the concentrations ranging between 0.001 and 100 nM BTZ;
- Ch-GA-BTZ NPs and Ch-GA-BTZ+PEGAuNPs at the concentrations ranging between 0.01 and 100 nM BTZ;
- Ch-GA NPs and Ch-GA-PEGAuNPs at the concentrations ranging between $1.1x10^{-7}$ to $3.3x10^{-3}$ mg/mL.

Following this incubation period 50 µL of PB reagent (diluted 1:10 in the DMEM medium) were added to each well and incubated for 45 min at 37ºC. The PB reagent is modified by the reducing environment of the viable cells turning into red colour and becoming fluorescent. The fluorescence was measured using a microplate reader (PowerWave HT Microplate Spectrophotometer, BioTek) at an excitation and emission wavelengths of 560 and 590 nm, respectively.

For the SRB assay, the cells were fixated with 10% TCA for 1 h on ice. After the incubation period the cell monolayers were washed and stained with 50 µL SRB dye for 30 min. The cells were then washed repeatedly with 1% acetic acid to remove unbound dye. The cells were dried and the protein-bound stain was solubilized with 10 mM Tris solution.

The SRB absorbance at 560 nm was measured using the PowerWave microplate reader [170]. Concentration for 50% growth inhibition (GI_{50}) was evaluated from the SRB assay. The absorbance of the wells containing the nanoparticles or drug and the absorbance of the wells containing untreated cells following a 48 h incubation period were subsequently compared with that of the wells containing the cells that have been fixated at time zero (when the nanoparticles and drug were added) [171] .

Statistical analysis for *in vitro* assays

For each assay, three independent experiments were measured in triplicate. Statistical significance ($p < 0.05$) was determined by the Student's t-Test.

Chapter 4

This chapter is based on the following publications:

Coelho SC, Rocha S, Juzenas P, Sampaio P, Almeida GM, Silva FS, et al. (2013) Gold nanoparticle delivery-enhanced proteasome inhibitor effect in adenocarcinoma cells. Expert Opin Drug Deliv 10 (10): 1345-52. doi:10.1517/17425247.2013.827659.

Coelho SC, Rocha S, Carmo Pereira M, Juzenas P, Coelho MAN Enhancing proteasome inhibitor effect by functionalized gold nanoparticles. J. Biomed. Nanotech. 2013, 9 (*in press)*.

4 BTZ loaded PEGAuNPs

Contents

4.1 Introduction

This study was conducted to evaluate the efficacy to delivery bortezomib by gold nanoparticles into pancreatic and prostate cancer cells.

Bortezomib (BTZ), also known as Velcade or PS-341, is a boronic dipeptide, which inhibits the function of the 26S proteasome, and is nowadays being studied for a wide diversity of cancer types [172, 173]. Proteasome inhibitors and their associated mechanism of action in protein degradation and recirculation foresee large-scale

effects in the organism. Thus, drugs controlling proteasome activity are ideally suited for unidirectional manipulation of cellular pathways such as apoptosis.

BTZ chemical structure is illustrated in Figure 4.1.

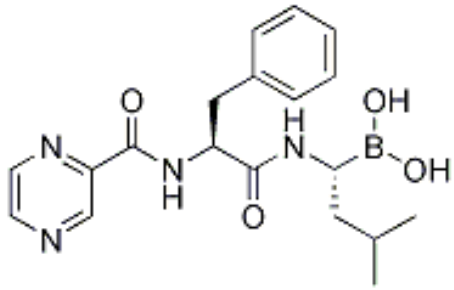

Figure 4.1 Chemical structure of BTZ.

BTZ blocks the activation of the transcription nuclear factor κB (NF-κB); induces apoptosis in prostate cancer cells - LNCaP, LAPC4, PC-3 and Du145 [173-176].

Limitations associated to anticancer drugs such as low bioavailability, little stability, poor specificity and development of resistance may be overcome by the use of nanoparticles (NPs), which offer the advantage of maximizing the retention of the drug in cancer cells and of minimizing its uptake in normal surrounding tissues [10, 78, 177]. Radiotherapy, which also causes toxicity by affecting healthy tissues, can benefit from this approach by selective absorption of radiation by NPs [10, 19, 78].

Nanoparticle based systems show the capacity to cross biological barriers and be internalized in different cell cycle phases[37]. Gold nanoparticles (AuNPs) have been studied as vectors for cancer therapy and diagnostics [14, 24, 37, 87 109 178, 179]. Several studies demonstrated that small sized AuNPs appear to be biocompatible, have low toxicity to human cells and show physical and chemical stability [14, 109, 180, 181]. They are able to improve the delivery and efficacy of anticancer drugs [20, 106, 182]. The AuNPs high reactive surface areas allow surface functionalization and immobilization of biomolecules [106, 109]. Their strong affinity for hydrophilic molecules like polyethylene

glycol (PEG) modified with thiol groups has been reported [106, 183, 184]. Pegylation of AuNPs (PEGAuNPs) increase their stability, and inhibits protein adsorption to their surface, which consequently prevents particle agglomeration [36, 185, 186]. This fact is explained by the steric repulsion effect induced by the attached PEG molecules. There is also evidence showing that the conformation of PEG chains around the nanoparticles is responsible for an efficient cell uptake and for prolonging the circulation lifetime in the blood, since PEG confers flexibility to the AuNPs [36, 187]. The bioconjugation with different molecules allows the formation of stable colloidal suspensions for targeted drug delivery applications [90 188 106]. These properties make functionalized AuNPs a promising system to deliver anticancer drugs in chemotherapy and to overcome the problem of multi-drug resistance (MDR) [14, 90].

Several *in vitro* studies have revealed that AuNPs can be used as delivery vehicles of anticancer drugs against pancreatic cancer cells, demonstrating inhibition of tumour cell proliferation [24, 90, 189]. The nanoparticle cell internalization mechanisms, which might contribute to increase the drug effect, are still not understood.

Recently, AuNPs have been proposed as potential candidates to assist radiotherapy by enhancing its efficiency [19, 78]. Because it is expected that the nanoparticles will absorb high-energy photons, they would act as radiation sensitizers (radiosensitizers) minimizing the total radiation dose necessary to eradicate the tumour [10, 19, 78].

The aim of this work is to provide insights into the mechanisms of activity enhancement of bortezomib (BTZ) by PEGAuNPs. The effect of PEGAuNPs combined with BTZ or ionizing radiation was studied on prostate cancer cells. Also, the potential application of PEGAuNPs as a delivery vehicle of BTZ was studied using human pancreatic cancer cell line S2-013 and immortalized human pancreatic duct epithelial cells (hTERT-HPNE). Laser scanning confocal microscopy (LSCM) imaging was performed to follow the nanoparticle uptake by pancreatic and prostate cells.

Our study demonstrates the synergistic effect between PEGAuNPs and BTZ and can be extended to other cancer cell lines and drugs as a preliminary approach for new therapies.

4.2 Results

4.2.1 Physical characterization

4.2.1.1 Particle size distribution, surface charge and morphology of BTZ loaded PEGAuNPs

The size distribution and zeta potential of the BTZ loaded PEGAuNPs was determined by Dynamic light scattering (DLS) and Laser Doppler velocimetry (LDV), respectively. Negatively charged AuNPs were prepared through the reduction of gold salt by trisodium citrate, and were functionalized with α-thiol-ω-carboxyl (polyethylene glycol) (PEG).

Their zeta potential was -47±4 mV and notably it changed to -13.6±0.5 mV after addition of 124.2 nM of BTZ, suggesting adsorption of the drug to the pegylated particles (Table 4.1). Schematic illustration of BTZ+PEGAuNPs is shown in Figure 4.2.

Table 4.1 Hydrodynamic diameter, polydispersity index (PdI) and zeta potential of gold nanoparticles.

	H_2O		
Parameters[1] / Sample	D (nm)	PdI	ZP (mV)
AuNPs 14.4 nM (stock)	22 ± 0.4	0.6	-40 ± 1
PEGAuNPs 12.2 nM (stock)	22 ± 0.3	0.6	-47 ± 4
124.2 nM BTZ+ 12.2 nM PEGAuNPs	24 ± 0.3	0.6	-13.6 ± 0.5

[1]D, diameter; ZP, zeta potential

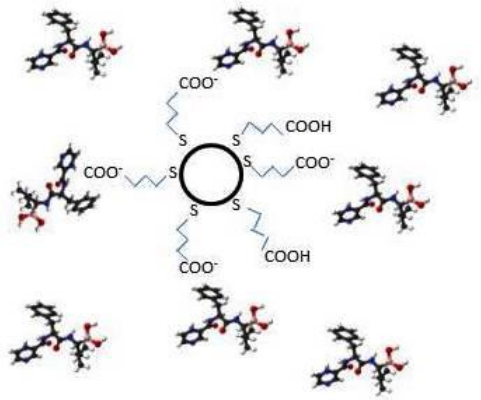

Figure 4.2 Schematic illustration of BTZ+PEGAuNPs.

The pegylation of AuNPs does not significantly change the size of the nanoparticles. The average hydrodynamic diameter of PEGAuNPs was 20 nm and the polydispersity index (PdI) was 0.6 (Table 4.1 and Figure 4.3).

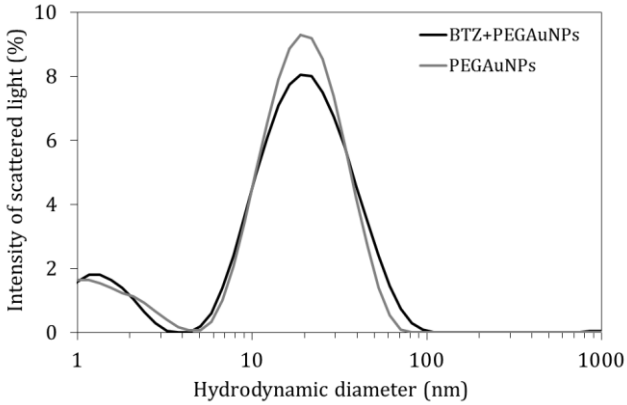

Figure 4.3 Characteristics of AuNPs: A) Size distribution chart of PEGAuNPs and BTZ+PEGAuNPs.

TEM and SEM analysis (Figure 4.4) showed nanoparticles in suspension with spherical shape and size of 20 nm that is in agreement with DLS measurements.

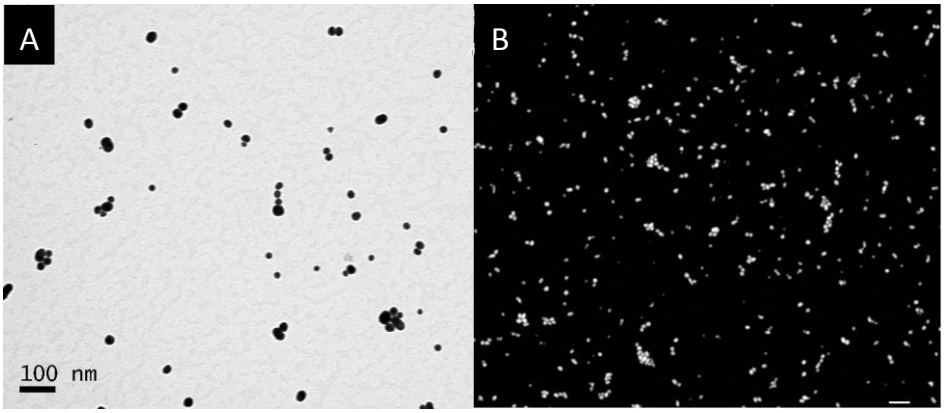

Figure 4.4 A) TEM image of PEGAuNPs; B) SEM micrographs of PEGAuNPs. The scale bar of TEM and SEM images is 100 nm.

The particles show, in aqueous dispersion, a typical and distinctive surface plasmon resonance band centered at 526 nm (Figure 4.5). The concentration of PEGAuNPs was 12.2 nM, estimated by the Lambert-Beer Law. The addition of nanomolar concentrations of BTZ did not change the absorption λ_{max} value of

PEGAuNPs and the BTZ absorption characteristic band was observed at 270 nm. The peak around 526 nm disappears for the nanoparticles suspended in RPMI medium due to the significant RPMI plasmon resonance band centered at 558 nm. From these results, we can conclude that the PEGAuNPs do not form aggregates in RPMI suspensions.

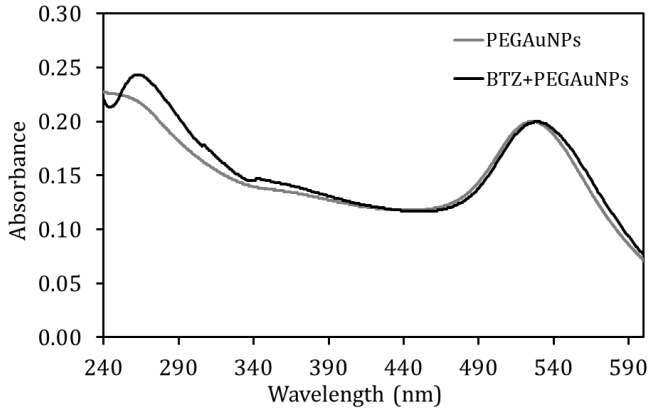

Figure 4.5 Absorption spectra of BTZ+PEGAuNPs and PEGAuNPs.

4.2.1.2Nanoparticle Stability

The particle stability, with and without BTZ, in the presence of salt/serum medium (RPMI-1640 medium + FBS) was evaluated by hydrodynamic diameter and zeta potential measurements. In the presence of RPMI medium, significant changes in the zeta potential values were observed, which could be justified by the presence of the amino-acids and ions that are responsible for the screening of charges. The addition of BTZ to the PEGAuNPs suspended in the RPMI-1640 medium does not show any effect in zeta potential value, contrarily to the results reported in DI water (Table 4.1 and Table 4.2).

Table 4.2 Hydrodynamic diameter, polydispersity index (PdI) and zeta potential of gold nanoparticles suspended in DI water and RPMI/FBS medium.

	H_2O			RPMI medium		
Parameters[1] / Sample	D (nm)	PdI	ZP (mV)	D (nm)	PdI	ZP (mV)
PEGAuNPs 1.6 nM	22 ± 1	0.6	-47 ± 1	40 ± 1	0.5	-8 ± 0.5
PEGAuNPs 0.1 nM	25 ± 1	0.4	-33 ± 2	41 ± 1	0.5	-8 ± 0.3
4.0 nM BTZ + PEGAuNPs[2]	27 ± 2	0.6	-16 ± 5	35 ± 1	0.5	-8 ± 1
40.0 nM BTZ + PEGAuNPs[2]	27 ± 0.3	0.6	-22 ± 1	34 ± 3	0.5	-8 ± 1
400.0 nM BTZ + PEGAuNPs[2]	28 ± 0.4	0.2	-13 ± 2	36 ± 0.4	0.5	-7 ± 1

[1] D, diameter; ZP, zeta potential

[2] PEGAuNPs concentration of 0.1nM

Based on the results presented in Table 4.1 and Table 4.2, the mean size of the nanoparticle suspended in the RPMI-1640 medium increases 27% relatively to the PEGAuNPs suspended in DI water. This means that PEGAuNPs tend to form larger complexes in the RPMI-1640 medium due to most likely the fetal bovine serum protein adsorption into the nanoparticle surface contributing to steric forces between AuNPs. The spherical PEGAuNPs were stable and well dispersed for several months when stored at 4ºC in the dark (denoted by the absence of color change, aggregation, size and zeta potential).

4.2.2 BTZ interactions with PEGAuNPs

4.2.2.1 ATR-FTIR analysis

Two different samples were analysed by ATR-FTIR spectroscopy: mixture of BTZ in powder plus dried PEGAuNPs (1) and the suspension of BTZ mixed with PEGAuNPs (BTZ+PEGAuNPs) that was dried (2). The spectra of the sample 2 showed a band at

1528 cm^{-1} (N-H bend), which is not observed for the sample prepared by simply mixing the dried components (Figure 4.6). Since BTZ has a small extent of dissociation (pKa is 13.82), it acts as a base and there will be an electrostatic attraction between the negatively charged PEGAuNPs surface and BTZ, which is confirmed by the decrease of the zeta potential values.

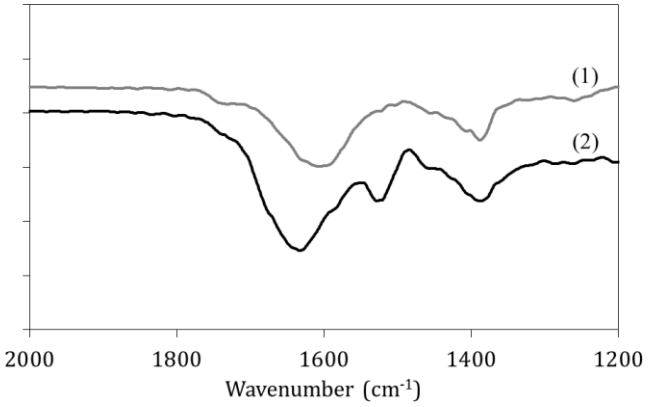

Figure 4.6 FTIR spectra of (1) mixture of BTZ in powder plus dried PEGAuNPs (2) BTZ+PEGAuNPs after drying. The spectra were shifted for a better visualization.

4.2.2.2 Assay of 20S Proteasome Activity

The behaviour and interactions of BTZ with gold nanoparticles were studied by 20S proteasome assay. In fact, to confirm the possibility of an enhancement of BTZ effect in the presence of PEGAuNPs, proteasome activity was measured in an aqueous model system.

For BTZ concentrations up to 10 nM and constant PEGAuNPs concentration of 0.1 nM, it is not possible to observe any activity because this concentration is below the detection limit of the method. According to the results presented in Figure 4.7, for BTZ concentrations of 20-50 nM, the fluorescence curves of BTZ alone and BTZ plus 0.1 nM PEGAuNPs are similar without any significant changes in the BTZ activity.

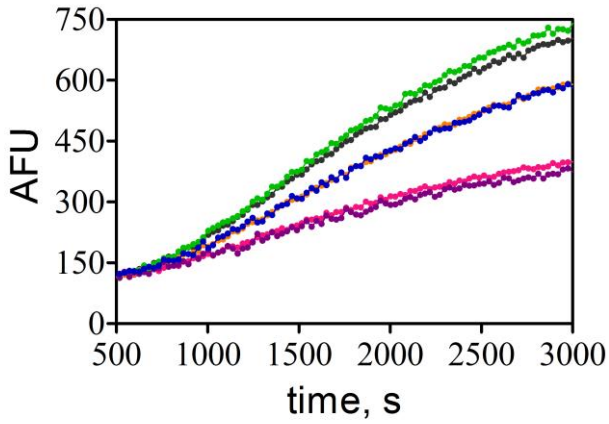

Figure 4.7 Kinetics of BTZ inactivation of 20S proteasome chymotrypsin-like activity. Arbitrary fluorescence units (AFU) versus time. Control (—●—), PEGAuNPs 0.1 nM (—●—), BTZ 20 nM (—●—), BTZ 20 nM plus PEGAuNPs 0.1 nM (—●—), BTZ 50 nM (—●—), BTZ 50 nM plus PEGAuNPs 0.1 nM (—●—).

4.2.3 *In vitro* release studies

The *in vitro* release experiment of BTZ+PEGAuNPs and BTZ alone were investigated using dialysis membranes (MWCO 8-10 kD) in DI water and in PBS 0.01 M at 37 ºC. The BTZ and PEGAUNPs concentrations were 210 µM and 5 nM, respectively.

The results of BTZ dialysis are depicted in Figure 4.8.

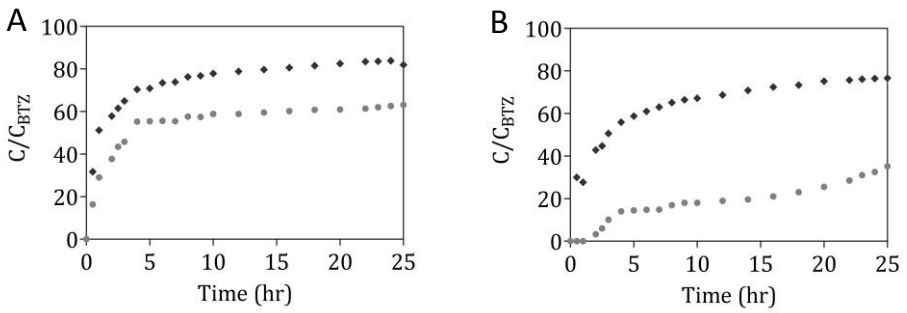

Figure 4.8 BTZ release profiles (◆) and BTZ+PEGAuNPs (●) versus time: A) in DI water; B) in PBS (0.01 M).

The release profiles showed that the BTZ release in PBS is much slower than in DI water (Figure 4.8). The BTZ release from the PEGAuNPs is pH dependent as it can be seen from the profiles in ultrapure water (pH 5.8) and in PBS 0.01 M (pH 7.0).

It was observed that in DI water, the BTZ release is slower with PEGAuNPs although after 4 h 55% of all the BTZ (C_{max}) was released (Figure 4.8A). The behavior of BTZ released in PBS is very different as depicted by the concentration profiles of Figure 4.8B. In PBS, a delay in the BTZ release is observed in the first two hours, in comparison with BTZ alone, due to the presence of PEGAuNPs. The amount of BTZ released after 4 h was 56% and 15% for BTZ alone and in combination with PEGAuNPs, respectively. Also, after 30 h, 77% of the BTZ alone was detected in the outer solution of the dialysis membrane, whereas only 36% was released from the PEGAuNPs. The presence of PBS has an effect on BTZ release from the PEGAuNPs suggesting a stronger adsorption of the drug to the surface of PEGAuNPs. These results corroborate the zeta potential measurements, indicating that PBS has an effect on BTZ adsorption to the surface of PEGAuNPs, slowing down significantly the release process. These findings are particularly important to explain the BTZ+PEGAuNPs behaviour in cellular medium and the BTZ activity.

4.2.4 Cellular imaging studies

The cellular uptake and intracellular distribution of the PEGAuNPs in prostate cancer cells (Du145), pancreatic cancer cells (S2-013) and immortalized human pancreatic duct epithelial cells (hTERT-HPNE) were assessed by Laser scanning confocal microscopy (LSCM) imaging technique (Figure 4.9 and Figure 4.10). An increase in the reflectance signal is observed in cells treated with PEGAuNPs compared to the untreated cells (control), which is attributed to the cellular uptake of PEGAuNPs [101].

LSCM images of the Du145 cancer cells with the internalized PEGAuNPs are presented in Figure 4.9.

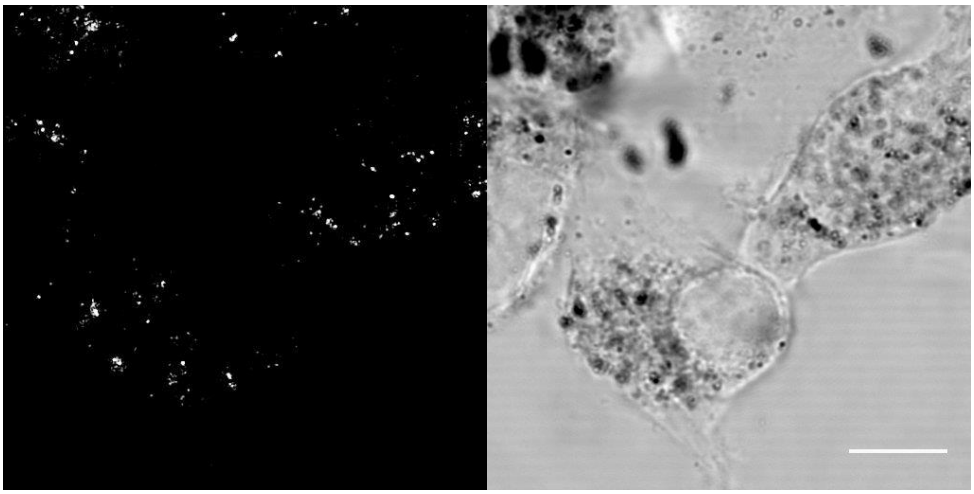

Figure 4.9 Confocal reflectance images of Du145 cells at 48 h of incubation. The cells were incubated with 0.5nM PEGAuNPs. Scale bar in all images is 10 µm.

On the contrary to other studies reporting the difficulty of cellular uptake of AuNPs after pegylation [182, 190], our observations show that PEGAuNPs are internalized by DU145, S2-013 and hTERT-HPNE cells. The PEGAuNPs are localized in the cytoplasm with higher concentration in the perinuclear region. The internalization of the nanoparticles by the pancreatic cells was detected after 30 min of incubation at

37ºC. Up to 48 h a well-defined accumulation of the PEGAuNPs is observed in endocytic vesicles at the perinuclear regions (Figure 4.10).

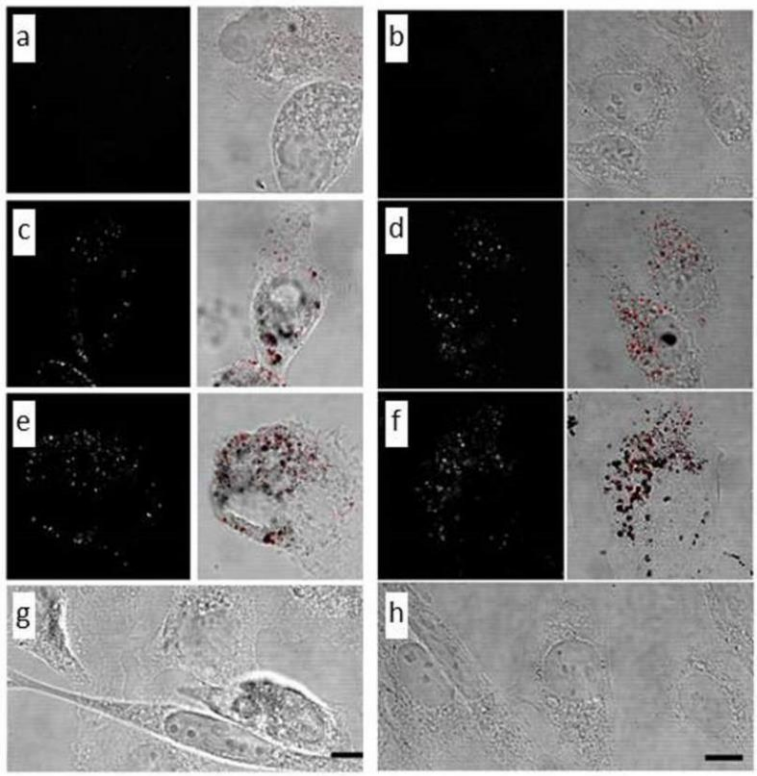

Figure 4.10 Confocal reflectance images of the S2-013 (a, c, e, g) and hTERT-HPNE (b, d, f, h) cells after 48 h incubation. (a and b) The cells were incubated with 1nM BTZ alone; (c and d) the cells were incubated with 0.5nM PEGAuNPs; (e and f) the cells were incubated with 1nM BTZ+ 0.5 nM PEGAuNPs; (g and h) the control untreated cells. Scale bar in all images is 10 µM.

Figure 4.11 corresponds to a 3D projection showing the PEGAuNPs distribution in the pancreatic cancer cell cytoplasm.

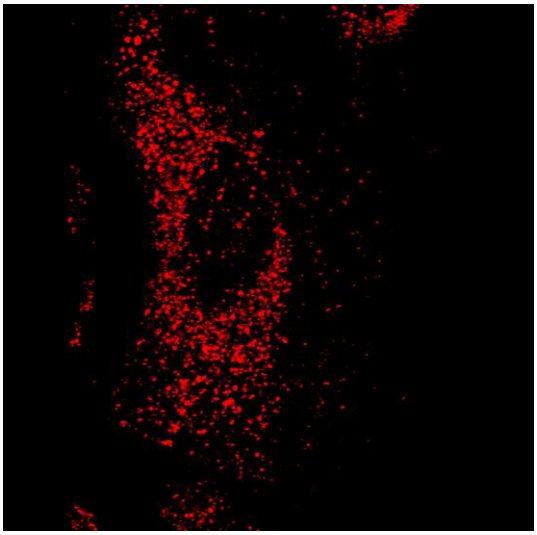

Figure 4.11 PEGAuNPs distribution in the cell cytoplasm.

The PEGAuNPs form dynamic clusters where the nanoparticles move fast, which could be explained by Coulomb forces and osmotic repulsion as a consequence of their confinement in the endocytic vesicles (Figure 4.12).

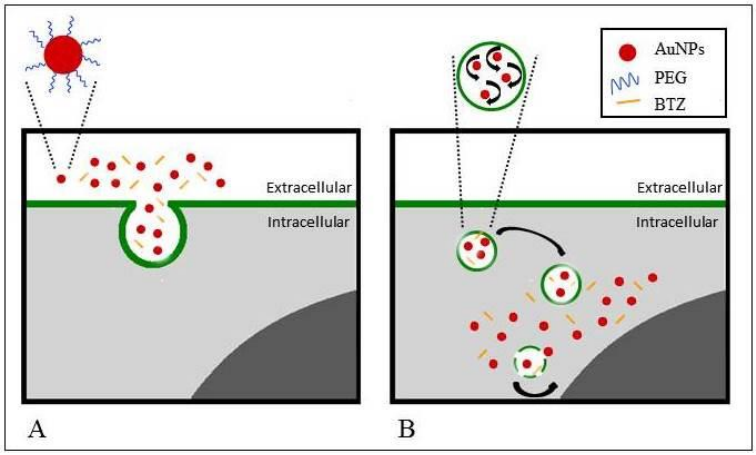

Figure 4.12 Schematic illustration of the gold nanoparticle uptake into the pancreatic cells: A) The PEGAuNPs and BTZ are internalized by endocytosis; B) The BTZ+PEGAuNPs confine in the vesicles and induce diffusion processes in the cytoplasm. Inside of the vesicles the nanoparticles move due to electrostatic repulsion and steric forces. Accumulation of the nanoparticles in the perinuclear region is observed due to disruption of some vesicles. Figure not to scale.

4.2.5 Cytotoxic studies

Following the observation of the PEGAuNPs cellular uptake, *in vitro* cytotoxicity studies were performed with BTZ and the PEGAuNPs. BTZ alone, PEGAuNPs and BTZ+PEGAuNPs were incubated with Du145, S2-013 and hTERT-HPNEs cells, at 37ºC, for 48 h and their effect was assessed by MB, PB and SRB methods.

4.2.5.1 Prostate cancer cell line, Du 145

As presented in Figure 4.13, PEGAuNPs up to 0.1 nM did not show any significant toxicity to the cells, which is corroborated by other findings [182, 191]

The effect of X-rays radiation (5 Gy) on prostate cell line in the presence of PEGAuNPs at different concentrations was analyzed (Figure 4.13). Irradiation with X-rays leads to a 20% decrease in the cell viability, regardless of whether the cells are

incubated or not with the colloidal solution (concentration range: 0.05–1.00 nM). Statistical analysis confirmed that the radiation and the non-radiation results are different (t test; p-value 0.0002) with means of 70% and 90%, respectively.

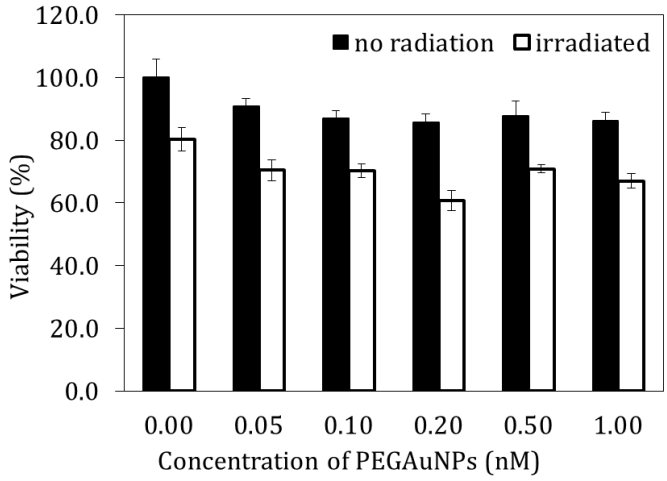

Figure 4.13 Viability of Du145 cells exposed to PEGAuNPs without BTZ and X-rays radiation (5 Gy).

The inhibitory effect of BTZ on the proliferation of Du145 cells was evaluated in the presence of PEGAuNPs at concentrations from 0.1 to 1.0 nM. All the results with BTZ combined with PEGAuNPs were obtained with a PEGAuNPs concentration of 0.1 nM. This concentration was selected because it was the lowest PEGAuNPs concentration that enhanced the BTZ effect. Some experiments were performed with higher concentrations of PEGAuNPs but the results were similar and did not show significant improvements in the BTZ activity.

A significant decrease in the cell viability occurred in the presence of 0.1 nM PEGAuNPs plus BTZ at concentrations from 4 to 124 nM (Figure 4.14).

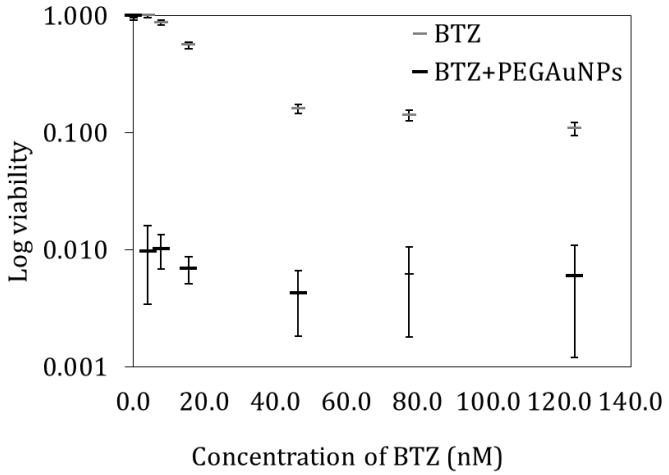

Figure 4.14 Viability of Du145 cells exposed to BTZ and BTZ+PEGAuNPs. PEGAuNPs concentration was 0.1 nM.

The mixture significantly decreased the cell viability to 1% already for 4 nM BTZ, whereas the drug alone at this concentration had no effect (Figure 4.14). A concentration of BTZ alone of 124 nM reduced the cell viability to about 11%. Such synergistic behavior can be explained by the formation of AuNPs clusters inside the cells and in intracellular vesicles [36, 101, 182]. The cells internalize AuNPs by the endocytosis process responsible for the high increase of BTZ concentration inside the Du145 cells when compared with the BTZ alone [182, 192, 193].

4.2.5.2 Pancreatic cell lines, S2-013 and hTERT-HPNE

Figure 4.15 showed that the PEGAuNPs at the concentrations up to 1.0 nM do not show any cytotoxicity on both pancreatic cell lines, sustaining by the cell integrity.

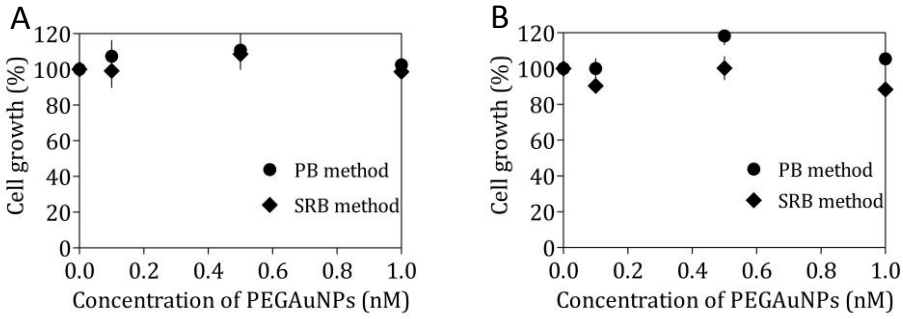

Figure 4.15 Effect of PEGAuNPs on the cell growth of S2-013 (A) and hTERT-HPNE (B) cells.

In the presence of BTZ combined with 1.0 nM of PEGAuNPs, the growth rate of the S2-013 cells decreased significantly when compared with BTZ alone (Figure 4.16).

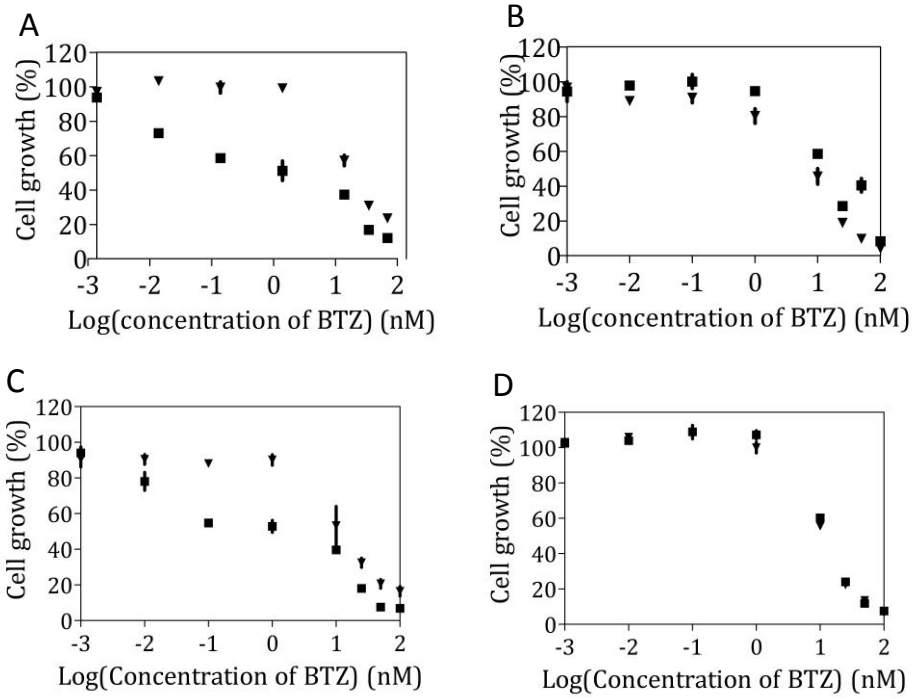

Figure 4.16 Effect of the BTZ+PEGAuNPs 1.0 nM (■) and BTZ alone (▼) on the cell growth of S2-013 (A, C) and hTERT-HPNE (B, D) cells. (A, B) SRB assay and (C, D) PB assay.

Analysing the effect of BTZ at the concentrations in the range 0.1 - 1.0 nM, a significant difference in the cell growth is evident, 90-100% for BTZ alone and about 50% for BTZ+PEGAuNPs (Figure 4.16A and Figure 4.16C). At this concentration range the drug toxicity on the hTERT-HPNE cells is not observed with the growth rate being 97-100% (Figure 4.16B and Figure 4.16D). Our interpretation of these results is that apparently the S2-013 cell uptake kinetics is dependent on the PEGAuNP concentration in contrast to the hTERT-HPNE cell response, which is almost independent on the nanoparticle concentration (Figure 4.17).

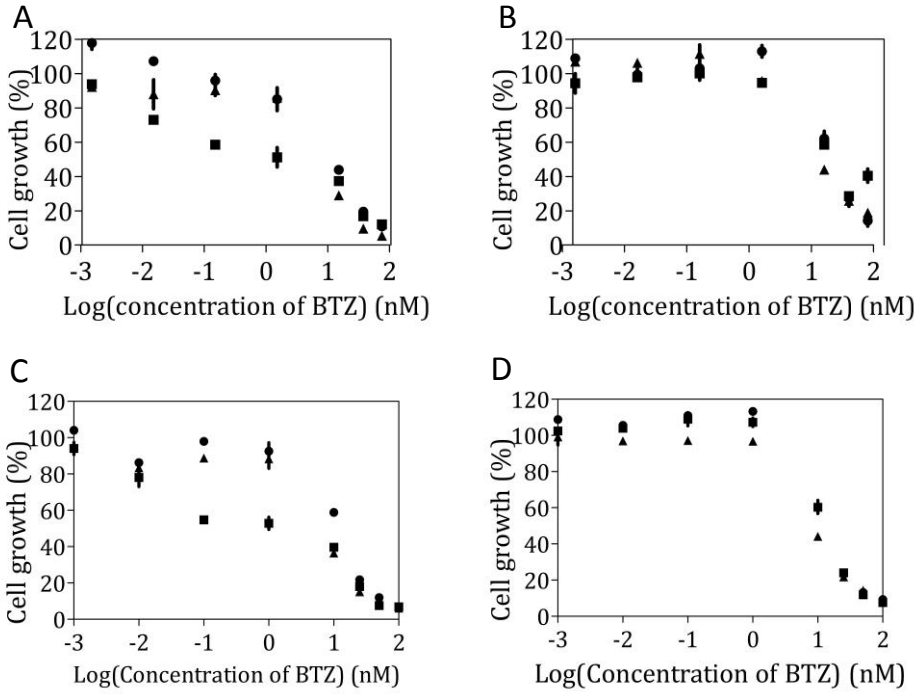

Figure 4.17 Effect of the BTZ+PEGAuNPs 1.0 nM (■), BTZ+PEGAuNPs 0.5 nM (●) and BTZ+PEGAuNPs 0.1 nM (▲) on the cell growth of the S2-013 (A, C) and hTERT-HPNE (B, D) cells. (A, B) SRB assay and (C, D) PB assay.

The analysis of the balance between cell proliferation and cell death showed an increase of the inhibitory growth effect with BTZ concentration (Table 4.3 and Figure 4.18).

Table 4.3 Effect of BTZ and mixture of BTZ and PEGAuNPs on the growth inhibition of the pancreatic cell lines.

	GI_{50} (nM)	
Sample	**S2-013**	**hTERT-HPNE**
BTZ	0.85 ± 0.17	2.57 ± 1.81
BTZ+PEGAuNPs 1.0 nM	0.24 ± 0.03	6.42 ± 0.84

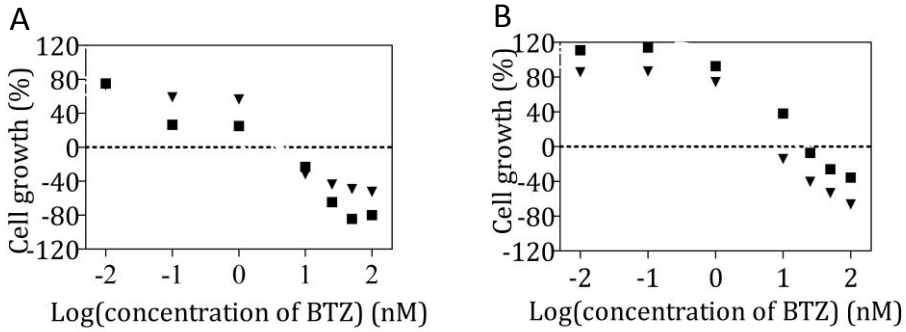

Figure 4.18 Effect of the BTZ+PEGAuNPs 1.0 nM (■) and BTZ alone (▼) on the cell growth of the S2-013 (A) and hTERT-HPNE (B) cells compared to the control, by the SRB assay.

The GI_{50} concentration, obtained by the SRB assay, is significantly ($p < 0.05$) lower for the BTZ+PEGAuNPs 1.0 nM when compared to BTZ alone in the S2-013 cells (0.24 and 0.85 nM, respectively). Also, the efficacy of the BTZ+PEGAuNPs on inducing cell death is more pronounced than that of BTZ alone for drug concentrations above 1.0 nM. For the hTERT-HPNE cells the GI_{50} concentration is significantly ($p < 0.05$) higher for the BTZ+PEGAuNPs 1.0 nM than that for BTZ alone (6.4 and 2.6 nM, respectively).

Moreover, the influence of the nanoparticle concentration on BTZ activity on S2-013 and hTERT-HPNE cells was analyzed. Our data show that BTZ+PEGAuNPs 1.0 nM decrease significantly the S2-013 cell growth rate in comparison with 0.1 and 0.5 nM PEGAuNPs (Figure 4.17A and Figure 4.17C). This effect is not observed in hTERT-HPNE cells (Figure 4.17B and Figure 4.17D). Such difference can be explained by the different nanoparticle uptake kinetics by the two pancreatic cell lines. The potential enhancement of BTZ activity in the presence of PEGAuNPs was also evaluated by measuring the kinetics of the inactivation of chymotrypsin-like activity of the 20S proteasome by BTZ. In the absence of cell microenvironment, BTZ inhibitory activity in the presence of the PEGAuNPs (0.1 nM) remains constant (BTZ concentration range of 20-50 nM). These results corroborate the cytotoxicity experiments and prove that the synergism between BTZ and PEGAuNPs on inhibiting the cell growth is only observed if cellular uptake of the nanoparticles occurs.

4.3 Conclusions

The present work demonstrates the ability of cells to internalize PEGAuNPs and the repercussion on the enhancement of permeation and retention of BTZ in prostate and pancreatic cancer cells, reducing the dose needed to decrease their viability.

The significant increase of BTZ toxicity with PEGAuNPs at low concentration levels can be explained by the BTZ surface adsorption to the nanoparticles and cellular uptake mechanism observed by LSCM images. In fact, the cell uptake mechanism induces a synergistic activity of the proteasome inhibitor and gold nanoparticles at very low drug concentrations. This response may be due to a more efficient delivery of BTZ into the cells by PEGAuNPs maintaining the original activity of BTZ. These findings are also supported by the dialysis experiments in which a time lag and a significant decrease in BTZ release rate in PBS are observed when BTZ is combined with PEGAuNPs.

The pegylated gold nanoparticles internalized by prostate adenocarcinoma cells show no toxicity. Moreover the *in vitro* results with 0.1 nM PEGAuNPs and 4 nM BTZ show that it is possible to reduce the drug concentration 30 times to have the same effect as that of the drug alone.

The effect of nanoparticle cell uptake and the formation of endocytic vesicles in the pancreatic cells increase the mass transfer rate across cell membranes and subsequently drug diffusion in the cytoplasm. The PEGAuNPs localized at the perinuclear region enhance the toxicity of BTZ at very low concentrations (0.1-1.0 nM) in the pancreatic cancer cells. At this level of concentrations, the passive transport of the drug alone through the cell membrane does not induce significant cytotoxicity.

This process leads to high BTZ concentrations inside the cells compared to its low bulk concentrations, at which *per se* BTZ is not able to produce any cytotoxicity.

The *in vitro* results reported pave the way for a better understanding of the AuNPs uptake mechanism by cancer cells and evidence the enhanced permeation and retention effect, opening the possibility to decrease MDR. Increasing the ability of drugs to penetrate tumour microenvironment in lethal concentration is particularly relevant in conventional chemotherapy of adenocarcinomas.

Chapter 5

This chapter is based on the following publications:

Coelho S, Moreno-Flores S, Toca-Herrera JL, Coelho MAN, Carmo Pereira M, Rocha S (2011) Nanostructure of polysaccharide complexes. Journal of Colloid and Interface Science 363 (2):450-455. doi:http://dx.doi.org/10.1016/j.jcis.2011.07.098.

Coelho SC, Rocha S, Sampaio P, Carmo Pereira M, Coelho MAN Encapsulation of a proteasome inhibitor with gold-polysaccharide nanocarriers. *Submitted to Journal of Nanoparticle Research*.

5 BTZ+PEGAuNPs loaded Ch-GA nanoparticles

Contents

5.1 Introduction

Polymeric nanoparticles are suitable drug nanocarriers due to their high capacity of encapsulation of molecules and endocytosis efficiency by enhanced permeation and retention (EPR) effect [194-196]. Also, it is reported that the circulation half-life time of drugs is improved and they are protected from inactivity during blood circulation and transport to the specific tissue [22, 120, 197-201]. Moreover, the nanoparticles are biocompatible, stable [202]. The control of the surfaces of the nanoparticles allows their interactions with negatively charged components from

plasma membrane. Nanoparticles are described to be internalized into cells by endocytosis [8, 100]. These properties lead to improve drug delivery and reduction of the undesirable systemic side-effects in normal surrounding tissues [203, 204]. Chitosan (Ch) is a cationic polysaccharide from the partial alkaline deacetylation of chitin [26, 199, 200]. It is a biodegradable and non-toxic polysaccharide that increases cell membrane permeability [120, 198, 205]. Gum Arabic (GA), approved by the Food and Drug Administration, is an anionic polysaccharide prepared from the exudates of acacia trees [205, 206]. As a result, these polysaccharides have several suitable characteristics to improve drug nanocarriers and enhance drug therapeutic efficacy.

Unique properties as biocompatibility, physical-chemical stability, namely high reactive surface, and non-toxicity make gold nanoparticles (AuNPs) eligible nanosystems for cancer treatment and diagnostics applications [14, 20, 87, 109, 181]. Actually, AuNPs have been investigated for targeting drugs directly *in situ*, reducing several effects in the body, minimizing the multi-drug resistance (MDR) [14]. Also, AuNPs were chosen to accumulate in tumours through the EPR effect [26].

The presented investigation is focused on targeting a proteasome inhibitor, the bortezomib (BTZ), in combination with pegylated gold nanoparticles (PEGAuNPs), by incorporating them into chitosan-gum Arabic nanoparticles (Ch-GA-PEGAuNPs) to protect normal cells from the drug. PEGAuNPs combined with BTZ into Ch-GA NPs matrix were incorporated during the preparation of the polysaccharide matrix by complex coacervation. There are electrostatic interactions between the two polysaccharides with opposite charged surface, in solution. This process is often used to encapsulate biomolecules and to control their release [205, 207]

The anticancer activity of the BTZ is expected to be enhanced by its incorporation into the Ch-GA-PEGAuNPs but also to increase the systemic bioavailability of BTZ. The physicochemical properties and the *in vitro* cell uptake and cell growth of BTZ loaded Ch-GA-PEGAuNPs nanoparticles (Ch-GA-BTZ+PEGAuNPs) were studied in the human pancreatic cancer cells, S2-013 and the immortalized

human pancreatic duct epithelial cells, hTERT-HPNE, by laser scanning confocal microscopy.

5.2 Results

5.2.1 Physical characterization

The complexes were prepared at pH 4.8 since at higher pH, chitosan has low solubility, whereas at pH below 4 the degree of ionization of GA is low. The chitosan molecules had two different degrees of deacetylation (DD), 75% (Ch75) and 93% (Ch93) and were prepared at two initial concentrations (C_{Ch} = 0.06 and 0.3%). The Ch concentrations after adding GA solution were 0.03% and 0.15%. The GA final concentrations depend on the ratios studied. GA/Ch weight ratios ($R_{GA/Ch}$) were 0.6, 1, 1.2 and 3, correlated to positive/negative charge ratios of 5.4, 3.3, 2.7, 1.1 for GA/Ch75 and 6.7, 4.0, 3.4, 1.4 for GA/Ch93.

5.2.1.1 Assess complex formation

GA/Ch75 mixtures at C_{Ch} = 0.03% and $R_{GA/Ch}$ 0.6, 1 and 1.2 were visually transparent, whereas all the other samples became turbid immediately after preparation (Figure 5.1A). The turbidity, monitored by spectrophotometry at 500 nm of the GA/Ch75 mixtures was close to zero at $R_{GA/Ch}$ up to 1.2 and increased to 0.50 at $R_{GA/Ch}$ of 3 (Figure 5.1B).

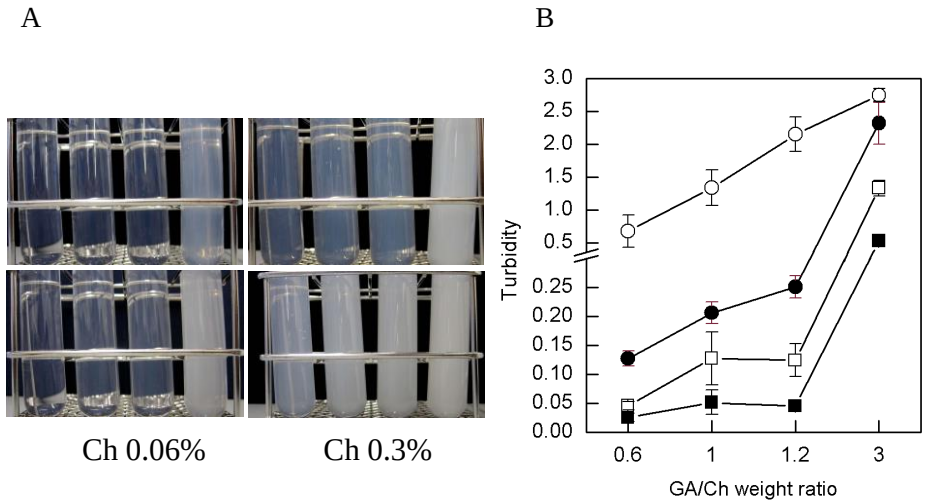

Figure 5.1 Macroscopic features (A) and turbidity (B) of GA/Ch complexes, immediately after preparation, at different ratios and two Ch concentrations: GA/Ch75 at 0.03% (■) and 0.15% (●); GA/Ch93 at 0.03% (□) and 0.15% (○).

At higher concentrations (C_{Ch} = 0.15%), the samples showed turbidity ranging from 0.10 ($R_{GA/Ch}$ of 0.6) to 2.3 ($R_{GA/Ch}$ of 3) (Figure 5.1B). The complexes with C_{Ch} = 0.15% and $R_{GA/Ch}$ of 3 precipitated after overnight incubation at room temperature. Ch DD93 at 0.03% and GA had turbidity close to zero for $R_{GA/Ch}$ of 0.6 which increased to 0.10 and 1.0 for $R_{GA/Ch}$ of 1/1.2 and 3, respectively (Figure 5.1B). At Ch DD93 concentration of 0.15% the turbidity increased from 0.70 to 2.7 ($R_{GA/Ch}$ 0.6 to 3) upon addition of GA. Precipitation of GA/Ch93 samples was observed at weight ratios of 3 for C_{Ch} = 0.03% and at all ratios for C_{Ch} = 0.15%.

The size of the complexes at C_{Ch} = 0.03% is similar and constant for both Ch DD75 and DD93 (240–260 nm) at $R_{GA/Ch}$ of 0.6 to 1.2, but increases to 360 nm at $R_{GA/Ch}$ of 3 (Figure 5.2).

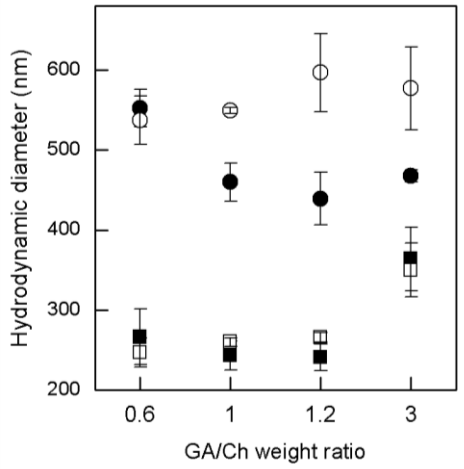

Figure 5.2 Mean hydrodynamic diameter of mixtures of GA/Ch: Ch DD75% at 0.03% (■) and 0.15% (●) or Ch DD93% at 0.03% (□) and 0.15% (○).

The hydrodynamic diameter of the complexes prepared with Ch DD75 at 0.15% decreased from 550 to 460 nm as the GA concentration increases from $R_{GA/Ch}$ 0.6 to 1, and is similar between ratios of 1 and 3 (Figure 5.2). The variation in the diameter of complexes containing Ch DD93 at 0.15% is less pronounced (540–600 nm). The polydispersity index (PdI) of the samples is greater than 0.1 and is higher for C_{Ch} = 0.15%, indicating broad size distribution (Table 5.1).

Table 5.1 Polydispersity index and zeta potential of GA/Ch complexes.

complexes	$R_{GA/Ch}$	(+/–) charge ratio	PdI		ZP	
			0.03%	0.15%	0.03%	0.15%
GA/Ch75	0.6	5.4	0.38 ± 0.05	0.50 ± 0.05	37 ± 2	44 ± 5
	1	3.3	0.31 ± 0.04	0.41 ± 0.09	38 ± 4	44 ± 3
	1.2	2.7	0.29 ± 0.03	0.42 ± 0.11	35 ± 3	42 ± 2
	3	1.1	0.39 ± 0.08	0.50 ± 0.01	28 ± 2	26 ± 6
GA/Ch93	0.6	6.7	0.22 ± 0.04	0.27 ± 0.02	38 ± 2	51 ± 4
	1	4.0	0.18 ± 0.05	0.25 ± 0.01	39 ± 4	48 ± 3
	1.2	3.4	0.16 ± 0.04	0.38 ± 0.07	37 ± 2	47 ± 1
	3	1.4	0.24 ± 0.03	0.37 ± 0.04	31 ± 1	33 ± 2

The complexes possess positive zeta potential indicating predominance of free amine groups at their surface (Table 5.1). At $R_{GA/Ch}$ of 3, the zeta potential values decrease and the complexes tend toward electroneutrality, which leads to their association and precipitation.

If the turbidity of GA and Ch DD75 mixtures is low and no phase separation is observed, the detection of particles by DLS at $R_{GA/Ch}$ up to 1.2 and C_{Ch} = 0.03% can be explained by the formation of soluble complexes. At higher concentrations or using Ch DD93, the complexes become insoluble. The hydrodynamic diameter of the complexes containing Ch DD75 at 0.15% decreases upon increasing the concentration of GA, from $R_{GA/Ch}$ 0.6 to 1 due to the shrinkage of the complexes when more carboxylic groups interact with amine groups of Ch molecules resulting in a reduction of the intramolecular repulsion. However, this tendency, which is usually observed upon increasing the number of opposite charges, is not observed for the other cases. The number of positive charges is always higher than that of negative ones (Table 5.1). Thus the core of the complexes must be composed of segments resulting from the local neutralization of positive charges of Ch. Given the fact that only 23% of GA residues are charged, its chains possess large non-charged segments, which might explain the lack of significant variation of their hydrodynamic diameters, despite the

increase in the number of negative charges in the medium. The increase in turbidity of mixtures containing 0.15% Ch indicates an increase in mass of the complexes. Increasing the GA/Ch ratio, macroscopic phase separation is observed. DLS measurements showed that there is a correlation between the average size and the polymer concentration. It was demonstrated that increasing the concentration of the polymer, its degree of ionization decreases, and it becomes more flexible as it is less expanded [158]. Thus, the charged sites are more available for interaction, which associated to the fact that the number of macromolecules available in concentrated systems is higher lead to the formation of complexes with larger average size. At lower concentrations the charged polymers will be expanded due to intramolecular electrostatic repulsions, resulting in macromolecule stiffness.

The strength of complexation depends on the charge density of the polymers. The charge density of weak polyelectrolytes is governed mainly by the pH, which is why solution pH plays a crucial role on the coacervation process [208-212]. A pH value has been defined for synthetic polyelectrolytes and proteins at which soluble complexes are formed and that preceded the pH of visual phase separation [213-218]. Weinbreck *et al.* proved that pH-induced structural transitions occurred for GA and whey protein [219]. Here structural transitions of GA/Ch complexes are described, at constant pH, by changing the Ch degree of deacetylation (charge density). Complexes prepared with chitosan DD75 at 0.03% detected by DLS appeared to be soluble, as there was no phase separation and the turbidity was low (up to $R_{GA/Ch}$ of 1.2). However, using Ch DD93, the turbidity increased already at low concentrations. There is an optimum concentration where complex coacervation is maximum [220]. Previous studies demonstrated that at chitosan concentrations of 0.5–1%, GA/Ch complexes precipitate at pH 4.5, particularly at ratios of 4 and 5 [158]. Our studies were performed with chitosan concentrations of 0.03 and 0.15% at $R_{GA/Ch} \leq 3$. Although GA/Ch ratios were kept low, at which soluble complexes are expected,[205] insoluble complexes evidenced by increased turbidity, were also observed.

5.2.1.2Imaging gum Arabic-chitosan complexes

GA/Ch75 complexes prepared with 0.03% of chitosan and weight ratios of 0.6 and 1.2 have a globular shape when adsorbed onto the polar mica substrate (Figure 5.3). The AFM images and section analysis also indicate that, after deposition on substrates, the complexes collapse into a core structure surrounded by a rough layer (Figure 5.3A). A profile analysis of an agglomerate observed at ratio of 1.2 (GA/Ch) (dashed line in Figure 5.3B) evidences diameters of 200-250 nm.

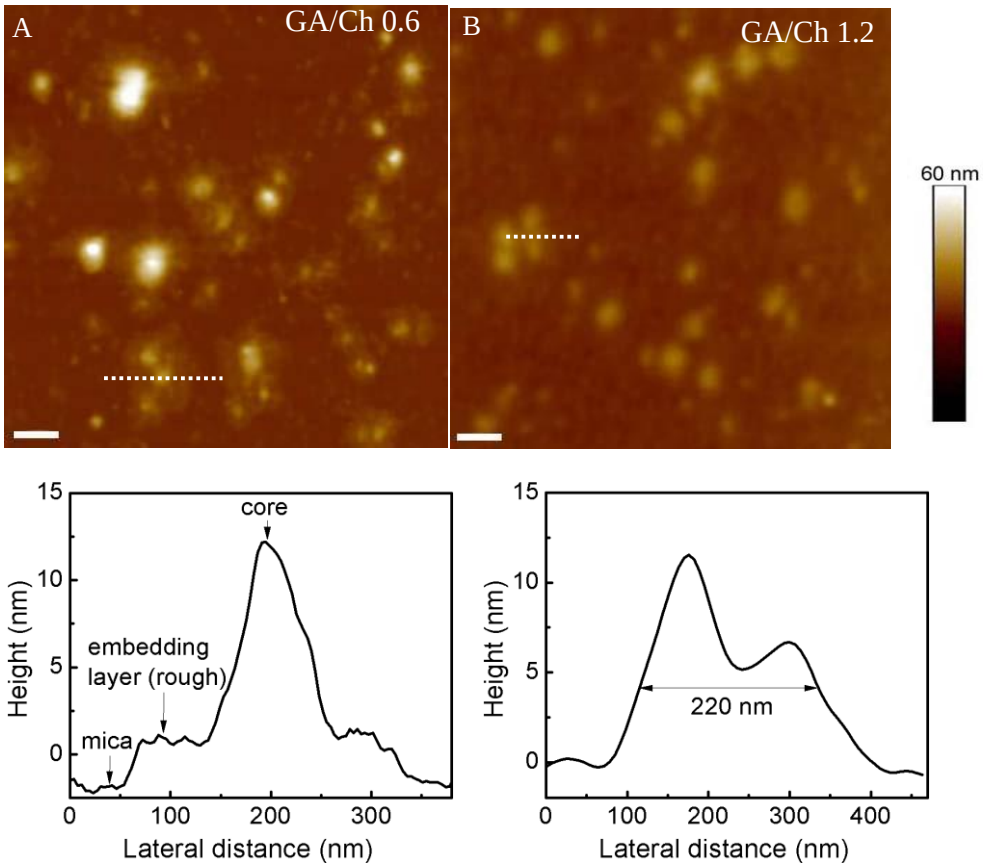

Figure 5.3 AFM height images of GA/Ch75 complexes at chitosan concentration of 0.03%: (A) RGA/Ch = 0.6 and (B) RGA/Ch = 1.2 (scale bar = 200 nm). The profile analysis of the complexes is shown below evidencing the complex core structure surrounded by a rough layer at RGA/Ch of 0.6 and one particle aggregate of 220 nm at RGA/Ch = 1.2.

Phase analysis shows more contrast than the topographic one as well as more sensitivity to material surface properties such as stiffness and viscoelasticity. GA/Ch75 complexes (weight ratio of 0.6 and 0.03% Ch) are agglomerates of homogeneous material as they show the same bright colour (Figure 5.4).

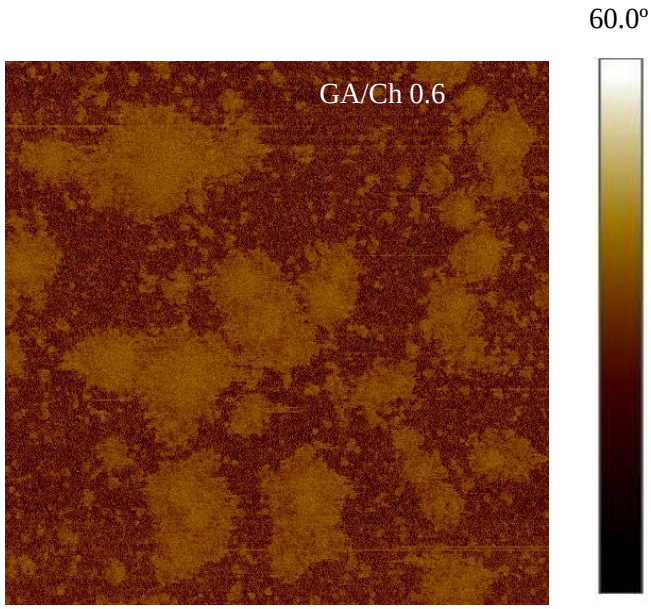

Figure 5.4 AFM phase image of GA/Ch75 complex at RGA/Ch = 0.6 and Ch final concentration of 0.03%.

GA/Ch93 complexes prepared with 0.03% of Ch form more uniform structures with spherical shape (Figure 5.5A). The average diameters, based on 20–30 direct measurements from AFM micrographs, are 240 ± 60 nm for $R_{GA/Ch}$ 1.2, which are in agreement with DLS measurements. Phase images show particle aggregates and soft material surrounding the particles (dark areas are softer then bright areas) (Figure 5.5B). The differences between particle core and surroundings are attributed to viscoelastic properties of the material. The core is composed of hydrophobic aggregates (neutralized segments of GA and Ch) which are harder than free charged segments of Ch or polar non charged segments of GA.

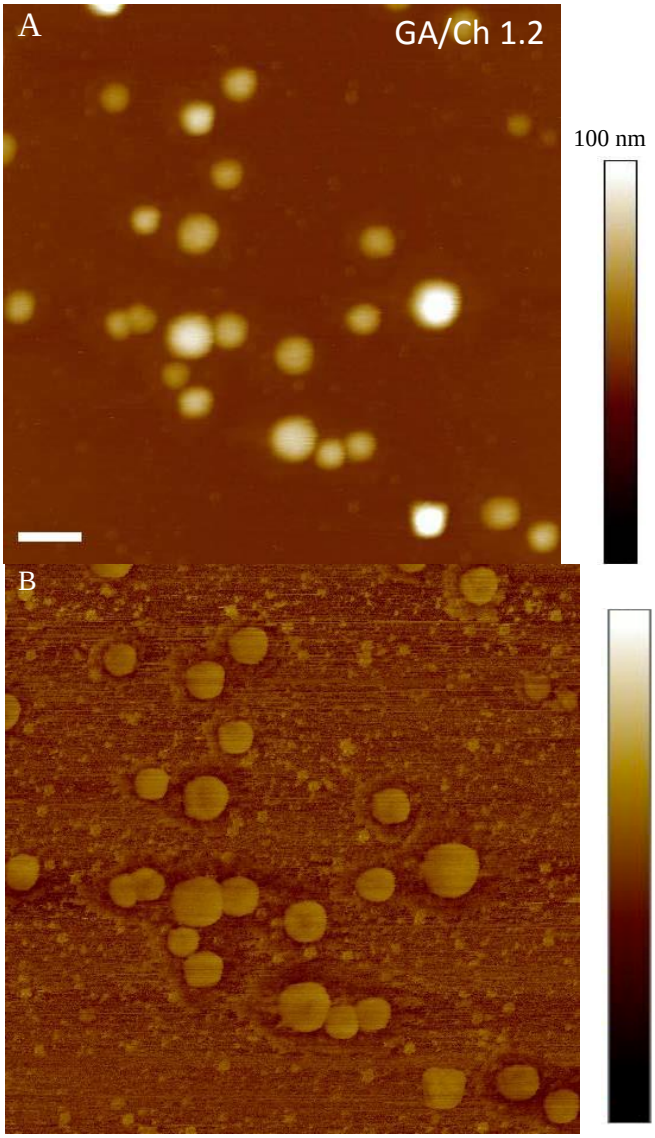

Figure 5.5 Structure of GA/Ch93 complex at weight ratio of 1.2 and chitosan final concentration of 0.03%, viewed by AFM (scale bar = 500 nm).

At higher biopolymer concentrations (C_{Ch} = 0.15%) the structure of the complexes is similar to that observed for 0.03% chitosan (Figure 5.6). A layer embedding the complexes is visible (Figure 5.6B).

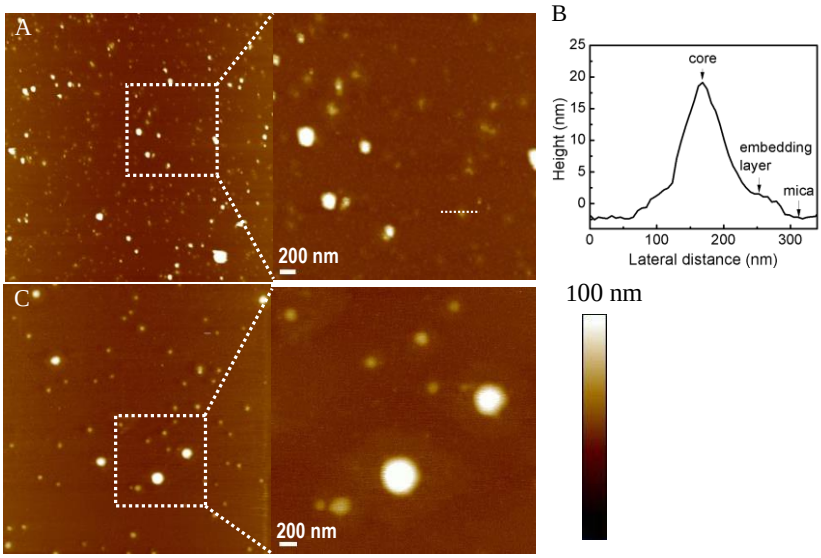

Figure 5.6 AFM height images of GA/Ch75 (a) and GA/Ch93 (c) complexes, at weight ratios of 0.6 and Chitosan final concentration of 0.15%. The profile analysis of GA/Ch75, shown in (b), evidences the presence of a rough embedding layer

Ch is positively charged and has a relatively extended conformation in solution, resulting that its charges are accessible [158, 221]. GA, in contrast, is negatively charged (with low charge density) and has a globular structure [205, 222]. Arising from electrostatic interaction, the two weak oppositely charged polyelectrolytes form a complex, thereby releasing counterions and water molecules, contributing to an entropy gain in the system [158, 223]. GA forms, with Ch DD75, complexes with a relatively globular shape, but less uniform than the ones obtained with Ch DD93, which are spherical particles. GA/Ch75 complexes appear also more polydispersed and flattener (their diameter: height ratios typically exceeded 10:1 at C_{Ch} = 0.03%), when compared with the particles formed by GA/Ch93. Ch molecules DD93 have more positive charges and efficiently neutralized the negatively charges of GA. The lower charge density of Ch DD75 is most likely the cause for inefficient assembly of the macromolecules. The formation of irregular aggregates by GA and Ch DD75 is attributed to the presence of non-charged polar monomers in chitosan molecule. This hypothesis is based on the work of Wolfert *et al*. with copolymers of cationic and

uncharged monomers, which have lost their ability to condense deoxyribonucleic acid (DNA) [224]. The copolymers could not induce hydrophobic self-assembly of polymer/DNA complexes even at charge neutrality. Also Sanchez *et al*. found vesicular structure for GA and lactoglobulin due to insufficiently neutralization of the macromolecular complexes [225].

It is well known that the solubility of polyelectrolyte complexes depends strongly on the molar mixing ratio of the macromolecules and their relative molecular weights [226-229]. Polyions with weak ionic groups that have significantly different molecular weights and/or are mixed in non-stoichiometric ratios form water-soluble micelle-like aggregates [228]. Such complexes adopt a structure similar to the ladder model, consisting of hydrophilic single-stranded and hydrophobic double-stranded segments, where complex formation takes place on a molecular level via conformational adaptation (zip mechanism) [229]. The formation of soluble GA/Ch complexes might follow a similar mechanism, due to large non-charged segments of GA (only approximately 23% of GA residues are charged). The driving force of complex formation is the release of counterions, but once the polyelectrolytes are in close contact, the distance between the charges also influences the complex structure. GA/Ch75 form, at low concentrations (C_{Ch} = 0.03%) and up to 1.2 ratio, soluble complexes (optical density low) with globular structure, whereas GA/Ch93 form spherical particles (insoluble complexes). The complexes appear to have a core-shell micellar structure, composed of hydrophobic core (charge neutralized segments) stabilized by non-neutralized Ch segments and non-charged segments of GA. The distance between the charges on the Ch molecule seems to have a higher influence on the structure of the complexes than the charge ratio itself, as observed in the case of cationic polymers and DNA complexes [224]. In addition to the degree of deacetylation of Ch, the formation of nanoparticles was dependent on the concentrations of the polymers, as observed for other cases such as for Ch-dextran system [230]. For both systems, small particles were formed only by using dilute polysaccharide solutions (final total concentration less than 0.07%). Similar results are

described for the system poly-gamma-glutamic acid and Ch. At low concentration of biopolymers, more stable nanocomplexes were formed, and the formation of smaller individual nanoparticles was favoured [231].

The objective of this characterization was to develop and optimize a system that could be used to deliver an anticancer drug. GA/Ch93 form soluble complexes with spherical structure of about 240 nm at weight ratios up to 1.2, if the concentrations are kept low (total biopolymer concentration up to 0.06%). Thus, these parameters were used to prepared BTZ and AuNPs-loaded polysaccharide NPs.

5.2.2 Particle size distribution, surface charge and morphology of BTZ loaded Ch-GA NPs and BTZ+PEGAuNPs loaded Ch-GA NPs

The Ch-GA based nanoparticles alone and loaded with PEGAuNPs and BTZ were prepared through a coacervation process. The initial concentration of chitosan was 0.04% (w/v) and a GA/Ch weight ratio of 1.2 was used. Figure 5.7A and Figure 5.7B confirmed the presence of PEGAuNPs inside the complexes without and with BTZ, respectively.

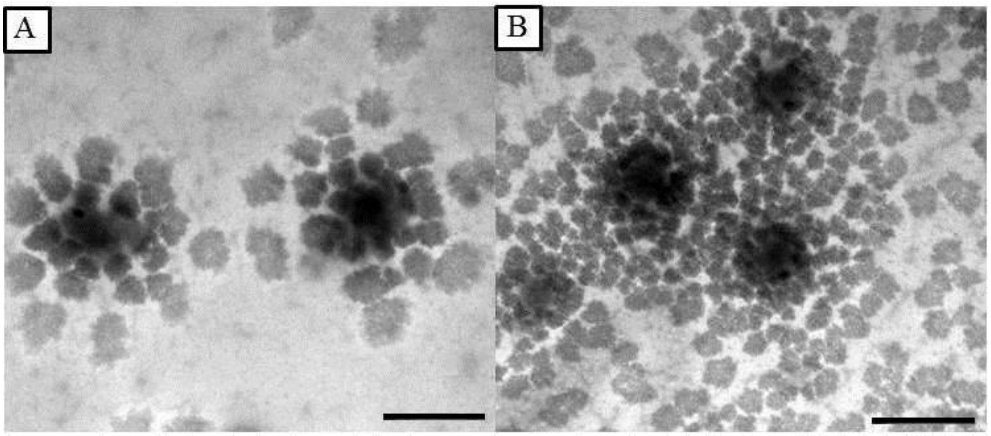

Figure 5.7 Transmission electron microscope images of (A) Ch-GA-PEGAuNPs, (B) Ch-GA-BTZ+PEGAuNPs. Scale bar represent 200 nm.

The Ch-GA-BTZ+PEGAuNPs show two typical absorption bands centered at 528.5 and 268.5 nm from PEGAuNPs and BTZ, respectively (data not shown). These nanosystems were stable for several weeks when stored at 4ºC in the dark. DLS measurements were in agreement with the TEM analysis, and are shown in Table 5.2.

Table 5.2 Hydrodynamic diameter, polydispersity index (PdI) and zeta potential of nanoparticle systems with initial Ch concentrations of 0.04% (w/v) and a RGA/Ch = 1.2.

Sample	C_{BTZ} (nM)	$C_{PEGAuNPs}$ (nM)	Diameter (nm)	PdI	ZP (mV)	pH
Ch-GA	-	-	315 ± 5	0.3	39 ± 1	4.8
PEGAuNPs (stock solution)	-	18.9	39 ± 1	0.6	-39 ± 3	5.3
Ch-GA-PEGAuNPs	-	2	428 ± 18	0.3	23 ± 3	4.7
Ch-GA-BTZ	200	-	341 ± 26	0.1	30 ± 3	4.8
Ch-GA-PEGAuNPs-BTZ	200	2	327 ± 73	0.2	33 ± 2	4.6

The average hydrodynamic diameter of Ch-GA NPs ranged from 315 nm to 327 nm (loaded with PEGAuNPs) and the polydispersity index (PdI) was 0.3. This diameter change occurs due to the presence of spherical PEGAuNPs with small diameters (39 nm). In BTZ loaded Ch-GA-PEGAuNPs, no significant change in the nanoparticle diameter was observed.

The average zeta potential was positive for the different formulations, which is attributed to the residual amine groups of Ch that neutralize the negative charges of GA and PEGAuNPs. Also, the strong positive charges on the surface of nanoparticles prevent the aggregation (Table 5.2) [130, 134, 232] .

5.2.3 *In vitro* release studies

The release profiles of BTZ from Ch-GA NPs and Ch-GA-PEGAuNPs were studied *in vitro* using a dialysis membrane in ultrapure water and in PBS 0.01 M at 37 ºC. The results are shown in Figure 5.8.

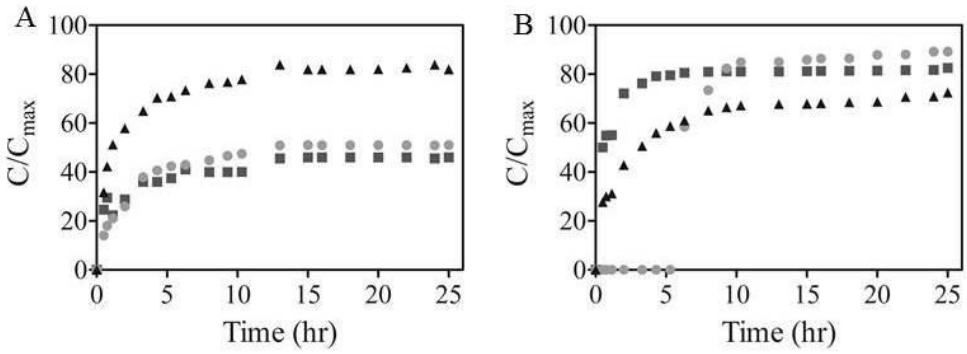

Figure 5.8 Release profiles of Ch-GA-BTZ+PEGAuNPs (●), Ch-GA-BTZ NPs (■) and BTZ alone (▲) in DI water (A) and PBS 0.01 M (B). C_{max} corresponds to the total amount of BTZ added.

The drug release from Ch-GA-BTZ+PEGAuNPs and Ch-GA-BTZ NPs is pH dependent as it can be seen from the profiles in ultrapure water (pH 5.8) and in PBS

0.01 M (pH 7.0). In DI water, the amount of BTZ release from Ch-GA-BTZ+PEGAuNPs and Ch-GA-BTZ NPs is lower than the amount detected in the sample with only free BTZ (Figure 5.8A). After 5 h 40% of the total BTZ was released, which might be attributed to diffusion of BTZ from the nanosystems Ch-GA-BTZ NPs and Ch-GA-BTZ+PEGAuNPs. Also, after 13 h, 51% was released from Ch-GA-BTZ+PEGAuNPs and Ch-GA-BTZ NPs, and 82% of BTZ alone was released. The release of BTZ in PBS is very different as depicted by the profiles of Figure 5.9B. In PBS, a delay in BTZ released from Ch-GA-BTZ+PEGAuNPs is observed in the first 5 h due to the presence of PEGAuNPs, comparing to the Ch-GA-BTZ NPs. For these systems, the BTZ release after 10 h was 85%. Also, PBS provides an effect on BTZ adsorption of Ch-GA-BTZ NPs and Ch-GA-BTZ+PEGAuNPs systems, slowing down the BTZ release for the last nanoparticles.

5.2.4 Cellular imaging studies

The cellular uptake of Ch-GA-BTZ+PEGAuNPs with BTZ concentration of 100 nM in pancreatic cells (S2-013) and immortalized human pancreatic duct epithelial cells (hTERT-HPNE) was investigated by confocal microscopy. From our observations we can conclude that PEGAuNPs were internalized and distributed throughout S2-013 and hTERT-HPNE cells after 48 h incubation, as illustrated in Figure 5.9c and Figure 5.9d. It was observed that the accumulation of the nanoparticles into the cytoplasm effectively improve the cytotoxicity in both cell lines.

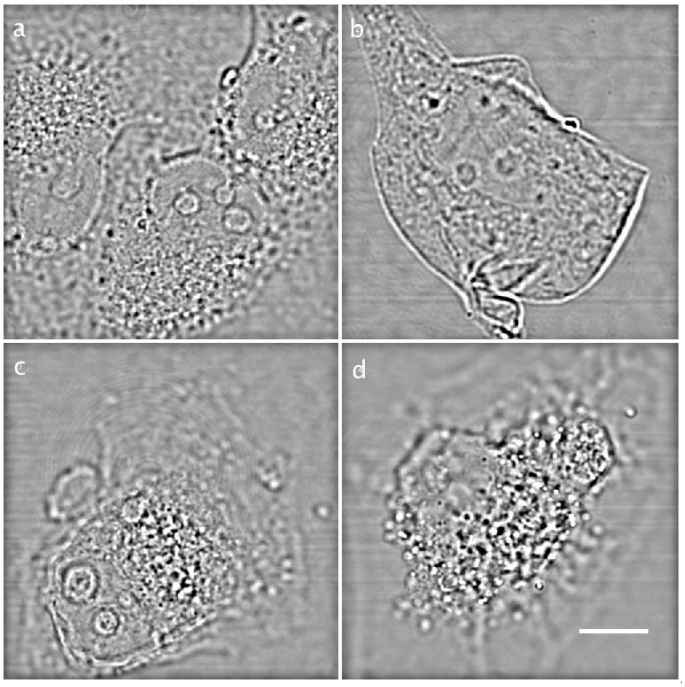

Figure 5.9 Transmission images of the S2-013 (a, c) and hTERT-HPNE (b, d) cells after 48 h incubation. The cells were incubated with Ch-GA-BTZ+PEGAuNPs with BTZ concentration of 100 nM; (a,b) the control untreated cells. Scale bar is 10 µm.

5.2.5 Cytotoxic studies

The *in vitro* cytotoxicity studies of the effects of Ch-GA-PEGAuNPs, Ch-GA NPs, BTZ alone, Ch-GA-BTZ+PEGAuNPs and Ch-GA-BTZ NPs were performed with S2-013 and hTERT-HPNE. The cells were exposed to a range of experimental concentration of BTZ loaded nanoparticles and blank nanoparticles for 48 h at 37ºC. Their effect was evaluated by SRB and PB methods. Ch-GA-PEGAuNPs and Ch-GA NPs with Ch concentration up to 3.3×10^{-3} mg/mL and $R_{GA/Ch}$ of 1.2 do not show any cytotoxicity on both cell lines (Figure 5.10), showing good biocompatibility.

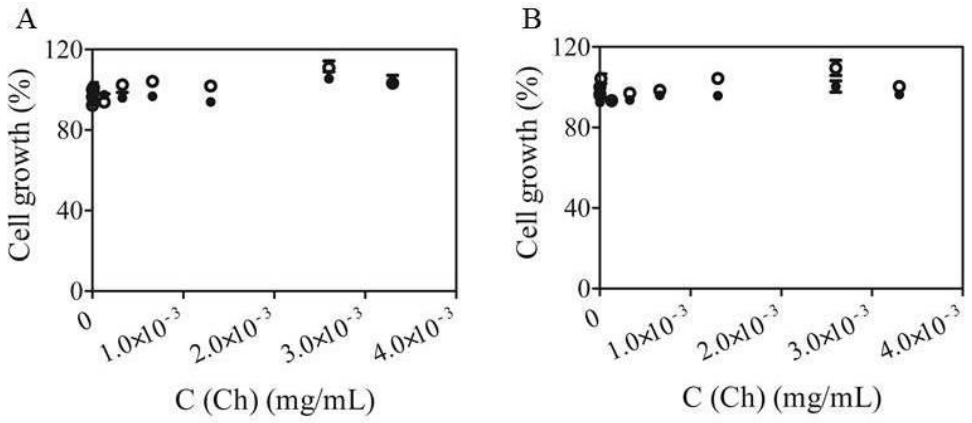

Figure 5.10 Cytotoxicity induced by Ch-GA-PEGAuNPs (●) and Ch-GA NPs (○) at $R_{GA/Ch}$ = 1.2 on S2-013 (A) and hTERT-HPNE (B) cells, by the SRB assay.

The inhibitory effect of BTZ on the proliferation of S2-013 and hTERT-HPNE was evaluated with the drug incorporated in the NPs, Ch-GA-BTZ+PEGAuNPs and Ch-GA-BTZ NPs. The effect of BTZ at concentrations from 0.1 to 100.0 nM was tested in these two systems with concentrations of Ch in the range $1.1x10^{-7}$ to $3.3x10^{-3}$ mg/mL and $R_{GA/Ch}$ of 1.2 (Figure 5.11).

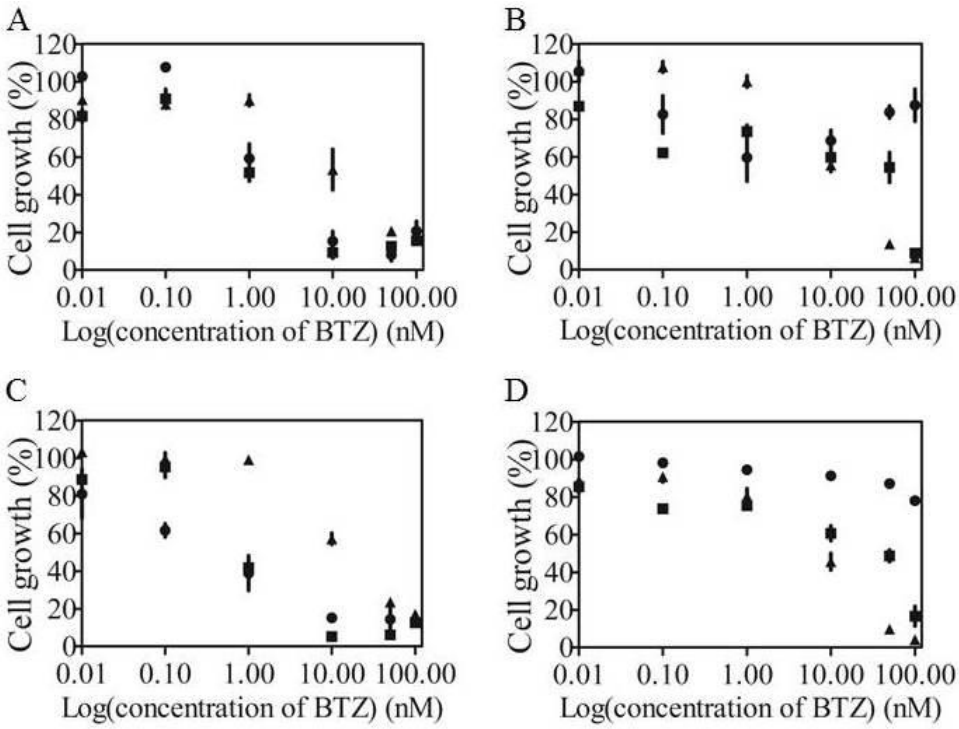

Figure 5.11 Effect of the Ch-GA-BTZ+PEGAuNPs (●), Ch-GA-BTZ NPs (■) and BTZ alone (▲) on the cell growth of S2-013 (A, C) and hTERT-HPNE (B, D) cells. (A, B) PB assay and (C, D) SRB assay.

As presented in Figure 5.11A and Figure 5.11C, BTZ loaded Ch-GA NPs and BTZ loaded Ch-GA-PEGAuNPs decrease the growth rate of the S2-013 cells, when compared with BTZ alone, especially to 1.0 and to 10.0 nM of BTZ concentration. A possible reason for the efficacy increase of cytotoxicity of BTZ is the efficient delivery by the nanoparticles. Ch-GA system might augment protection of BTZ. Also for 10.0 nM BTZ loaded in Ch-GA NPs and loaded in Ch-GA-PEGAuNPs reduced the cell growth to about 13% compared with 58% to BTZ alone. This suggests a good efficiency of the Ch-GA nanosystem through the EPR effect [200]. Moreover, at this concentration range Ch-GA-BTZ+PEGAuNPs does not show toxicity to hTERT-HPNEs (Figure 5.11D).

The inhibiting cell growth effect of BTZ loaded Ch-GA NPs and Ch-GA-PEGAuNPs were achieved by following SRB assay. In fact, as showed in Figure 5.12 and Table 5.3,

there is an increase of cell death with the increase of BTZ concentration, which is given by the analysis of the cell proliferation and cell death.

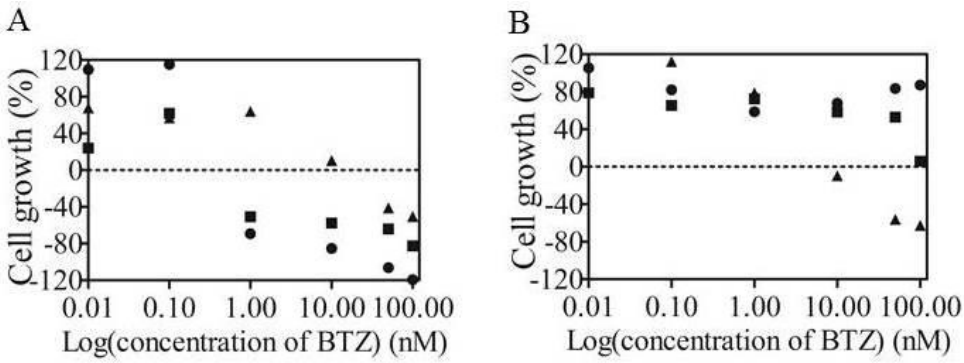

Figure 5.12 Effect of the Ch-GA-BTZ+PEGAuNPs (●), Ch-GA-BTZ NPs (■) and BTZ alone (▲) on the cell growth of S2-013 (A) and hTERT-HPNE (B) cells compared to the control, by the PB assay.

Table 5.3 Effect of BTZ, Ch-GA-BTZ NPs and Ch-GA-BTZ+PEGAuNPs on the growth inhibition of the pancreatic cell lines S2-013 and hTERT-HPNE.

	GI_{50} (nM)	
Sample	**S2-013**	**hTERT-HPNE**
BTZ	0.74 ± 0.35	1.49 ± 0.20
Ch-GA-BTZ	0.21 ± 0.06	10.0 ± 0.00
Ch-GA-PEGAuNPs-BTZ	0.60 ± 0.00	23.86 ± 22.40

In S2-013 cells, the GI_{50} concentration is lower in the case of Ch-GA-BTZ+PEGAuNPs (0.47 nM) and Ch-GA-BTZ NPs (0.83 nM) when compared to BTZ alone (13.95 nM) ($p < 0.05$). Also, Ch-GA-BTZ+PEGAuNPs are more efficient in inducing cell death than BTZ alone for drug concentrations over 1.0 nM. BTZ alone is significantly ($p < 0.05$) more effective at decreasing cell survival and has more inhibitory effect on cell

growth, as it presents the lowest GI_{50} value (Table 5.3). Moreover, Figure 5.12 show that BTZ loaded nanoparticles decrease significantly the S2-013 cell growth rate when compared to BTZ alone. Also, it is showed that in hTERT-HPNEs the same effect is not observed. In fact, hTERT-HPNE cell growth did not change with BTZ loaded nanoparticles in the concentration range of 0.1 and 100.0 nM (Figure 5.12B). This could be explained by the effect of the carbohydrate matrix on the BTZ release in normal cells.

5.3 Conclusions

A novel chitosan-gum Arabic-gold nanoparticle system with positively charged was developed for the delivery of the proteasome inhibitor, bortezomib. BTZ was entrapped into the polysaccharides-gold nanoparticles' system. Confocal images indicate that Ch-GA-BTZ+PEGAuNPs were internalized by the pancreatic cells through endocytic mechanism and are able to enhance permeation and retention of BTZ activity. There is a decreasing in the required drug concentration to induce cell proliferation. The *in vitro* cytotoxic study revealed that 10.0 nM BTZ loaded Ch-GA-PEGAuNPs had a significant toxicity to human pancreatic cancer cells as compared to the drug alone. Also, at the same BTZ concentration, the nanosystem has no toxic effect to immortalized human pancreatic duct epithelial cells, suggesting that these nanoparticles can have good applicability to overcome limitations associated to low bioavailability, *in situ* delivery and, therefore, fewer side effects.

Chapter 6

6 Concluding Remarks

This thesis reports the concept of enhancing the effect of anticancer drugs on cancer cells by pegylated gold nanoparticles. Our approach is based on the increase of the permeation and retention effect by the functionalized gold nanoparticles in prostate and pancreatic cancer cells, and opens the possibility to overcome multi-drug resistance

In cell cultures, our results show that gold nanoparticles intensify the anticancer response of the drug bortezomib, a proteasome inhibitor. The pegylated gold nanoparticles localized at the perinuclear regions enhance the toxicity of bortezomib in both types of cancer cells.

Our concept is based on the formation of endocytic vesicles with high electron density where the nanoparticles move at high speed, increasing the drug mass transfer rate across cell membranes and diffusion process in the cytoplasm to perinuclear region. The effect of this mechanism on the drug mass transfer rate across cell membranes and diffusion process can be further explored by the research teams working in the development of new anticancer drugs.

The incorporation of bortezomib and pegylated gold nanoparticles into a positively charged chitosan-gum Arabic-gold matrix was also evaluated. The objective of this work was to protect the systemic bioavailability of BTZ and avoid that normal cells are exposed to the drug toxicity. The results demonstrated that the toxicity in normal cells decreases, suggesting the potential of these nanoparticles to protect the drug activity and reduce the side effects.

The design of suitable nanocarriers for molecular transport can be fine-tuned to influence the enhanced permeation and retention effect. Since no chemical modification of the drug is needed, the present approach can be potentially applied to other anticancer drugs with potential efficacy in the angiogenesis process. The

benefits of this approach for future cancer drugs/therapies/diagnosis require further research to evaluate *in vivo* drug efficacy to understand the pharmacokinetics, pharmacodynamics and response of the immune system to the nanosystems.

Appendix

A Press release

Cancer Treatment Going for the Gold

21 Tuesday May 2013

Posted by AAPS Blog in AAPS Events

≈ 3 Comments

Tags
2013 AAPS National Biotechnology Conference, cancer, Gold, Nanoparticles, Silvia Coelho

Kim Brown is the AAPS communications and social media manager in the Public Outreach Department.

As is well known, cancer is a major public health problem worldwide. Most cancers are recognized primarily due to symptoms or specific medical tests to a definitive diagnostic. There are different therapy options available, such as surgery, chemotherapy, radiation therapy, and palliative care. Due to cancer heterogeneity and development of multi-drug resistance, chemotherapy may not be effective for every patient. For example, anticancer drugs often have a short half-life time into the body and, sometimes, their efficacy is compromised by adverse effects. The drugs cause damage not only in cancer, but also in surrounding tissues.

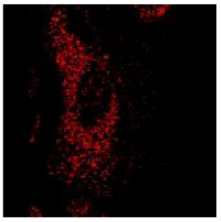

Silvia Coelho and a team of researchers from the University of Porto, the University of Nebraska, and Oslo University are working to develop nanosystems based in gold nanoparticles to be tested as combined strategies for cancer therapy. These small structures show no toxic leeway to the human body and can be combined with anticancer drugs.

The team's first achievements have paved the way for a better understanding of the mechanism uptake of gold nanoparticles by cancer cells, which now induces a synergistic activity of the anticancer drug and gold nanoparticles at very low concentrations. The approach can be fine-tuned for therapeutic drugs to minimize their side effects and overcome multi-drug resistance.

Learn more about the research that Coelho and her team are presenting today at 1:30 p.m. PDT, by viewing their abstract, no. T2021, in the 2013 AAPS National Biotechnology Conference MyAgenda Planner.

thoughts on "Cancer Treatment Going for the Gold"

ASPIC

envie informação pesquisa

início sobre nós torne-se membro notícias reuniões emprego parceiros contacto

envie a um amigo share this

< voltar à listagem

Tratar o cancro do pâncreas e da próstata com nanopartículas de ouro

Quinta, 04.07.2013

Uma equipa multidisciplinar da Universidade do Porto - constituída por investigadores do Laboratório de Engenharia de Processos Ambiente e Energia (LEPAE) da FEUP, do IBMC e do IPATIMUP – em conjunto com investigadores da Universidade Técnica de Chalmers (Suécia), do University of Nebraska Medical Center (EUA) e do Institute for Cancer Research da Noruega estudou, durante três anos, a utilização de nanopartículas de ouro como forma de tratar o cancro, tendo chegado à conclusão que estas tornam mais eficiente o efeito de retenção e permeação de drogas terapêuticas nos tecidos atingidos pela doença.

Segundo explicou ao site da ASPIC a investigadora Sílvia Coelho, da Faculdade de Engenharia da Universidade do Porto e primeira autora do estudo, «a droga (nomeadamente a conhecida «multi anti-drug resistance» (MDR), entra nas nanopartículas e fica muito mais potente, ou seja tem efeitos muito mais elevados nas células tumorais. Isto permite diminuir a dose normal, que é muito forte, e obter efeitos superiores nas células tumorais e, por razões ainda não conhecidas, sem consequências negativas para as células não tumorais».

As nanopartículas de ouro podem ser utilizadas tanto no tratamento de quimioterapia como de radioterapia, tendo já sido testadas em linhas celulares tumorais e não-tumorais pancreáticas e da próstata.

Com viabilidade para ser introduzido no mercado farmacêutico, este tratamento já despertou o interesse de uma investigadora da Pfizer, nos Estados Unidos, para a aplicação destas nanopartículas na passagem de drogas através da barreira hematoencefálica.
O projecto, que foi financiado pela FCT (140 000 €) e pelo Research Council of Norway (180 000 NK), foi recentemente apresentado nos Estados Unidos, numa conferência da American Association of Pharmaceutical Scientists (AAPS) e, segundo o investigador que liderou o projecto, Manuel Coelho, será publicado dentro de um mês no «Journal of Biomedical Nanotechnology».

Créditos da foto: Faculdade de Engenharia da Universidade do Porto

PARCEIROS

IPATIMUP FUNDAÇÃO CALOUSTE GULBENKIAN IPOPORTO NOVARTIS AstraZeneca

www.aspic.pt/pt-pt/noticias/tratar-o-cancro-do-pâncreas-e-da-próstata-com-nanopartículas-de-ouro#.Ue--T43CZ8E

Bibliography

Bibliography

1. Cedervall T, Lynch I, Lindman S, Berggård T, Thulin E, Nilsson H, et al. Understanding the nanoparticle–protein corona using methods to quantify exchange rates and affinities of proteins for nanoparticles. Proceedings of the National Academy of Sciences 2007 February 13, 2007;104(7):2050-55.
2. Swatantra K.S. Kushwaha AR, A.K. Rai, Satyawan Singh. Novel Drug Delivery System for Anticancer Drug: A Review. International Journal of PharmTech Research 2012;4(2):542-53.
3. Papasani MR, Wang G, Hill RA. Gold nanoparticles: the importance of physiological principles to devise strategies for targeted drug delivery. Nanomedicine 2012;8(6):804-14.
4. Zamboni WC, Torchilin V, Patri AK, Hrkach J, Stern S, Lee R, et al. Best practices in cancer nanotechnology: perspective from NCI nanotechnology alliance. Clin Cancer Res 2012;18(12):3229-41.
5. De Jong WH, Borm PJ. Drug delivery and nanoparticles:applications and hazards. Int J Nanomedicine 2008;3(2):133-49.
6. Shahshahan MA, Beckley MN, Jazirehi AR. Potential usage of proteasome inhibitor bortezomib (Velcade, PS-341) in the treatment of metastatic melanoma: basic and clinical aspects. Am J Cancer Res 2011;1(7):913-24.
7. Coelho J, Ferreira P, Alves P, Cordeiro R, Fonseca A, Góis J, et al. Drug delivery systems: Advanced technologies potentially applicable in personalized treatments. EPMA Journal 2010 2010/03/01;1(1):164-209.
8. Beija M, Salvayre R, Lauth-de Viguerie N, Marty J-D. Colloidal systems for drug delivery: from design to therapy. Trends in Biotechnology 2012;30(9):485-96.
9. Chomoucka J, Drbohlavova J, Huska D, Adam V, Kizek R, Hubalek J. Magnetic nanoparticles and targeted drug delivering. Pharmacological Research 2010;62(2):144-9.
10. Praetorius NP, Mandal TK. Engineered nanoparticles in cancer therapy. Recent Pat Drug Deliv Formul 2007;1(1):37-51.
11. Ravi Kumar MN. Nano and microparticles as controlled drug delivery devices. J Pharm Pharm Sci 2000;3(2):234-58.

12. Kumar A, Zhang X, Liang X-J. Gold nanoparticles: Emerging paradigm for targeted drug delivery system. Biotechnology Advances 2013;31(5):593-606.
13. Nikunj Trivedi NP, U M Upadhyay, Viral Shah. Gold Nanoparticulate Drug Delivery System: A Review. Pharmacie Globale, International Journal of Comprehensive Pharmacy 2012;2(3).
14. Parveen S, Misra R, Sahoo SK. Nanoparticles: a boon to drug delivery, therapeutics, diagnostics and imaging. Nanomedicine 2012;8(2):147-66.
15. Suri SS, Fenniri H, Singh B. Nanotechnology-based drug delivery systems. J Occup Med Toxicol 2007;2:16.
16. Arruebo M, Fernández-Pacheco R, Ibarra MR, Santamaría J. Magnetic nanoparticles for drug delivery. Nano Today 2007;2(3):22-32.
17. Persson E, Gustafsson A-S, Carlsson A, Nilsson R, Knutson L, Forsell P, et al. The Effects of Food on the Dissolution of Poorly Soluble Drugs in Human and in Model Small Intestinal Fluids. Pharmaceutical Research 2005 2005/12/01;22(12):2141-51.
18. Lysik MA, Wu-Pong S. Innovations in oligonucleotide drug delivery. Journal of Pharmaceutical Sciences 2003;92(8):1559-73.
19. Juzenas P, Chen W, Sun Y-P, Coelho MAN, Generalov R, Generalova N, et al. Quantum dots and nanoparticles for photodynamic and radiation therapies of cancer. Advanced Drug Delivery Reviews 2008;60(15):1600-14.
20. Ghosh P, Han G, De M, Kim CK, Rotello VM. Gold nanoparticles in delivery applications. Advanced Drug Delivery Reviews 2008;60(11):1307-15.
21. Wang AZ, Langer R, Farokhzad OC. Nanoparticle Delivery of Cancer Drugs. Annual Review of Medicine 2012;63(1):185-98.
22. Iyer AK, Khaled G, Fang J, Maeda H. Exploiting the enhanced permeability and retention effect for tumor targeting. Drug Discovery Today 2006;11(17–18):812-18.
23. Zhao M, Hu B, Gu Z, Joo K-I, Wang P, Tang Y. Degradable polymeric nanocapsule for efficient intracellular delivery of a high molecular weight tumor-selective protein complex. Nano Today 2013;8(1):11-20.
24. Yang F, Jin C, Subedi S, Lee CL, Wang Q, Jiang Y, et al. Emerging inorganic nanomaterials for pancreatic cancer diagnosis and treatment. Cancer Treatment Reviews 2012;38(6):566-79.
25. Patel S, Bhirde AA, Rusling JF, Chen X, Gutkind JS, Patel V. Nano Delivers Big: Designing Molecular Missiles for Cancer Therapeutics. Pharmaceutics 2011;3(1):34-52.

26. Nitta S, Numata K. Biopolymer-Based Nanoparticles for Drug/Gene Delivery and Tissue Engineering. International Journal of Molecular Sciences 2013;14(1):1629-54.
27. Maeda H, Wu J, Sawa T, Matsumura Y, Hori K. Tumor vascular permeability and the EPR effect in macromolecular therapeutics: a review. J Control Release 2000;65(1-2):271-84.
28. Nishida N, Yano H, Nishida T, Kamura T, Kojiro M. Angiogenesis in cancer. Vasc Health Risk Manag 2006;2(3):213-9.
29. Bartczak D, Muskens OL, Sanchez-Elsner T, Kanaras AG, Millar TM. Manipulation of in Vitro Angiogenesis Using Peptide-Coated Gold Nanoparticles. ACS Nano 2013 2013/06/25;7(6):5628-36.
30. Jain RK, Stylianopoulos T. Delivering nanomedicine to solid tumors. Nat Rev Clin Oncol 2010;7(11):653-64.
31. Banerjee D, Harfouche R, Sengupta S. Nanotechnology-mediated targeting of tumor angiogenesis. Vasc Cell 2011 2011/01/31;3(1):1-13.
32. Yoo SY, Kwon SM. Angiogenesis and Its Therapeutic Opportunities. Mediators of Inflammation 2013;2013:11.
33. Jang SH, Wientjes MG, Lu D, Au JL. Drug delivery and transport to solid tumors. Pharmaceutical Research 2003;20(9):1337-50.
34. Gao H, Yang Z, Zhang S, Cao S, Shen S, Pang Z, et al. Ligand modified nanoparticles increases cell uptake, alters endocytosis and elevates glioma distribution and internalization. Sci Rep 2013;3(2534).
35. dos Santos T, Varela J, Lynch I, Salvati A, Dawson KA. Effects of transport inhibitors on the cellular uptake of carboxylated polystyrene nanoparticles in different cell lines. PLoS ONE 2011;6(9):19.
36. Verma A, Stellacci F. Effect of Surface Properties on Nanoparticle–Cell Interactions. Small 2010;6(1):12-21.
37. Kim JA, Åberg C, Salvati A, Dawson KA. Role of cell cycle on the cellular uptake and dilution of nanoparticles in a cell population. Nat Nanotechnol 2012;7(1):62-68.
38. Geiser M, Quaile O, Wenk A, Wigge C, Eigeldinger-Berthou S, Hirn S, et al. Cellular uptake and localization of inhaled gold nanoparticles in lungs of mice with chronic obstructive pulmonary disease. Part Fibre Toxicol 2013 2013/05/16;10(1):1-10.
39. Abulateefeh SR, Spain SG, Thurecht KJ, Aylott JW, Chan WC, Garnett MC, et al. Enhanced uptake of nanoparticle drug carriers via a thermoresponsive shell enhances cytotoxicity in a cancer cell line. Biomaterials Science 2013;1(4):434-42.
40. Singh J, Michel D, Chitanda J, Verrall R, Badea I. Evaluation of cellular uptake and intracellular trafficking as determining factors of gene

expression for amino acid-substituted gemini surfactant-based DNA nanoparticles. Journal of nanobiotechnology 2012;10(1):7.
41. Paciotti GF, Myer L, Weinreich D, Goia D, Pavel N, McLaughlin RE, et al. Colloidal gold: a novel nanoparticle vector for tumor directed drug delivery. Drug Deliv 2004;11(3):169-83.
42. Barraud L, Merle P, Soma E, Lefrançois L, Guerret S, Chevallier M, et al. Increase of doxorubicin sensitivity by doxorubicin-loading into nanoparticles for hepatocellular carcinoma cells in vitro and in vivo. Journal of Hepatology 2005;42(5):736-43.
43. Perez AT, Domenech GH, Frankel C, Vogel CL. Pegylated liposomal doxorubicin (Doxil) for metastatic breast cancer: the Cancer Research Network, Inc., experience. Cancer Invest 2002;2:22-9.
44. Cheng F-Y, Su C-H, Wu P-C, Yeh C-S. Multifunctional polymeric nanoparticles for combined chemotherapeutic and near-infrared photothermal cancer therapy in vitro and in vivo. Chemical Communications 2010;46(18):3167-69.
45. Koziara JM, Lockman PR, Allen DD, Mumper RJ. Paclitaxel nanoparticles for the potential treatment of brain tumors. Journal of Controlled Release 2004;99(2):259-69.
46. Parveen S, Mitra M, Krishnakumar S, Sahoo SK. Enhanced antiproliferative activity of carboplatin-loaded chitosan-alginate nanoparticles in a retinoblastoma cell line. Acta Biomater 2010;6(8):3120-31.
47. Singh M, Chakrapani A, O'Hagan D. Nanoparticles and microparticles as vaccine-delivery systems. Expert Rev Vaccines 2007;6(5):797-808.
48. Janssen Products L. DOXIL® (doxorubicin HCl liposome injection) 2013 [cited; Available from: http://www.doxil.com/#isi
49. Center ULCC. Doxorubicin Hydrochloride Liposome and Bortezomib in Treating Patients With Refractory Hematologic Cancer or Malignant Solid Tumor or Metastatic Breast Cancer. 2012.
50. Johnson & Johnson Pharmaceutical Research & Development L. A Study of Docetaxel Monotherapy or DOXIL and Docetaxel in Patients With Advanced Breast Cancer. 2013.
51. Medicine NYUSo. Pharmacokinetic Study of Avastin and Doxil in Ovarian Cancer. 2012.
52. Medicine WUSo. Liposomal Doxorubicin and PSC 833 in Treating Patients With AIDS-Related Kaposi's Sarcoma or Other Advanced Cancers. 2013.
53. Pharma B. Livatag®. 2013 [cited 2013; Available from: http://www.bioalliancepharma.com/en/category/medias-4/communiques-de-presse/livatag/

54. Blackwell K. Temperature-Sensitive Liposomal Doxorubicin and Hyperthermia in Treating Women With Locally Recurrent Breast Cancer. 2013.
55. Celsion. A Study of ThermoDox™ in Combination With Radiofrequency Ablation (RFA) in Primary and Metastatic Tumors of the Liver. 2009.
56. Nakanishi T, Fukushima S, Okamoto K, Suzuki M, Matsumura Y, Yokoyama M, et al. Development of the polymer micelle carrier system for doxorubicin. J Control Release 2001;74(1-3):295-302.
57. Matsumura Y, Hamaguchi T, Ura T, Muro K, Yamada Y, Shimada Y, et al. Phase I clinical trial and pharmacokinetic evaluation of NK911, a micelle-encapsulated doxorubicin. Br J Cancer 2004;91(10):1775-81.
58. Corporation C. ABRAXANE (paclitaxel protein-bound particles for injectable suspension. 2013 [cited 2013; Available from: http://www.abraxane.com/
59. Corporation C. Study of Dose-dense Adriamycin Plus Cytoxan (AC) Followed by Either ABI-007 (Abraxane) or Taxol With Bevacizumab as Adjuvant Therapy for Patients With Breast Cancer. 2013.
60. (NCI) NCI. Paclitaxel, Bevacizumab And Adjuvant Intraperitoneal Carboplatin in Treating Patients Who Had Initial Debulking Surgery for Stage II, Stage III, or Stage IV Ovarian Epithelial, Primary Peritoneal, or Fallopian Tube Cancer. 2013.
61. (NCI) NCI. Carboplatin, Paclitaxel, and Radiation Therapy With or Without Thalidomide in Patients With Stage III Non-small Cell Lung Cancer. 2013.
62. Group S. Genexol-PM. 2007 [cited 2013; Available from: http://www.evaluategroup.com/Universal/View.aspx?type=Story&id=267402
63. Lee KS, Chung HC, Im SA, Park YH, Kim CS, Kim SB, et al. Multicenter phase II trial of Genexol-PM, a Cremophor-free, polymeric micelle formulation of paclitaxel, in patients with metastatic breast cancer. Breast Cancer Res Treat 2008;108(2):241-50.
64. Werner ME, Cummings ND, Sethi M, Wang EC, Sukumar R, Moore DT, et al. Preclinical evaluation of Genexol-PM, a nanoparticle formulation of paclitaxel, as a novel radiosensitizer for the treatment of non-small cell lung cancer. Int J Radiat Oncol Biol Phys 2013;86(3):463-8.
65. Koziara JM, Oh JJ, Akers WS, Ferraris SP, Mumper RJ. Blood compatibility of cetyl alcohol/polysorbate-based nanoparticles. Pharm Res 2005;22(11):1821-8.
66. (CC) NIoHCC. TNF-Bound Colloidal Gold in Treating Patients With Advanced Solid Tumors. 2012.

67. (CC) NIoHCC. Tumor Necrosis Factor in Patients Undergoing Surgery for Primary Cancer or Metastatic Cancer. 2012.
68. Sciences C. AURIMUNE™ (CYT-6091). 2013 [cited; Available from: http://www.cytimmune.com/go.cfm?do=page.view&pid=26
69. Kelsen DP, Martin D, O'Neil J, Schwartz G, Saltz L, Sung MT, et al. Phase I trial of PN401, an oral prodrug of uridine, to prevent toxicity from fluorouracil in patients with advanced cancer. J Clin Oncol 1997;15(4):1511-7.
70. Nanocarrier Co. L. NC-6004(Nanoplatin) and Gemcitabine to Treat Pancreatic Cancer in Asia. 2013.
71. nanocarrier Co. L. NC-6004 Nanoplatin. 2013 [cited 2013; Available from: http://www.nanocarrier.co.jp/en/research/pipeline/02.html
72. Corporation SB. A Trial to Determine the Maximum Tolerated Dose and Evaluate the Safety and Pharmacokinetics of Docetaxel-PNP, Polymeric Nanoparticle Formulation of Docetaxel, in Subjects With Advanced Solid Malignancies. 2010.
73. FDA approves DaunoXome as first-line therapy for Kaposi's sarcoma. Food and Drug Administration: J Int Assoc Physicians AIDS Care. 1996 May;2(5):50-1.
74. Brigger I, Dubernet C, Couvreur P. Nanoparticles in cancer therapy and diagnosis. Advanced Drug Delivery Reviews 2002;54(5):631-51.
75. Koziara JM, Whisman TR, Tseng MT, Mumper RJ. In-vivo efficacy of novel paclitaxel nanoparticles in paclitaxel-resistant human colorectal tumors. J Control Release 2006;112(3):312-9.
76. Gu Y-J, Cheng J, Man CW-Y, Wong W-T, Cheng SH. Gold-doxorubicin nanoconjugates for overcoming multidrug resistance. Nanomedicine: Nanotechnology, Biology and Medicine 2012;8(2):204-11.
77. Brown SD, Nativo P, Smith J-A, Stirling D, Edwards PR, Venugopal B, et al. Gold Nanoparticles for the Improved Anticancer Drug Delivery of the Active Component of Oxaliplatin. Journal of the American Chemical Society 2010 2010/04/07;132(13):4678-84.
78. Jelveh S, Chithrani DB. Gold Nanostructures as a Platform for Combinational Therapy in Future Cancer Therapeutics. Cancers 2011;3(1):1081-110.
79. Sonntag Cv. The chemical basis of radiation biology. London; Philadelphia, PA: Taylor & Francis, 1989.
80. Butterworth KT, Coulter JA, Jain S, Forker J, McMahon SJ, Schettino G, et al. Evaluation of cytotoxicity and radiation enhancement using 1.9 nm gold particles: potential application for cancer therapy. Nanotechnology 2010;21(29):0957-4484.

81. Carter JD, Cheng NN, Qu Y, Suarez GD, Guo T. Nanoscale Energy Deposition by X-ray Absorbing Nanostructures. The Journal of Physical Chemistry B 2007 2007/10/01;111(40):11622-25.
82. Rahman WN, Bishara N, Ackerly T, He CF, Jackson P, Wong C, et al. Enhancement of radiation effects by gold nanoparticles for superficial radiation therapy. Nanomedicine: Nanotechnology, Biology and Medicine 2009;5(2):136-42.
83. Kong T, Zeng J, Wang X, Yang X, Yang J, McQuarrie S, et al. Enhancement of radiation cytotoxicity in breast-cancer cells by localized attachment of gold nanoparticles. Small 2008;4(9):1537-43.
84. Hainfeld JF, Dilmanian FA, Slatkin DN, Smilowitz HM. Radiotherapy enhancement with gold nanoparticles. Journal of Pharmacy and Pharmacology 2008;60(8):977-85.
85. Minelli C, Lowe SB, Stevens MM. Engineering Nanocomposite Materials for Cancer Therapy. Small 2010;6(21):2336-57.
86. Xia Y, Li W, Cobley CM, Chen J, Xia X, Zhang Q, et al. Gold nanocages: from synthesis to theranostic applications. Acc Chem Res 2011;44(10):914-24.
87. Duncan B, Kim C, Rotello VM. Gold nanoparticle platforms as drug and biomacromolecule delivery systems. Journal of Controlled Release 2010;148(1):122-27.
88. Tao AR, Habas S, Yang P. Shape Control of Colloidal Metal Nanocrystals. Small 2008;4(3):310-25.
89. Daniel M-C, Astruc D. Gold Nanoparticles: Assembly, Supramolecular Chemistry, Quantum-Size-Related Properties, and Applications toward Biology, Catalysis, and Nanotechnology. Chemical Reviews 2003;104(1):293-346.
90. Patra CR, Bhattacharya R, Wang E, Katarya A, Lau JS, Dutta S, et al. Targeted Delivery of Gemcitabine to Pancreatic Adenocarcinoma Using Cetuximab as a Targeting Agent. Cancer Research 2008 March 15, 2008;68(6):1970-78.
91. Giljohann DA, Seferos DS, Daniel WL, Massich MD, Patel PC, Mirkin CA. Gold nanoparticles for biology and medicine. Angew Chem Int Ed Engl 2010;49(19):3280-94.
92. Hainfeld JF, Slatkin DN, Focella TM, Smilowitz HM. Gold nanoparticles: a new X-ray contrast agent. British Journal of Radiology 2006 March 1, 2006;79(939):248-53.
93. Bhattacharya R, Patra CR, Earl A, Wang S, Katarya A, Lu L, et al. Attaching folic acid on gold nanoparticles using noncovalent interaction via different polyethylene glycol backbones and targeting of cancer cells. Nanomedicine : nanotechnology, biology, and medicine 2007;3(3):224-38.

94. Goulet PJG, Lennox RB. New Insights into Brust–Schiffrin Metal Nanoparticle Synthesis. Journal of the American Chemical Society 2010 2010/07/21;132(28):9582-84.
95. Frens G. Controlled nucleation for regulation of particle-size in monodisperse gold suspensions. Nature-Physical Science 1973;241(105).
96. Turkevich J, Stevenson PC, Hillier J. A study of the nucleation and growth processes in the synthesis of colloidal gold. Discussions of the Faraday Society 1951;11:55-75.
97. Cho EC, Xie J, Wurm PA, Xia Y. Understanding the role of surface charges in cellular adsorption versus internalization by selectively removing gold nanoparticles on the cell surface with a I2/KI etchant. Nano Lett 2009;9(3):1080-4.
98. Ferrari M. Nanogeometry: beyond drug delivery: Nat Nanotechnol. 2008 Mar;3(3):131-2. doi: 10.1038/nnano.2008.46.
99. Zhu Z-J, Ghosh PS, Miranda OR, Vachet RW, Rotello VM. Multiplexed Screening of Cellular Uptake of Gold Nanoparticles Using Laser Desorption/Ionization Mass Spectrometry. Journal of the American Chemical Society 2008 2008/10/29;130(43):14139-43.
100. Gratton SEA, Ropp PA, Pohlhaus PD, Luft JC, Madden VJ, Napier ME, et al. The effect of particle design on cellular internalization pathways. Proceedings of the National Academy of Sciences 2008 August 19, 2008;105(33):11613-18.
101. Chithrani BD, Ghazani AA, Chan WC. Determining the size and shape dependence of gold nanoparticle uptake into mammalian cells. Nano Lett 2006;6(4):662-8.
102. Wang J, Yue Y, Chen G, Xia J. Protease-promoted drug delivery using peptide-functionalized gold nanoparticles. Soft Matter 2011;7(16):7217-22.
103. Sandhu KK, McIntosh CM, Simard JM, Smith SW, Rotello VM. Gold Nanoparticle-Mediated Transfection of Mammalian Cells. Bioconjugate Chemistry 2001 2002/01/01;13(1):3-6.
104. Muthu MS, Singh S. Targeted nanomedicines: effective treatment modalities for cancer, AIDS and brain disorders. Nanomedicine 2008 2009/01/01;4(1):105-18.
105. Vigderman L, Zubarev ER. Therapeutic platforms based on gold nanoparticles and their covalent conjugates with drug molecules. Adv Drug Deliv Rev 2012;18:18.
106. Yeh Y-C, Creran B, Rotello VM. Gold nanoparticles: preparation, properties, and applications in bionanotechnology. Nanoscale 2012;4(6):1871-80.

107. Zhang X-Q, Xu X, Lam R, Giljohann D, Ho D, Mirkin CA. Strategy for Increasing Drug Solubility and Efficacy through Covalent Attachment to Polyvalent DNA–Nanoparticle Conjugates. ACS Nano 2011 2011/09/27;5(9):6962-70.
108. Wang F, Wang Y-C, Dou S, Xiong M-H, Sun T-M, Wang J. Doxorubicin-Tethered Responsive Gold Nanoparticles Facilitate Intracellular Drug Delivery for Overcoming Multidrug Resistance in Cancer Cells. ACS Nano 2011 2011/05/24;5(5):3679-92.
109. Patra CR, Bhattacharya R, Mukhopadhyay D, Mukherjee P. Fabrication of gold nanoparticles for targeted therapy in pancreatic cancer. Advanced Drug Delivery Reviews 2010;62(3):346-61.
110. Cai Weibo GT, Hong Hao, Sun Jiangtao. Applications of gold nanoparticles in cancer nanotechnology. Nanotechnology, Science and Applications 2008;1:17-32.
111. Glazer ES, Zhu C, Massey KL, Thompson CS, Kaluarachchi WD, Hamir AN, et al. Noninvasive radiofrequency field destruction of pancreatic adenocarcinoma xenografts treated with targeted gold nanoparticles. Clin Cancer Res 2010;16(23):5712-21.
112. Huang X, Qian W, El-Sayed IH, El-Sayed MA. The potential use of the enhanced nonlinear properties of gold nanospheres in photothermal cancer therapy. Lasers Surg Med 2007;39(9):747-53.
113. Libutti SK, Paciotti GF, Byrnes AA, Alexander HR, Jr., Gannon WE, Walker M, et al. Phase I and pharmacokinetic studies of CYT-6091, a novel PEGylated colloidal gold-rhTNF nanomedicine. Clin Cancer Res 2010;16(24):6139-49.
114. Yang YY, Wang Y, Powell R, Chan P. Polymeric core-shell nanoparticles for therapeutics. Clin Exp Pharmacol Physiol 2006;33(5-6):557-62.
115. Saravanakumar G, Jo DG, Park JH. Polysaccharide-based nanoparticles: a versatile platform for drug delivery and biomedical imaging. Curr Med Chem 2012;19(19):3212-29.
116. Panyam J, Labhasetwar V. Biodegradable nanoparticles for drug and gene delivery to cells and tissue. Adv Drug Deliv Rev 2003;55(3):329-47.
117. Vila A, Sánchez A, Tobío M, Calvo P, Alonso MJ. Design of biodegradable particles for protein delivery. Journal of Controlled Release 2002;78(1–3):15-24.
118. Mu L, Feng SS. A novel controlled release formulation for the anticancer drug paclitaxel (Taxol): PLGA nanoparticles containing vitamin E TPGS. J Control Release 2003;86(1):33-48.
119. Duncan R. The dawning era of polymer therapeutics. Nat Rev Drug Discov 2003;2(5):347-60.

120. Goodarzi N, Varshochian R, Kamalinia G, Atyabi F, Dinarvand R. A review of polysaccharide cytotoxic drug conjugates for cancer therapy. Carbohydrate Polymers 2013;92(2):1280-93.
121. Singer JW, Bhatt R, Tulinsky J, Buhler KR, Heasley E, Klein P, et al. Water-soluble poly-(L-glutamic acid)-Gly-camptothecin conjugates enhance camptothecin stability and efficacy in vivo. J Control Release 2001;74(1-3):243-7.
122. Sinha VR, Kumria R. Polysaccharides in colon-specific drug delivery. International Journal of Pharmaceutics 2001;224(1-2):19-38.
123. Liu Z, Jiao Y, Wang Y, Zhou C, Zhang Z. Polysaccharides-based nanoparticles as drug delivery systems. Advanced Drug Delivery Reviews 2008;60(15):1650-62.
124. Boddohi S, Moore N, Johnson PA, Kipper MJ. Polysaccharide-based polyelectrolyte complex nanoparticles from chitosan, heparin, and hyaluronan. Biomacromolecules 2009;10(6):1402-9.
125. Sun W, Mao S, Mei D, Kissel T. Self-assembled polyelectrolyte nanocomplexes between chitosan derivatives and enoxaparin. European Journal of Pharmaceutics and Biopharmaceutics 2008;69(2):417-25.
126. Il'ina AV, Varlamov VP. Chitosan-based polyelectrolyte complexes: a review. Prikladnaia biokhimiia i mikrobiologiia 2005;41(1):9-16.
127. Agnihotri SA, Mallikarjuna NN, Aminabhavi TM. Recent advances on chitosan-based micro- and nanoparticles in drug delivery. Journal of Controlled Release 2004;100(1):5-28.
128. Harish Prashanth KV, Tharanathan RN. Depolymerized products of chitosan as potent inhibitors of tumor-induced angiogenesis. Biochimica et Biophysica Acta 2005;11(1):22-9.
129. Lehr C-M, Bouwstra JA, Schacht EH, Junginger HE. In vitro evaluation of mucoadhesive properties of chitosan and some other natural polymers. Int J Pharm 1992;78(1–3):43-48.
130. Avadi MR, Sadeghi AMM, Mohamadpour Dounighi N, Dinarvand R, Atyabi F, Rafiee-Tehrani M. Ex vivo evaluation of insulin nanoparticles using chitosan and arabic gum, 2011.
131. Islam AM, Phillips GO, Sljivo A, Snowden MJ, Williams PA. A review of recent developments on the regulatory, structural and functional aspects of gum arabic. Food Hydrocolloids 1997;11(4):493-505.
132. Liu C-P, Lin F-S, Chien C-T, Tseng S-Y, Luo C-W, Chen C-H, et al. In-situ Formation and Assembly of Gold Nanoparticles by Gum Arabic as Efficient Photothermal Agent for Killing Cancer Cells. Macromolecular Bioscience 2013:n/a-n/a.
133. Effiong U, Williams D, Otto W, Anderson W. Gum Arabic surface-modified magnetic nanoparticles for cancer therapy. Bioengineering

Conference, 2004 Proceedings of the IEEE 30th Annual Northeast; 2004 17-18 April 2004; 2004. p. 243-44.
134. Avadi MR, Sadeghi AMM, Mohammadpour N, Abedin S, Atyabi F, Dinarvand R, et al. Preparation and characterization of insulin nanoparticles using chitosan and Arabic gum with ionic gelation method. Nanomedicine : nanotechnology, biology, and medicine 2010;6(1):58-63.
135. Fonseca C, Simões S, Gaspar R. Paclitaxel-loaded PLGA nanoparticles: preparation, physicochemical characterization and in vitro anti-tumoral activity. Journal of Controlled Release 2002;83(2):273-86.
136. Yang H, Li K, Liu Y, Liu Z, Miyoshi H. Poly(D,L-lactide-co-glycolide) nanoparticles encapsulated fluorescent isothiocyanate and paclitaxol: preparation, release kinetics and anticancer effect. J Nanosci Nanotechnol 2009;9(1):282-7.
137. Su Young Chae CYC, Mi Kyeong Jang, Teok Rae Jung, Jae-Woon Nah, inventor Anti-cancer agent loaded hydrophobic bile acid conjugated hydrophilic chitosan oligosaccharide nanoparticles and preparation method thereof. 2007.
138. Sahu SK, Maiti S, Maiti TK, Ghosh SK, Pramanik P. Hydrophobically modified carboxymethyl chitosan nanoparticles targeted delivery of paclitaxel. J Drug Target 2011;19(2):104-13.
139. Kimling J, Maier M, Okenve B, Kotaidis V, Ballot H, Plech A. Turkevich Method for Gold Nanoparticle Synthesis Revisited. The Journal of Physical Chemistry B 2006;110(32):15700-07.
140. Baptista P, Doria G, Henriques D, Pereira E, Franco R. Colorimetric detection of eukaryotic gene expression with DNA-derivatized gold nanoparticles. J Biotechnol 2005;119(2):111-7.
141. Holoubek J. Some applications of light scattering in materials science. Journal of Quantitative Spectroscopy and Radiative Transfer;106(1-3):104-21.
142. Schärtl W. Light scattering from polymer solutions and nanoparticle dispersions: Springer Laboratory, 2001.
143. Hosokawa M. Nanoparticle technology handbook: Elsevier, 2007.
144. David Bernard Williams CBC. Transmission electron microscopy: a textbook for materials science. Basics, Part 1. 2nd ed: Springer, 2009.
145. Illum L, Jabbal-Gill I, Hinchcliffe M, Fisher AN, Davis SS. Chitosan as a novel nasal delivery system for vaccines. Advanced Drug Delivery Reviews 2001;51(1-3):81-96.
146. BLANCHARD CR. Atomic Force Microscopy. Springer 1996;1(5).
147. Pier Carlo Braga DR. Atomic force microscopy: biomedical methods and applications: Humana Press, 2004.

148. Bharat Bhushan HF. Applied Scanning Probe Methods: Characterization: Springer, 2006.
149. Dietler BCG. Force-distance curves by atomic force microscopy. Surface Science Reports 1999;34.
150. Fluorescence Tutorials. 2011 [cited 2011; Available from: http://probes.invitrogen.com/resources/education/tutorials/1Intro/player.html
151. Iain Johnson MTZS. The Molecular Probes® Handbook—A Guide to Fluorescent Probes and Labeling Technologies 11th ed.
152. Harris DC. Exploring chemical analysis: W.H. Freeman, 2004.
153. Silva HMAR. Espectroscopia no infravermelho por transformada de Fourier (FTIR). Fundamentos e aplicação na caracterização de materiais de construção: LNEC, 2007.
154. Oliveira MA, Ciarlini PC, Feitosa JPA, de Paula RCM, Paula HCB. Chitosan/"angico" gum nanoparticles: Synthesis and characterization. Materials Science and Engineering: C 2009;29(2):448-51.
155. Ebnesajjad S. Surface Treatment of Materials for Adhesion Bonding. William Andrew Publishing 2006.
156. Peter R. Griffiths JADH. Fourier Transform Infrared Spectrometry: Wiley-Interscience, 2007.
157. Hideshima T, Richardson P, Chauhan D, Palombella VJ, Elliott PJ, Adams J, et al. The Proteasome Inhibitor PS-341 Inhibits Growth, Induces Apoptosis, and Overcomes Drug Resistance in Human Multiple Myeloma Cells. Cancer Research 2001 April 1, 2001;61(7):3071-76.
158. Espinosa-Andrews H, Baez-Gonzalez JG, Cruz-Sosa F, Vernon-Carter EJ. Gum arabic−chitosan complex coacervation. Biomacromolecules 2007;8(4):1313-18.
159. Nanoparticles for enhanced x-ray treatment of cancer tumors. 2009 [cited 2011 June 2011]; Available from: http://www.understandingnano.com/nanomedicine-nanoparticle-xray-cancer-treatment.html
160. Cancer Treatments: Radiation Therapy. 2001 [cited 2011 June 2011]; Available from: http://www.livingwellwithcancer.com/index.html
161. Martínez A, González C, Porras M, Gutiérrez JM. Nano-sized latex particles obtained by emulsion polymerization using an amphiphilic block copolymer as surfactant. Colloids and Surfaces A: Physicochemical and Engineering Aspects 2005;270-271:67-71.
162. Ngwa W, Makrigiorgos GM, Berbeco RI. Gold nanoparticle-aided brachytherapy with vascular dose painting: estimation of dose enhancement to the tumor endothelial cell nucleus. Med Phys 2012;39(1):392-8.

163. Ngwa W, Korideck H, Kassis AI, Kumar R, Sridhar S, Makrigiorgos GM, et al. In vitro radiosensitization by gold nanoparticles during continuous low-dose-rate gamma irradiation with I-125 brachytherapy seeds. Nanomedicine 2013;9(1):25-7.
164. Cho SH, Jones BL, Krishnan S. The dosimetric feasibility of gold nanoparticle-aided radiation therapy (GNRT) via brachytherapy using low-energy gamma-/x-ray sources. Phys Med Biol 2009;54(16):4889-905.
165. Hainfeld JF, Slatkin DN, Smilowitz HM. The use of gold nanoparticles to enhance radiotherapy in mice. Physics in Medicine and Biology 2004;49(18):N309.
166. Hainfeld JF, Dilmanian FA, Zhong Z, Slatkin DN, Kalef-Ezra JA, Smilowitz HM. Gold nanoparticles enhance the radiation therapy of a murine squamous cell carcinoma. Physics in Medicine and Biology 2010;55(11):3045.
167. Finlay GJ, Baguley BC, Wilson WR. A semiautomated microculture method for investigating growth inhibitory effects of cytotoxic compounds on exponentially growing carcinoma cells. Analytical Biochemistry 1984;139(2):272-7.
168. Dent MF, Hubbold L, Radford H, Wilson AP. The methylene blue colorimetric microassay for determining cell line response to growth factors. Cytotechnology 1995;17(1):27-33.
169. Vichai V, Kirtikara K. Sulforhodamine B colorimetric assay for cytotoxicity screening. Nat Protoc 2006;1(3):1112-6.
170. Skehan P, Storeng R, Scudiero D, Monks A, McMahon J, Vistica D, et al. New Colorimetric Cytotoxicity Assay for Anticancer-Drug Screening. Journal of the National Cancer Institute 1990 July 4, 1990;82(13):1107-12.
171. Monks A, Scudiero D, Skehan P, Shoemaker R, Paull K, Vistica D, et al. Feasibility of a High-Flux Anticancer Drug Screen Using a Diverse Panel of Cultured Human Tumor Cell Lines. Journal of the National Cancer Institute 1991 June 5, 1991;83(11):757-66.
172. Boccadoro M, Morgan G, Cavenagh J. Preclinical evaluation of the proteasome inhibitor bortezomib in cancer therapy. Cancer Cell Int 2005 2005/06/01;5(1):1-9.
173. Adams J, Palombella VJ, Sausville EA, Johnson J, Destree A, Lazarus DD, et al. Proteasome Inhibitors: A Novel Class of Potent and Effective Antitumor Agents. Cancer Research 1999 June 1, 1999;59(11):2615-22.
174. An J, Sun Y-P, Adams J, Fisher M, Belldegrun A, Rettig MB. Drug Interactions between the Proteasome Inhibitor Bortezomib and Cytotoxic Chemotherapy, Tumor Necrosis Factor (TNF) α, and TNF-Related Apoptosis-Inducing Ligand in Prostate Cancer. Clinical Cancer Research 2003 October 1, 2003;9(12):4537-45.

175. Goktas S, Baran Y, Ural AU, Yazici S, Aydur E, Basal S, et al. Proteasome Inhibitor Bortezomib Increases Radiation Sensitivity in Androgen Independent Human Prostate Cancer Cells. Urology 2010;75(4):793-98.
176. Whang PG, Gamradt SC, Gates JJ, Lieberman JR. Effects of the proteasome inhibitor bortezomib on osteolytic human prostate cancer cell metastases. Prostate Cancer Prostatic Dis 2005;8(4):327-34.
177. Rocha S, Generalov R, Pereira MdC, Peres I, Juzenas P, Coelho MAN. Epigallocatechin gallate-loaded polysaccharide nanoparticles for prostate cancer chemoprevention. Nanomedicine 2011;6(1):79-87.
178. Stone J, Jackson S, Wright D. Biological applications of gold nanorods. Wiley Interdisciplinary Reviews: Nanomedicine and Nanobiotechnology 2011;3(1):100-09.
179. Wen J, Betty YSK, James TR, Warren CWC. Nanoparticle-mediated cellular response is size-dependent. Nature Nanotechnology 2008;3(3):145-50.
180. Manju S, Sreenivasan K. Gold nanoparticles generated and stabilized by water soluble curcumin-polymer conjugate: blood compatibility evaluation and targeted drug delivery onto cancer cells. Journal of Colloid and Interface Science 2012;368(1):144-51.
181. Huang H-C, Barua S, Sharma G, Dey SK, Rege K. Inorganic nanoparticles for cancer imaging and therapy. Journal of Controlled Release 2011;155(3):344-57.
182. Arnida, Malugin A, Ghandehari H. Cellular uptake and toxicity of gold nanoparticles in prostate cancer cells: a comparative study of rods and spheres. Journal of Applied Toxicology 2010;30(3):212-17.
183. Patra CR, Verma R, Kumar S, Greipp PR, Mukhopadhyay D, Mukherjee P. Fabrication of Gold Nanoparticle for Potential Application in Multiple Myeloma. Journal of Biomedical Nanotechnology 2008;4(4):499-507.
184. Qian W, Murakami M, Ichikawa Y, Che Y. Highly Efficient and Controllable PEGylation of Gold Nanoparticles Prepared by Femtosecond Laser Ablation in Water. The Journal of Physical Chemistry C 2011 2011/12/01;115(47):23293-98.
185. Gu Y-J, Cheng J, Lin C-C, Lam YW, Cheng SH, Wong W-T. Nuclear penetration of surface functionalized gold nanoparticles. Toxicology and Applied Pharmacology 2009;237(2):196-204.
186. Liu Y, Shipton MK, Ryan J, Kaufman ED, Franzen S, Feldheim DL. Synthesis, Stability, and Cellular Internalization of Gold Nanoparticles Containing Mixed Peptide−Poly(ethylene glycol) Monolayers. Analytical chemistry 2007 2007/03/01;79(6):2221-29.

187. Simpson CA, Agrawal AC, Balinski A, Harkness KM, Cliffel DE. Short-chain PEG mixed monolayer protected gold clusters increase clearance and red blood cell counts. ACS Nano 2011;5(5):3577-84.
188. Han G, Ghosh P, Rotello VM. Multi-functional gold nanoparticles for drug delivery. Adv Exp Med Biol 2007;620:48-56.
189. Khan JA, Kudgus RA, Szabolcs A, Dutta S, Wang E, Cao S, et al. Designing nanoconjugates to effectively target pancreatic cancer cells in vitro and in vivo. PLoS ONE 2011;6(6):27.
190. Cho EC, Zhang Q, Xia Y. The effect of sedimentation and diffusion on cellular uptake of gold nanoparticles. Nat Nanotechnol 2011;6(6):385-91.
191. Connor EE, Mwamuka J, Gole A, Murphy CJ, Wyatt MD. Gold Nanoparticles Are Taken Up by Human Cells but Do Not Cause Acute Cytotoxicity. Small 2005;1(3):325-27.
192. Wang S-H, Lee C-W, Chiou A, Wei P-K. Size-dependent endocytosis of gold nanoparticles studied by three-dimensional mapping of plasmonic scattering images. Journal of nanobiotechnology 2010;8(1):33.
193. Brandenberger C, Muhlfeld C, Ali Z, Lenz AG, Schmid O, Parak WJ, et al. Quantitative evaluation of cellular uptake and trafficking of plain and polyethylene glycol-coated gold nanoparticles. Small 2010;6(15):1669-78.
194. Garnett MC, Kallinteri P. Nanomedicines and nanotoxicology: some physiological principles. Occupational Medicine 2006 August 1, 2006;56(5):307-11.
195. Lee J, Twomey M, Machado C, Gomez G, Doshi M, Gesquiere AJ, et al. Caveolae-mediated endocytosis of conjugated polymer nanoparticles. Macromol Biosci 2013;13(7):913-20.
196. Sinha R, Kim GJ, Nie S, Shin DM. Nanotechnology in cancer therapeutics: bioconjugated nanoparticles for drug delivery. Molecular Cancer Therapeutics 2006 August 1, 2006;5(8):1909-17.
197. Peres I, Rocha S, Loureiro J, Carmo Pereira M, Ivanova G, Coelho M. Carbohydrate particles as protein carriers and scaffolds: physico-chemical characterization and collagen stability. J Nanopart Res 2012 2012/09/01;14(9):1-11.
198. Liu J, Xu L, Liu C, Zhang D, Wang S, Deng Z, et al. Preparation and characterization of cationic curcumin nanoparticles for improvement of cellular uptake. Carbohydrate Polymers 2012;90(1):16-22.
199. Ruíz-Ramos JO, Pérez-Orozco JP, Báez-González JG, Bósquez-Molina E, Pérez-Alonso C, Vernon-Carter EJ. Interrelationship between the viscoelastic properties and effective moisture diffusivity of emulsions with the water vapor permeability of edible films stabilized by mesquite gum–chitosan complexes. Carbohydrate Polymers 2006;64(2):355-63.

200. Nam HY, Kwon SM, Chung H, Lee SY, Kwon SH, Jeon H, et al. Cellular uptake mechanism and intracellular fate of hydrophobically modified glycol chitosan nanoparticles. J Control Release 2009;135(3):259-67.
201. Yousefpour P, Atyabi F, Vasheghani-Farahani E, Movahedi AA, Dinarvand R. Targeted delivery of doxorubicin-utilizing chitosan nanoparticles surface-functionalized with anti-Her2 trastuzumab. Int J Nanomedicine 2011;6:1977-90.
202. Gomes JF, Rocha S, do Carmo Pereira M, Peres I, Moreno S, Toca-Herrera J, et al. Lipid/particle assemblies based on maltodextrin-gum arabic core as bio-carriers. Colloids Surf B Biointerfaces 2010;76(2):449-55.
203. Kim B, Han G, Toley BJ, Kim CK, Rotello VM, Forbes NS. Tuning payload delivery in tumour cylindroids using gold nanoparticles. Nat Nanotechnol 2010;5(6):465-72.
204. Choi S, Jang S, Park J, Jeong S, Park J, Ock K, et al. Cellular uptake and cytotoxicity of positively charged chitosan gold nanoparticles in human lung adenocarcinoma cells. J Nanopart Res 2012 2012/11/03;14(12):1-13.
205. Moschakis T, Murray BS, Biliaderis CG. Modifications in stability and structure of whey protein-coated o/w emulsions by interacting chitosan and gum arabic mixed dispersions. Food Hydrocolloids 2010;24(1):8-17.
206. Alvarez-Lorenzo C, Blanco-Fernandez B, Puga AM, Concheiro A. Crosslinked ionic polysaccharides for stimuli-sensitive drug delivery. Adv Drug Deliv Rev 2013;29(13):00101-4.
207. Coelho S, Moreno-Flores S, Toca-Herrera JL, Coelho MAN, Carmo Pereira M, Rocha S. Nanostructure of polysaccharide complexes. Journal of Colloid and Interface Science 2011;363(2):450-55.
208. Sanchez C, Mekhloufi G, Renard D. Complex coacervation between [beta]-lactoglobulin and Acacia gum: A nucleation and growth mechanism. Journal of Colloid and Interface Science 2006;299(2):867-73.
209. de Kruif CG, Weinbreck F, de Vries R. Complex coacervation of proteins and anionic polysaccharides. Current Opinion in Colloid & Interface Science 2004;9(5):340-49.
210. Turgeon SL, Schmitt C, Sanchez C. Protein-polysaccharide complexes and coacervates. Current Opinion in Colloid & Interface Science 2007;12(4-5):166-78.
211. Schmitt C, Sanchez C, Desobry-Banon S, Hardy J. Structure and technofunctional properties of protein-polysaccharide complexes: A review. Critical Reviews in Food Science and Nutrition 1998;38(8):689-753.
212. Stuart MAC. Supramolecular perspectives in colloid science. Colloid and Polymer Science 2008 Aug;286(8-9):855-64.

213. Dubin PL, Gao J, Mattison K. Protein-purification by selective phase-separation with polyelectrolytes. Separation and Purification Methods 1994;23(1):1-16.
214. Mattison KW, Brittain IJ, Dubin PL. Protein-polyelectrolyte phase boundaries. Biotechnology Progress 1995 Nov-Dec;11(6):632-37.
215. Wang YF, Gao JY, Dubin PL. Protein separation via polyelectrolyte coacervation: Selectivity and efficiency. Biotechnology Progress 1996 May-Jun;12(3):356-62.
216. Wen Yp, Dubin PL. Potentiometric Studies of the Interaction of Bovine Serum Albumin and Poly(dimethyldiallylammonium chloride). Macromolecules 1997;30(25):7856-61.
217. Mattison KW, Wang YF, Grymonpre K, Dubin PL. Micro- and macro-phase behavior in protein-polyelectrolyte complexes. Macromolecular Symposia 1999 May;140:53-76.
218. Kaibara K, Okazaki T, Bohidar HB, Dubin PL. pH-induced coacervation in complexes of bovine serum albumin and cationic polyelectrolytes. Biomacromolecules 2000 Spr;1(1):100-07.
219. Weinbreck F, de Vries R, Schrooyen P, de Kruif CG. Complex Coacervation of Whey Proteins and Gum Arabic. Biomacromolecules 2003;4(2):293-303.
220. Schmitt C, Sanchez C, Thomas F, Hardy J. Complex coacervation between beta-lactoglobulin and acacia gum in aqueous medium. Food Hydrocolloids 1999 Nov;13(6):483-96.
221. Schatz C, Lucas J-M, Viton C, Domard A, Pichot C, Delair T. Formation and properties of positively charged colloids based on polyelectrolyte complexes of biopolymers. Langmuir 2004;20(18):7766-78.
222. Burgess DJ, Singh ON. Spontaneous formation of small-sized albumin acacia coacervate particles. Journal of Pharmacy and Pharmacology 1993 Jul;45(7):586-91.
223. Biesheuvel PM, Cohen Stuart MA. Cylindrical cell model for the electrostatic free energy of polyelectrolyte complexes. Langmuir 2004;20(11):4764-70.
224. Wolfert MA, Dash PR, Nazarova O, Oupicky D, Seymour LW, Smart S, et al. Polyelectrolyte Vectors for Gene Delivery: Influence of Cationic Polymer on Biophysical Properties of Complexes Formed with DNA. Bioconjugate Chemistry 1999;10(6):993-1004.
225. Sanchez C, Mekhloufi G, Schmitt C, Renard D, Robert P, Lehr CM, et al. Self-assembly of β-lactoglobulin and acacia gum in aqueous solvent: Structure and phase-ordering kinetics. Langmuir 2002;18(26):10323-33.

226. Dautzenberg H, Polyelectrolyte complex formation in highly aggregating systems: Methodical aspects and general tendencies. . In: Radeva T., Physical Chemistry of Polyelectrolytes. New York, USA., 2001.
227. Thünemann AF, Muller M, Dautzenberg H, Joanny JFO, Lowne H. Polyelectrolyte complexes. Adv Polym Sci 2004;166:113-71.
228. Kiriy A, Yu J, Stamm M. Interpolyelectrolyte complexes: A Single-molecule insight. Langmuir 2006;22(4):1800-03.
229. Kabanov VA, Basic Properties of Interpolyelectolyte Complexes Applied to Bioengineering and Cell Transformation. In: Dubin P., Bock J., Davies R.M., Schulz D.N., Thies C. (ed) , Macromolecular Complexes in Chemistry and Biology. Berlin, New York: Springer Verlag 1994.
230. Chen Y, Mohanraj V, Wang F, Benson H. Designing chitosan-dextran sulfate nanoparticles using charge ratios. AAPS PharmSciTech 2007;8(4):131-39.
231. Hajdu I, Bodnár M, Filipcsei G, Hartmann J, Daróczi L, Zrínyi M, et al. Nanoparticles prepared by self-assembly of chitosan and poly-γ-glutamic acid. Colloid & Polymer Science 2008;286(3):343-50.
232. Wang X, Chi N, Tang X. Preparation of estradiol chitosan nanoparticles for improving nasal absorption and brain targeting. Eur J Pharm Biopharm 2008;70(3):735-40.